



## Continuous Culture Microbioreactors

Schäpper, Daniel

*Publication date:*  
2010

[Link back to DTU Orbit](#)

*Citation (APA):*  
Schäpper, D. (2010). *Continuous Culture Microbioreactors*. Technical University of Denmark.

---

### General rights

Copyright and moral rights for the publications made accessible in the public portal are retained by the authors and/or other copyright owners and it is a condition of accessing publications that users recognise and abide by the legal requirements associated with these rights.

- Users may download and print one copy of any publication from the public portal for the purpose of private study or research.
- You may not further distribute the material or use it for any profit-making activity or commercial gain
- You may freely distribute the URL identifying the publication in the public portal

If you believe that this document breaches copyright please contact us providing details, and we will remove access to the work immediately and investigate your claim.

*Daniel Schäpper*

# Continuous Culture Microbioreactors

DTU Chemical Engineering  
Department of Chemical and Biochemical Engineering

PhD Thesis, March 2010





*Daniel Schäpper*

# **Continuous Culture Microbioreactors**

PhD Thesis, March 2010



Continuous Culture Microbioreactors,

**This report was prepared by**

Daniel Schäpper

**Supervisors**

Krist V. Gernaey	Department of Chemical and Biochemical Engineering, DTU
Anna Eliasson Lantz	Department of Systems Biology, DTU
Stuart Stocks	Novozymes A/S, Bagsværd, Denmark

Department of Chemical and Biochemical Engineering  
Center for Process Engineering and Technology (PROCESS)  
Technical University of Denmark  
Søltofts Plads, building 229  
DK-2800 Kgs. Lyngby  
Denmark

[www.kt.dtu.dk](http://www.kt.dtu.dk)

Tel: (+45) 45 25 35 00

Fax: (+45) 45 93 29 06

E-mail: [kt@kt.dtu.dk](mailto:kt@kt.dtu.dk)

---

Release date: Date published

Category: 1 (public)

Edition: First

Comments: This report is part of the requirements to achieve the PhD in Chemical Engineering at the Technical University of Denmark.

Rights: ©Schäpper, 2010



# Preface

---

This project was born through an idea of Nicolas Szita who had gained some experience in the field previously and was then started in May 2006 under the main supervision of Krist Gernaey within the framework of the *Novozymes Bioprocess Academy* with the aims of

- performing continuous culture experiments on a miniaturized scale,
- combining such microbioreactors with analytical methods for rapid measurement of relevant variables such as product or biomass concentration and
- demonstrating industrially relevant applications of the microbioreactors, for example based on continuous cell cultures or enzymatic conversion processes.

Yeast was to be used as a model strain, and benchmarking against bench-scale continuous cultivations would prove the viability of the microbioreactor results. Anna Eliasson Lantz and Nicolas Szita were included as co-supervisors from the university side, whilst Stuart Stocks was to represent Novozymes' support of the project. As Nicolas had more knowledge about microbioreactors, it was decided to locate me in his department,

After I had spent the first months learning a lot about the state-of-the-art of microbioreactors (I had previously worked with large-bore low-speed diesel engines for ships), their application and also the required fabrication techniques Nicolas Szita left for a more permanent position at University College London (UCL). As I did not fancy the prospect of living in busy London I decided to stay in Denmark and continue my studies here at a new department.

This change also required a change of office and laboratory, as Nicolas' group was to be dissolved. So I moved to the *Department of Chemical and Biochemical Engineering (KT)* and started applying my newly-won knowledge to the setup of a new lab. As I was (and still am) Krist's first PhD student and thus was the first member of his new group, the laboratory was completely empty when I started. Considerable effort was put into selecting, buying and also installing not only fabrication machinery such as a micromilling machine and a spinning

machine but also all the necessary components for a microbioreactor setup such as measurement apparatus, a computer and means for the control of some reactor parameters. This resulted in a fully functional mini-lab, where Krist's second microbioreactor PhD student—Nazrul—could start working some months later.

Parallel to the setup of the laboratory the microbioreactor design was also evolving. I started out with a design which was very similar to Nicolas', where alternating layers of PMMA and PDMS are clamped together. As this always brought leakage problems with it, my final design now consists of one single layer of PDMS. This design is working nicely now, obviously—however—there is still some way to go before the product can meet industrial demands with regards to quality, repeatability and ease-of-use.

Another major part of the research work consisted of the development and design of the measurement and control systems for temperature, optical density, pH and dissolved oxygen. Even though the basic functioning of the necessary systems was known, their application in my system proved to have its hurdles. Especially the software programming required some serious work—LabView is used for both measurement and control of the setup—as several components were not at all straightforward and easy to implement.

I would very much like to thank the many people around me who supported me in all possible ways: Krist, Anna, Stuart and Nicolas for their professional support and opinions, Rita and Patricia for their work done in their respective master theses and last but not least my wife and my daughter for putting up with an irritable workaholic for so long—without the two of you I might not have pulled this through. My thanks also go to the Novozymes Bioprocess Academy for helping finance this project—I hope you got your money's worth out of it. Naturally there are many others who have in one form or other contributed or supported me and my project—a heartfelt 'thank you' to them too.

Kgs. Lyngby, March 25 2010

# Summary

---

Efficient fermentations at industrial scale are usually preceded by an enormous amount of research work aimed at optimizing the productivity of the strain in question. Before that, the question of the selection of the correct strain already accounts for a substantial amount of work. Today, most screening is done in microtiterplates which allow for cultivations similar to those in shake flasks, however, due to the much smaller volume, microtiterplates are much more streamlined for parallel, machine-controlled operation. Out of these cultivations, a number of strains are selected for further investigation, which typically means performing cultivations in larger and larger scales. As the size of the reactor increases from shake flask to bench-scale reactors to pilot-plant installations the number of strains decreases until only one strain is left at production scale which hopefully is the ideal strain. However, precisely this scaling-up can give problems, as strains may behave differently in a shake flask than in a production scale reactor. There is therefore a need for a small-scale production platform which can offer more reliable upscaling; Or in other words a platform which is better at mimicking full-scale operation is needed. Apart from the fermentation industry, research also depends on well-controlled cultivations with tight measurement and control in order to obtain meaningful data about the strain metabolism.

Microbioreactors have the potential to be the platform needed to fulfill the above requirements: The working volumes are relatively small, typically  $< 1$  mL, and they can be operated in different operating conditions such as batch or continuous cultivations. Additionally, their small size offers a number of possibilities: Under the presence of good mixing, one can assume the contents of a microbioreactor to be free of gradients (e.g. nutrients, oxygen) which allows for a precise determination of the state of the cultivation. Additionally, the large surface to volume ratio opens up the possibility for quick changes in temperature, so that e.g. the influence of step changes on the metabolism can be investigated. The advance of miniature online measuring techniques makes it possible to measure at least the basic culture variables such as dissolved oxygen (DO), cell density (OD) and pH continuously and without disturbing the cultivation. Online measurements are at this scale very susceptible to the presence of bubbles—as is a microbioreactor itself as already small bubbles can disturb



the flow in microchannels. Bubble-less aeration through a membrane elegantly solves both problems and also separates the broth from external influences.

The microbioreactor developed here was designed to fulfill the above requirements; Additionally, much focus was put on the single-use aspect. This includes both being cheap in fabrication and in operation, and also requires the reactor to be sterilizable by industrial methods. It consists entirely of polydimethylsiloxane (PDMS) and contains two optical sensor spots for the measurement of DO and pH as well as a micro-stirrer for agitation of the broth. It has provisions for the measurement of cell density (by means of optical density measurement) as well as membrane aeration. Both temperature and pH can be controlled online and automatically.

The device has outer dimensions of 14 mm diameter and 4.2 mm height. The reactor chamber is a cylinder with 8 mm diameter and 2 mm height resulting in a culture volume of 100  $\mu\text{L}$ . The fluidic connections are done by piercing the reactor side walls with needles—the PDMS will tightly enclose the needle to prevent leakage. The reactor chamber is sealed with a semi-permeable membrane (thickness approximately 80  $\mu\text{m}$ ), through which the gases can diffuse. Both oxygen and off-gases are exchanged this way. Additionally, pH can be controlled by the addition of  $\text{CO}_2$  or  $\text{NH}_3$  to the aeration gas flow to lower or increase pH respectively. The density of the culture broth is measured by a transmittance measurement—light is shone through 0.5 mm of culture broth, and the intensity of the transmitted light is measured. This gives an indication of the amount of cells in the broth. Both DO and pH are measured with fluorescent sensor spots: Oscillating light is shone onto the sensor spots which in turn emit oscillating fluorescent light with a certain phase shift respective to the exciting light. This phase shift relates to the DO or pH of the broth, respectively.

Mixing is solved by means of a small magnetic stirrer bar which, contrarily to what is seen in other microbioreactor solutions, rotates freely within the reactor. Experiments had shown that a stirrer bar rotating in the middle of the reactor will only force the broth into a swirling motion where the outer edges of the reactor do not have enough updraft anymore. The freely spinning stirrer bar however will hit the wall and ricochet chaotically into the reactor chamber again. Thus, over time, all of the reactor floor will be covered which prevents the formation of dead zones.

Temperature is controlled by means of an external (and thus re-usable) heating plate which contains both a temperature sensor and a resistance heating wire. As the floor of the microbioreactor only consists of a membrane which offers virtually no heat resistance, this allows for a precise control of the broth temperature.

In order to provide benchmarking data to be able to evaluate the reactor performance, batch cultivations were done in both shake flasks and bench-scale reactors. Finally, corresponding cultivations were performed in the microbioreactor.

Additionally, as an entirely theoretical case study of something completely new, the application of the topology optimization methodology on microbioreactors and the resulting gains in productivity was studied.

## Dansk Resumé

---

Forud for implementering af fermenteringer i industriel skala er et omfangsrigt forskningsarbejde nødvendigt, som har til formål at øge produktiviteten af den valgte mikrobielle stamme. Udvælgelsen af en passende produktionsstamme udgør en betydelig del af arbejdet. I dag foregår størstedelen af screeningsarbejdet i mikrotiterplader, hvilket muliggør kultiveringer lignende dem i rysteflasker, men pga. det meget mindre volumen er mere effektiviserede til parallel maskinstyret drift. Ud fra disse kultiveringer vælges et antal stammer til videre analyse, hvilket indebærer kultiveringer i voksende skala. Efterhånden som størrelsen af reaktoren øges fra rysteflasker til laboratorieskala til pilot plant installationer mindskes antallet af stammer indtil en stamme, som forhåbentlig er den mest egnede, er tilbage når processen når produktionsskala. Denne opskalering kan dog give problemer, da stammer kan reagere anderledes i rysteflasker end i reaktorer i produktionsskala. Der er derfor brug for en produktionsplatform i mindre skala, som kan give en mere pålidelig opskalering. Også uden for fermenteringsindustrien er bioteknologisk og mikrobiel forskning afhængig af kultiveringer med præcise målinger og effektiv kontrol for at kunne skaffe brugbar information om f.eks. cellemetabolismen.

Mikrobioreaktorer har potentiale for at opfylde ovennævnte krav til en ny fermenteringsplatform: Arbejdsvolumenet er relativt lille, typisk  $< 1$  mL og de giver mulighed for forskelligartet drift som f.eks. batch og kontinuert kultivering. Størrelsen giver et antal muligheder: Under god omrøring kan det antages at bioreaktoren er fri for gradienter (som f.eks. næringsstoffer og ilt), hvilket tillader præcis bestemmelse af procesbetingelserne. Derudover giver det store relative forhold mellem overfladeareal og volumen mulighed for hurtige ændringer i temperatur, så f.eks. effekten af trinændringer på cellemetabolismen kan undersøges. Udviklingen af online-måleteknikker i mikroskala muliggør som et minimum kontinuerlige målinger af de basale variabler knyttet til cellekultivering, såsom opløst ilt (DO), celledensitet (OD) og pH, uden at forstyrre kultiveringen. Da selv små bobler kan forstyrre strømmingen i mikrokanaler, er online-målinger meget følsomme overfor bobler og det samme er mikrobioreaktoren. Boblefri beluftning gennem en membran løser elegant begge problemer og adskiller derudover fermenteringsvæsken fra eksterne påvirkninger.

Mikrobioreaktoren udviklet her blev designet til at opfylde ovennævnte krav.

Der blev derudover lagt vægt på at reaktoren var egnet til engangsbrug, hvilket indebærer billig fabrikation og drift samt at reaktoren kan steriliseres ved industrielle metoder. Reaktoren består udelukkende af polydimethylsiloxane (PDMS) og indeholder to optiske sensor-spots til måling af DO og pH samt en mikroomrører. Den er klargjort til måling af celledensitet (vha. måling af optisk densitet) og membranbeluftning. Både temperatur og pH kan kontrolleres online og automatisk.

Hele anordningen måler 14 mm i diameter og er 4.3 mm høj. Selve reaktorkammeret er en cylinder som måler 8 mm i diameter og er 2 mm høj, hvilket giver et volumen på 100  $\mu\text{L}$ . Væsketilførsel udføres ved at gennembore sidevæggen i reaktoren med nåle—PDMS vil slutte tæt om nålen og dermed undgå lækager. Reaktorkammeret er forseglet med en semipermeabel membran (ca. 80  $\mu\text{m}$  tyk) gennem hvilken gasser kan diffundere. Både ilt og affaldsgasser overføres på denne måde. Derudover kan pH kontrolleres ved at tilsætte  $\text{CO}_2$  eller  $\text{NH}_3$  til beluftningsgassen for henholdsvis at sænke eller øge pH. Densiteten af cellekulturen måles ved en transmittans måling—lys sendes gennem 0.5 mm af fermenteringsvæsken og intensiteten af det overførte lys måles. Dette giver en indikation af mængden af celler i kultiveringsvæsken. Både DO og pH måles med fluorescerende sensor-spots: Oscillerende lys sendes på sensor-spottene som udsender oscillerende fluorescerende lys med et bestemt fase skift i forhold til det eksisterende lys. Dette faseskift afhænger af henholdsvis DO eller pH i væsken. Omrøring foregår vha. en lille magnetomrører, som modsat hvad der er set i andre mikrobioreaktorer roterer frit i reaktoren.

Eksperimenterne viste at en omrører, der roterer i midten af reaktoren, vil tvinge væsken ind i en hvirvlende bevægelse, hvor de ydre kanter af reaktoren ikke har den nødvendige opdrift. Den frit roterende omrører vil derimod ramme væggen og rikochettere kaotisk ind i reaktorkammeret. Dermed vil alle dele af reaktorgulvet blive dækket, hvilket forhindrer døde zoner i at opstå.

Temperaturen kontrolleres vha. en ekstern (og dermed genanvendelig) varmeplade som indeholder både temperatursensor og en varmetråd. Eftersom bunden af mikrobioreaktoren består af en membran, som stort set ingen modstand giver, kan der opnås en effektiv kontrol af temperaturen i kultiveringsvæsken. Derudover er alle de elektriske kontakter, der er brugt til temperaturkontrollen, ikke en del af mikrobioreaktoren, hvilket øger pålideligheden betydeligt.

For at skaffe benchmarking data til evaluering af reaktoren blev batch kultiveringer udført i både rysteflasker og laboratorieskala reaktorer. Endelig blev tilsvarende kultiveringer udført i mikrobioreaktoren.

Ydermere, som et komplet, nyt teoretisk studie, blev indførelsen af topologisk optimering af mikrobioreaktorer og den deraf øgede produktivitet studeret.

# Contents

---

List of Figures	x
List of Tables	xiii
Nomenclature	xv
<b>1 Introduction</b>	<b>1</b>
<b>2 State-of-the-art in microbioreactor technology</b>	<b>3</b>
2.1 Introduction to microbioreactor technology . . . . .	3
2.2 Materials . . . . .	4
2.3 Mass and heat transfer in microbioreactors . . . . .	7
2.3.1 Mixing . . . . .	7
2.3.2 Aeration and evaporation . . . . .	10
2.3.3 Fluidics - pumping mechanism & connections . . . . .	12
2.4 Sensing and control . . . . .	15
2.4.1 Temperature . . . . .	16
2.4.2 pH . . . . .	17
2.4.3 Cell concentration . . . . .	19
2.4.4 Dissolved oxygen concentration . . . . .	21
2.4.5 CO <sub>2</sub> . . . . .	22
2.4.6 Spectroscopy . . . . .	22
2.5 Discussion . . . . .	23
2.6 Conclusions from the literature review . . . . .	27

2.7	Goals of the PhD project . . . . .	27
<b>3</b>	<b>Microbioreactor Design</b>	<b>29</b>
3.1	Current state-of-the-art . . . . .	29
3.2	Microbioreactor design and fabrication . . . . .	31
3.2.1	Overview . . . . .	31
3.2.2	Dissolved oxygen . . . . .	33
3.2.3	pH . . . . .	36
3.2.4	Optical density . . . . .	40
3.2.5	Mixing . . . . .	43
3.2.6	Evaporation . . . . .	44
3.2.7	Fluidics . . . . .	44
3.2.8	Temperature . . . . .	44
3.3	LabView control program . . . . .	46
3.3.1	Lock-in Amplifiers . . . . .	50
<b>4</b>	<b>Results</b>	<b>53</b>
4.1	Dissolved Oxygen . . . . .	53
4.2	pH . . . . .	54
4.3	Optical Density . . . . .	57
4.4	Mixing . . . . .	58
4.5	Temperature . . . . .	58
<b>5</b>	<b>Cultivations</b>	<b>65</b>
5.1	Cultivations of microorganisms . . . . .	65
5.1.1	Batch operation . . . . .	66
5.2	Model system <i>S. cerevisiae</i> . . . . .	68
5.3	Bench-scale and shake flask cultivations: data for benchmarking with microscale . . . . .	69
5.4	Cultivations in the microbioreactor and their comparison with the larger scale cultivations . . . . .	72
5.4.1	Standardization of microscale cultivations . . . . .	74
<b>6</b>	<b>Topology Optimization</b>	<b>77</b>
6.1	Biological motivation . . . . .	79
6.2	Microfluidics modeling and optimization . . . . .	80

6.2.1	Fluid dynamic modeling of the flow . . . . .	80
6.2.2	Implementation of the biological model . . . . .	82
6.2.3	Model for topology optimization: spatial dependency . . .	83
6.3	Simulation results . . . . .	85
6.4	Benchmarking . . . . .	86
6.5	Outlook . . . . .	86
<b>7</b>	<b>Conclusion and perspectives</b>	<b>91</b>
7.1	Conclusions on the final microbioreactor design . . . . .	91
7.2	Perspectives and future work . . . . .	92
	<b>References</b>	<b>96</b>
	<b>Appendix</b>	<b>107</b>
<b>A</b>	<b>Microbioreactor: Mechanical drawings</b>	<b>107</b>
<b>B</b>	<b>Optical density: Mechanical drawings</b>	<b>113</b>
<b>C</b>	<b>Dissolved oxygen &amp; pH: Mechanical drawings</b>	<b>123</b>
<b>D</b>	<b>Photodiodes: Mechanical drawings</b>	<b>127</b>
<b>E</b>	<b>Procedure for the production of PDMS membranes</b>	<b>131</b>
<b>F</b>	<b>Transmittance/absorbance measurements of different materials</b>	<b>137</b>
<b>G</b>	<b>Culture media</b>	<b>139</b>
G.1	YPD . . . . .	139
G.2	CBS / Delft medium . . . . .	140
<b>H</b>	<b>LabView program</b>	<b>143</b>
<b>I</b>	<b>Details of the topology optimization routine</b>	<b>155</b>

x

---

# List of Figures

---

2.1	Section of a typical microbioreactor . . . . .	6
2.2	Schematic of a complete microbioreactor setup . . . . .	9
2.3	Example of mixing in a microbioreactor . . . . .	10
2.4	Passive staggered herringbone mixer . . . . .	11
2.5	Automatic cell culture system . . . . .	13
2.6	Rigidly mounted fluidic connection . . . . .	14
2.7	Needle-based fluidic connection . . . . .	15
2.8	Multiplexed microbioreactor setup . . . . .	26
2.9	Final goal of PhD project . . . . .	28
3.1	Photo of the microbioreactor . . . . .	32
3.2	3D CAD sketch of the current microbioreactor design . . . . .	32
3.3	Microbioreactor holder plate . . . . .	34
3.4	Microbioreactor lying on holder plate . . . . .	35
3.5	Close-up of the meandering aeration channel . . . . .	36
3.6	Close-up of the dissolved oxygen sensor . . . . .	37
3.7	Close-up of the pH sensor . . . . .	38
3.8	Calibration curve for the pH measurement. . . . .	39
3.9	pH control scheme . . . . .	40
3.10	OD beamsplitter block . . . . .	41
3.11	Close-up of the optical density measurement . . . . .	42
3.12	Temperature control scheme . . . . .	46



3.13	Overview over the LabView program . . . . .	47
3.14	Schematic of the LabView program: high-speed part . . . . .	48
3.15	Schematic of the LabView program: low-speed part . . . . .	49
3.16	Schematic of the LabView program: Digital part . . . . .	50
3.17	Schematic depicting the operating mode of the lock-in amplifier. . . . .	51
4.1	pH set point tracking . . . . .	56
4.2	Calibration curve for the OD measurement. . . . .	57
4.3	Mixing in the microbioreactor . . . . .	59
4.4	Temperature rise with increasing heating power . . . . .	60
4.5	Total heating energy applied. . . . .	61
4.6	Stepping up/down of the reactor temperature . . . . .	62
4.7	Control system response to a disturbance in temperature . . . . .	62
4.8	Temperature difference between different locations . . . . .	63
5.1	Growth of a typical microbial culture in batch conditions. . . . .	66
5.2	Bench-scale batch cultivation: Biomass, glucose and ethanol. . . . .	71
5.3	Bench-scale batch cultivation: Oxygen and CO <sub>2</sub> . . . . .	71
5.4	Shake flask cultivation: Biomass. . . . .	72
5.5	Shake flask cultivation: Glucose and ethanol. . . . .	73
5.6	Microbioreactor cultivation: OD, DO and temperature. . . . .	74
5.7	Microbioreactor cultivation: Variation between cultivations. . . . .	76
6.1	Yeast metabolism: pathways . . . . .	82
6.2	Topology optimization routine . . . . .	85
6.3	Optimized structure for low glucose concentrations . . . . .	87
6.4	Rates for low glucose concentrations . . . . .	87
6.5	Optimized structure for high glucose concentrations . . . . .	88
6.6	Rates for low glucose concentrations . . . . .	88
E.1	Membranes of Series A . . . . .	133
E.2	Membranes of Series B . . . . .	133
E.3	Membranes of Series C . . . . .	134
E.4	Membranes of Series D . . . . .	134
E.5	Membrane of Series A . . . . .	135

F.1	Transmittance for various transparent materials . . . . .	138
F.2	Scaled absorbtion for various transparent materials . . . . .	138



# List of Tables

---

2.1	Current microbioreactor platforms . . . . .	5
5.1	Comparison between the different reactor scales . . . . .	74
6.1	Comparison of the total protein outputs for the homogenous and the structurally optimized reactor designs at different glucose feed concentrations. . . . .	89
E.1	Summary of Results . . . . .	132
I.1	List of model parameters . . . . .	157



# Nomenclature

---

## Abbreviations:

DO	dissolved oxygen
OD	optical density
PMMA	poly(methylmethacrylate)
PDMS	polydimethylsiloxane
RTD	resistance temperature detector
ISFET	ion-sensitive field-effect transistor

$\alpha(\vec{r})$	proportionality factor [-]
$\eta$	viscosity [Pa·s]
$\gamma$	set of design variables
$\mu$	specific growth rate [-]
$\Omega$	design region
$\Phi$	objective function
$\rho$	density [kg·m <sup>-3</sup> ]
$\varepsilon$	molar absorptivity of the absorber [L·mol <sup>-1</sup> ·cm <sup>-1</sup> ]
$\vec{r}$	position coordinate vector
$\vec{u}$	flow velocity [m/s]
$A$	absorbance [-]
$a$	interfacial area [m <sup>2</sup> /m <sup>3</sup> ]
$c$	concentration of the absorbing species [mol·L <sup>-1</sup> ]
$D$	dilution rate [h <sup>-1</sup> ]
$D_A$	diffusion coefficient for $A$ [m <sup>2</sup> /s]

---

$E$	ethanol concentration [ $\text{g}\cdot\text{L}^{-1}$ ]
$G$	glucose concentration [ $\text{g}\cdot\text{L}^{-1}$ ]
$I$	power [W]
$k_L$	mass transfer coefficient [m/h]
$k_L a$	volumetric oxygen transfer coefficient [ $\text{h}^{-1}$ ]
$l$	path length [cm]
$p$	pressure [Pa]
$P(\vec{r})$	product/protein concentration [units $\text{L}^{-1}$ ]
$R$	rate of formation [units/( $\text{L} \cdot \text{s}$ )]
$X_f$	total free (suspended) biomass [ $\text{g}\cdot\text{L}^{-1}$ ]
$X_f^+$	plasmid bearing freely suspended biomass
$X_{im}$	immobilized cells [ $\text{g}_{cells}/\text{g}_{carrier}$ ]
$X_{im}^+$	immobilized cells with plasmid [ $\text{g}_{cells}/\text{g}_{carrier}$ ]

# Introduction

---

This project has a quite broad scope going from mechanical engineering over electronics and programming as a necessary basis for the fabrication of a micro-bioreactor system to biotechnology and cultivation technology as the final goal. This is reflected accordingly in the structure of the thesis:

In *Chapter 2* I will give an overview over the current state of the art in micro-bioreactor technology, with special emphasis on reactors that allow for the (preferably continuous) cultivation of suspended cells. The basis for this chapter is the review paper which we published in *Analytical and Bioanalytical Chemistry* in 2009 (1).

In *Chapter 3* the current reactor design is presented. I emphasize the design considerations and the fabrication methods used; The measurement and control concepts are also explained in detail. The basis for this chapter is a research paper which was published online in *Chemical Engineering Journal* in March 2010 (2).

Once the reactor has been produced the measurements of the most important culture variables have to be calibrated (*Chapter 4*). These variables are temperature, pH, cell density and dissolved oxygen. Of these the former two are controlled whereas the latter two are only measured. However, the control algorithm for dissolved oxygen is very similar to that of pH, so this would probably require relatively little time to implement. The basis for this chapter are the article in *Chemical Engineering Journal* (2) and two other research articles: An article discussing temperature control was accepted for publication by *Journal of Micromechanics and Microengineering* in 2010 (3), and one discussing the gaseous control of pH is in preparation.

All this mechanical and measurement & control work is irrelevant if it does not lead to biological cultivations (*Chapter 5*). I present and discuss some results of cultivations done in the micro-bioreactor. Additionally, the results from the microscale are compared with bench-scale reactors in order to investigate the scaling-up properties.

An interesting side path (*Chapter 6*) was opened up by a course I took at the



Department for Nanotechnology (then *Department of Micro- and Nanotechnology*): Topology optimization. This is a fascinating field of design, mostly mechanical design, where the computer strives to optimize a system with respect to some predefined quality criteria. This reverses the design pathway where the reactor is normally designed by the engineer and then its operation is optimized. Whilst this technology has been presented in various fields, nobody has investigated (micro-)biological systems with it. We have investigated a kind of perfusion reactor where the cells are not evenly distributed but optimized for the production of a protein. The basis for this chapter is a scientific article that is in preparation.

Finally (*Chapter 7*), I summarize the work done and also voice some opinions on where microbioreactor technology might be going and which factors have to be addressed in order to make this vision possible.

# State-of-the-art in microbioreactor technology

---

This chapter gives an introduction into the world of microbioreactors, shows the current state of the art and also the limitation of the various aspects of microbioreactor technology and shows where microbioreactor technology might be heading in the future. Based on this introduction the project name ‘Development of continuous culture microbioreactors’ is spelled out into specific requirements and tasks at the end of this chapter. The chapter is based in large parts on our review paper which was published in *Analytical and Bioanalytical Chemistry* in 2009 (1).

## 2.1 Introduction to microbioreactor technology

Microbioreactor technology offers the potential to develop disposable and miniaturized versions of bench-scale bioreactors for carrying out fermentation experiments. Such a scaled down version of a bioreactor would then ideally combine the ease of handling of shake flask operations while preserving the online sensing and control capabilities of stirred-tank bench-scale bioreactors. Microbioreactor technology thus offers academia and industry the capacity to acquire real-time experimental data via cheap and high throughput experimentation under well-controlled conditions (4).

Bench-scale bioreactors typically operate with a volume of 0.5–5 L. Such bioreactors are the most versatile experimental tool available for studying fermentation processes. They enable cultivations in batch, fed-batch, and continuous modes under a broad range of environmental conditions. Indeed, temperature, pH, and—at least for aerobic fermentations—dissolved oxygen concentrations are typically quantified on-line with well-established probes, and each variable can be maintained close to a desired set point or set point profile with a suitable controller. In addition, bench-scale bioreactors usually offer online measurement of acid and base consumption used for pH control, substrate consumption, off-

gas composition (especially CO<sub>2</sub>), and sometimes also biomass concentration (5).

Microbioreactors with working volumes of between 50 to 800  $\mu$ L have been realized (see Table 2.1). Due to their small size, they offer a number of cost-reducing advantages for assessing biological processes (6–8). These include lower running costs due to the reduced amount of substrate and utilities such as water or power consumption needed per experiment, and reduced space requirements for parallel operation due to their small footprint. Furthermore, compared to bench-scale bioreactors, disposable microbioreactors also reduce the labor and effort required to prepare fermentation experiments; for example, they do not have to be cleaned and sterilized, and there is the potential to automate experiments.

The scope of this chapter is restricted to microbioreactors that allow fermentations with microorganisms growing in suspension, since the majority of industrial fermentations are based on this type of process. Moreover, in this literature review, we will only consider microbioreactors with an operating volume smaller than 1 mL, which are designed to mimic typical bench-scale reactors. Therefore, the term ‘microbioreactor’ will exclusively refer to this type of reactor throughout the manuscript. Larger reactors have already been looked at in other reviews (7; 8; 16).

This review starts with a concise overview of the materials most commonly used for microbioreactor fabrication. Once the reactor is established, the key requirements to obtain a successful fermentation experiment are then an adequate temperature and supply of nutrients, sufficient mixing, and—for aerobic fermentations—a sufficient supply of oxygen. The second part of the review therefore focuses on mass and heat transfer in microbioreactors. In the third part of the review, the state of the art in on-line measurement techniques for microbioreactors is highlighted, and methods currently used to control the main microbioreactor variables—temperature, pH, dissolved oxygen concentration—are presented. The final part of the review consists of an extended discussion of microbioreactor technology considering the needs of the fermentation industry, as well as the outlook for future developments. These are based on the literature presented here—Our own conclusions and outlook will be presented in chapter 7.

## 2.2 Materials

Microbioreactor prototypes are typically made from poly(methylmethacrylate) (PMMA) and polydimethylsiloxane (PDMS) (9; 11; 13; 14; 17). These are the most commonly used substrates for the fabrication of microbioreactor prototypes due to their low material cost, easy handling, biocompatibilities, nontoxicities, good solvent and chemical compatibilities, and durabilities. Additionally, they also exhibit high optical transmission in the visible wavelength range, which facilitates optical measurements (18; 19). Moreover, using PMMA and PDMS substrates, it is possible to fabricate two- or three-dimensional (2D or 3D) microfluidic geometries using a rather straightforward and relatively cheap micromachining process (20; 21). Whilst the bonding (or structuring) of multiple layers of PMMA is normally done using replication methods like injection molding or hot embossing (20; 21), the fabrication of PDMS-based reactors

Table 2.1: Current microbioreactor platforms and their basic characteristics

Source	Volume [ $\mu L$ ]	Organism	Fermen- tation mode	Mixing	Minimization of evaporation	$k_L a$ [ $h^{-1}$ ]	OD max.	OD measure- ment
(9)	5-50	<i>E. coli</i>	batch	Diffusion	Humid air	60	8	Transmittance
(10)	50	<i>S. cerevisiae</i>	batch	Stirrer on axis	Water replenish- ment from elevat- ed reservoir	-	6.87	Transmittance
(11)	100	<i>E. coli</i>	batch	Peristaltic	Oxygen feed hum- idified	500	40	Transmittance
(12)	250	<i>E. coli</i>	batch	Shaken steel bead	Sealed	150	2.5	Transmittance
(13), (14)	150	<i>E. coli</i> (13), <i>S. cerevisiae</i> (14)	batch	Stirrer on axis	Water replenish- ment from elevat- ed reservoir	20-75	6 (13), 7 (14)	Transmittance
(15)	700	<i>E. coli</i>	batch	Shaken	Sealed	-	-	Transmittance

merely involves a few casting and curing steps (20; 22). Pressing a PDMS slab between two PMMA layers (see Fig. 2.1 for an example) with metal screws or clamps is an alternative way to ensure watertight seals in multilayered reactors consisting of PMMA-PDMS substrates (17). Their low material cost coupled with their cheap fabrication processes are ideal characteristics for low-cost mass production and rapid prototyping. This also allows for the fabrication of disposable microbioreactors—a useful advantage, as disposable reactors prevent sample contamination and reduce the effort involved in reactor preparation significantly.

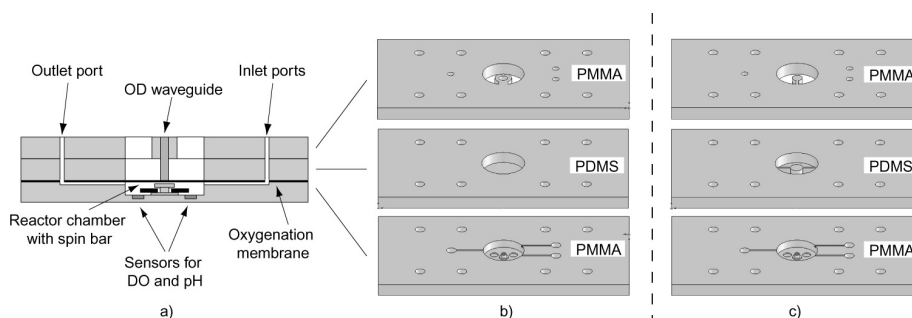


**Figure 2.1:** (a) Longitudinal section of a microbioreactor consisting of alternating layers of PDMS and PMMA clamped together with screws. (b) Solid models of the different layers with a PMMA waveguide. (c) Solid models of the different layers with a PDMS waveguide. (13)

An important advantage of PDMS substrates over other thermoplastic polymers like PMMA, polyetheretherketone (PEEK) or polycarbonate (PC) is that PDMS enables the integration of microfluidic devices such as microvalves, micropumps, and mixers as an integral part of the reactor (11; 23). While the integration of microfluidic devices may complicate the reactor design, it—more importantly—decreases the cost of the entire microbioreactor setup because fewer macroscale devices are needed to drive the system. Furthermore, PDMS also exhibits high permeability to oxygen and carbon dioxide, which makes it highly suitable for cell-based systems (20). Despite all of these advantages, PDMS also suffers from several drawbacks. One drawback is that the gas permeability of PDMS can lead to unwanted levels of evaporation (17; 20). Evaporation is discussed further later on in this review (see the section on aeration and evaporation). PDMS also swells in most organic solvents (20), although this is not really an issue for standard microbial fermentations because most fermentation media are prepared using water as a solvent. However, the swelling could become a problem for novel reactor designs where a solvent is added to the fermentation broth; for example, to remove product or inhibitory compounds from the water phase in an attempt to increase the productivity (24; 25).

Silicon and glass can also be used as substrates for the fabrication of microbioreactors, but these are rather difficult to work with. Moreover, the fabrication techniques used for these substrates are expensive, time consuming, and require access to clean-room facilities (22).

## 2.3 Mass and heat transfer in microbioreactors

Adequate mass transfer and heat transfer are required in order to achieve successful fermentation experiments, and this of course also applies to fermentation in microbioreactors. Therefore, this part of the review focuses on established mixing and aeration concepts in microbioreactors, the importance of minimizing evaporation, and microfluidic pumping for different modes of operation.

### 2.3.1 Mixing

Mixing is one of the most important operations in a submerged cultivation: the mixing quality directly influences the distribution and suspension of substrate and microorganisms in the reactor, and thus affects both the growth characteristics (e.g., the availability of oxygen and nutrients, removal of waste products, etc.) and the quality of the measurements. Also, optimal mixing ensures an even temperature profile throughout the reactor. Mixing becomes more difficult as the scale of the reactor decreases, as it becomes impossible to achieve the turbulent conditions associated with good mixing. This is due to the small Reynolds numbers that can be achieved, which in turn can be explained by the small characteristic lengths (26). In addition, the influence of the volume boundaries becomes much more apparent due to both the molecular forces present and the much higher proportion of cells growing on the walls compared to, for example, a bench-scale fermentor. If the system also contains particles (e.g., cells), then the mixing problem is further accentuated: the mixing system must then also provide some updraft that lifts the particles, and dead zones (with insufficient mixing) must be avoided even more rigorously, as they would lead, for example, to the local accumulation of particle heaps on the reactor floor.

Optimal mixing is a compromise between ensuring homogeneous conditions and efficient mass and heat transfer and avoiding damage to the cells, and thus affects the quality of the achieved growth. Key here is a trade-off where mixing is ‘as good as necessary’ while being ‘as gentle as possible’. The severity of the mixing problem depends very much on the type of microorganism used (*Saccharomyces cerevisiae* cells will, for example, sediment much quicker than *Escherichia coli* cells, but they are quite robust; also, different microorganisms can have different sensitivities to concentration gradients), on the reactor geometry (shape, such as the ratio of height to diameter), and on the mixing scheme chosen.

Mixing can be achieved in microfluidic bioreactors by active methods that utilize moving parts to disturb the fluid and passive methods that have no moving parts (27; 28). Passive mixing can also be subdivided into molecular diffusion and chaotic advection. In molecular diffusion, the natural Brownian motion of the molecules is utilized. Good mixing is then achieved with large interfacial areas, large gradients, and high diffusion coefficients. Large interfacial areas can be achieved by, for example, laying many thin layers of the fluids to be mixed upon each other, similar to an alternating stack of differently colored paper sheets. Thus, the same molecular diffusion rate becomes a more effective mixing operation. Chaotic advection further enhances mixing by stretching, folding, and breaking up the fluid streams. This is achieved by forcing motion transverse to the flow direction upon the fluid, by fabricating obstacles that are placed in the microfluidic channel for instance.

When active mixing is used, it is important to take into account the fact that microbioreactors often consist of completely filled volumes without any headspace. Shaking the entire reactor will only move the small liquid volume as a whole; very little mixing will be induced. Therefore, in such reactors, there is a need to actively induce the mixing inside the chamber of the microbioreactor. This will also aid in the retention of microbial cells in suspension. Mimicking the agitation methods of larger-scale reactors, many microbioreactors include a stirrer bar mounted on and revolving around a rigid vertical post (13; 14) (Figs. 2.2 and 2.3). These bars can also potentially be microfabricated to mimic the shapes of larger-scale impellers. Whilst these systems create defined liquid movement in the reactor volume, they require very precise fabrication of both the impeller and also the axis needed to mount the impeller. The utilization of this type of microimpeller cannot guarantee that there are no dead zones in the reactor: the corners between the vertical walls and the horizontal floor are typically the most critical points. A simpler solution has been achieved by replacing impellers with steel beads (12), thus avoiding the need for precise manufacturing. However, the fact that an optical density of only 2.5 was reported by Maharbiz et al. (12) may indicate that mixing with steel beads does not work properly for high cell concentrations.

Another active mixing approach involves moving the boundaries of the reactor. Lee et al. (11) arranged a series of inflatable air cushions in the ceiling of the reactor chamber. Periodic inflation of these cushions created peristaltic movement of the liquid in the reactor. Cultivations done with *E. coli* successfully demonstrated that high cell densities can be achieved. Zanzotto et al. (9) fabricated shallow microfluidic bioreactors with operating volumes of between 5 and 50  $\mu\text{L}$ . Due to the shallow design of the reactor chamber and the motility of the *E. coli* cells used, diffusion was efficient enough to support growth. The fermentation results of Zanzotto et al. (9) compared well with those obtained from 500 mL bench-scale reactors. Passive mixing requires some kind of flow of the broth through a microchannel, for example by recirculating the fermentation broth in and out of the reactor chamber. Molecular diffusion can be enhanced with, for example, parallel lamination, where the broth stream is split into various substreams and is later rejoined, preferably in a different order so that different streams meet each other. While this will mix the fluid, the channel length will be quite substantial (depending of course on fluid velocity, etc.). Chaotic advection can significantly reduce channel length and thus increase mixing efficiency.

One possibility here is to use passive mixing structures such as the staggered herringbone mixer (31) that impose a transverse swirling motion upon the fluid (Fig. 2.4). Another possibility is to increase the recirculation flow velocity such that the fluid motion in the reactor chamber is no longer truly laminar but approaches transition phase conditions, which in turn reduces diffusion lengths. This can, for example, be implemented with a system of three serially connected reactors where the broth is pumped back and forth between the two outer chambers using the middle chamber as a mixing chamber (32). Mixing can then further be enhanced by arranging the inlet/outlet ports eccentrically such that the fluid is forced into a swirling motion in the main reactor chamber, which further reduces diffusion lengths and thus increases the quality of mixing. Whilst passive mixing elegantly removes the need for some kind of active mixing in the chamber, it creates additional fluidic requirements, such

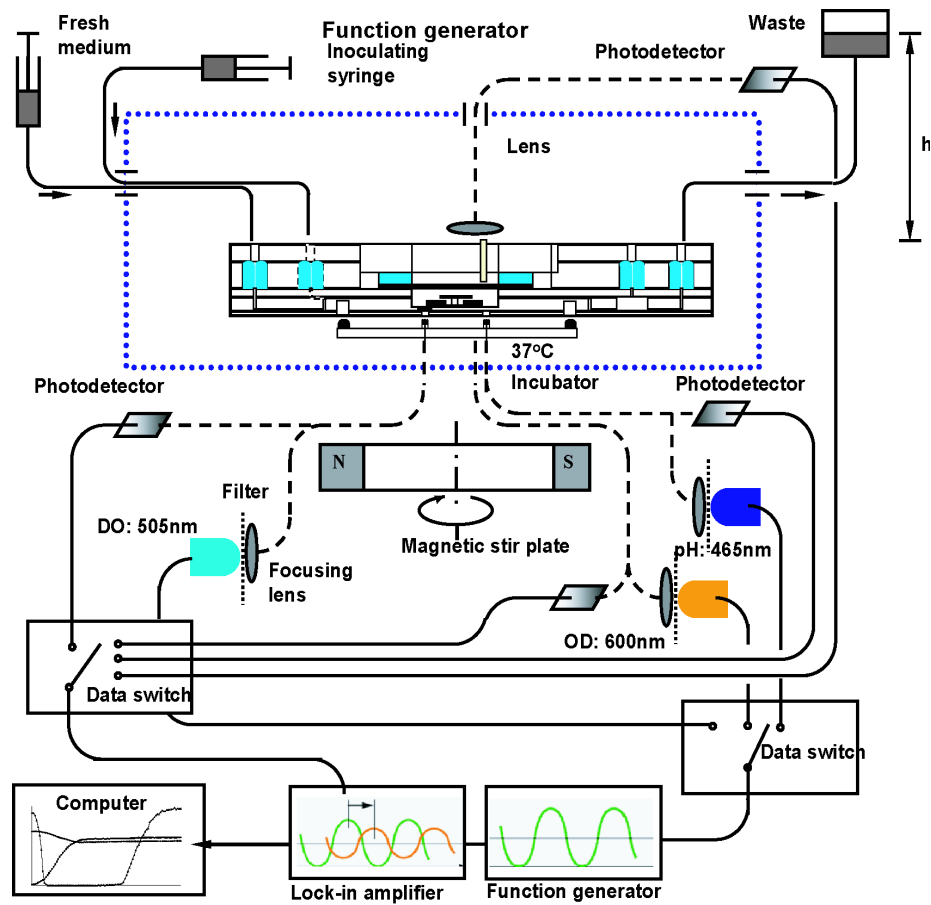


**Figure 2.2:** Schematic of a microbioreactor setup complete with actuation, fluidic connections (*solid lines*), and optical fibers (*dashed lines*) for the sensing of OD, DO, and pH (29)



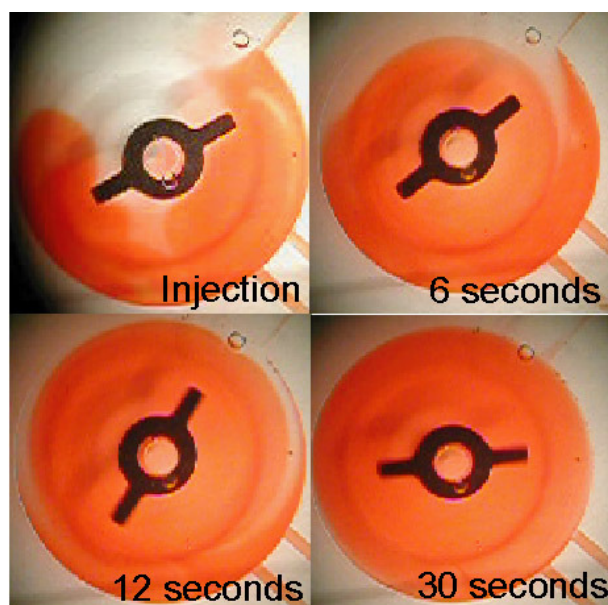


**Figure 2.3:** Photographs of the mixing of phenol red dye in a microbioreactor using a stirring speed of 180 rpm (30)

as pumps to move the liquid through the passive mixing elements and possibly valves to separate the recirculation stream from the dilution flow (for example), as needed for continuous cultivations. Also, as with active mixing, great care must be taken to prevent dead zones where particles could sediment.

While many of these methods have been shown to create sufficiently thorough mixing for the fermentation of microorganisms, mostly *E. coli*, they often require delicate manufacturing. Whilst a micro-impeller, for example, requires very precise manufacturing of both the impeller itself and the vertical axis that supports and guides the impeller, a system with moving boundaries (11) requires elaborate pneumatic installations. Both systems are also technically feasible for mass fabrication. They will, however, result in higher production costs than a mechanically simpler solution. Therefore, ideally, it would be desirable to find a simple and cheap mixing solution that provides sufficient mixing for a wide range of microorganisms.

### 2.3.2 Aeration and evaporation

Aeration is relevant for aerobic fermentations, and is achieved in most if not all microsystems through a thin PDMS membrane (9; 11; 13; 14). This method allows for the diffusion of both oxygen as well as off-gases at sufficiently high rates whilst also ensuring continuous sterility of the fermentation broth. Additionally, if other parts of the reactor are also fabricated from PDMS, handling of the fragile membrane then becomes very easy. Indeed, the membrane can be directly bonded to other PDMS elements, making the membrane an integral part of another reactor component.

Unfortunately, the membrane also allows for the diffusion of other molecules

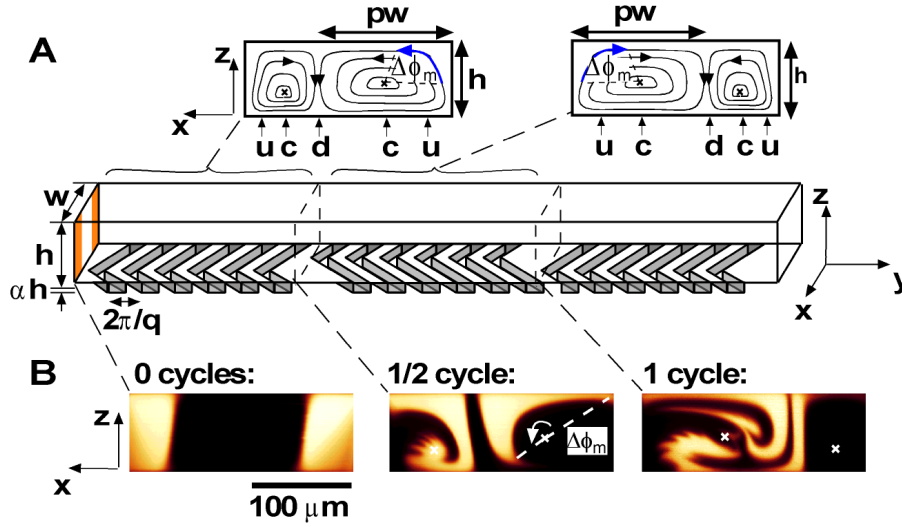


**Figure 2.4:** Effect of a passive mixing element (staggered herringbone mixer). One mixing cycle consists of two sequential regions of ridges; the direction of asymmetry of the herringbone switches with respect to the centerline of the channel from one region to the next (31)

such as water vapor out of the reactor (33). With evaporation rates on the order of  $5\ \mu\text{L}\cdot\text{h}^{-1}$  (water at  $37\ ^\circ\text{C}$  (10)), a  $100\ \mu\text{L}$  reactor would completely dry out after 20 h. Apart from increasing the concentrations of cells, substrate, and products in the remaining liquid, the gas bubbles that appear in the reactor due to evaporation may well disturb any online measurements in the microbioreactors, rendering them useless.

This, therefore, calls for solutions that either prevent or minimize the evaporation of water or rely on continuous replenishment of the evaporated volume. In most cases the first approach is utilized by placing the whole reactor into a humidified chamber, thereby reducing evaporation out of the reactor to negligible amounts (13). This, however, makes direct access to the reactor more difficult, and also requires that all connections to and from the reactor lead into the chamber. Another solution is to passively replenish the evaporated water by connecting an elevated water reservoir to the reactor, which places the reactor under a slight overpressure, as demonstrated in (13). Whenever water evaporates, the same amount automatically flows in from the elevated reservoir. This method efficiently keeps the water volume in the reactor constant, although it increases the risk of contamination too. Also, this solution is difficult to install if the cultivation needs to run continuously or in fed-batch mode, since it creates an input/output port with undefined characteristics. Therefore, in continuous or fedbatch operation, preventing evaporation instead of replenishing water seems to be the best solution.

### 2.3.3 Fluidics - pumping mechanism & connections

Fermentations can be run in a variety of operating modes, ranging from batch fermentations to fed-batch to continuous cultivations. Batch cultivations are (from the fluidic point of view) the easiest to handle as it is only necessary to cope with the evaporation of culture liquid. In continuous and fed-batch cultures, on the other hand, it is necessary to handle the evaporation and also to control the in- and outflow of liquid to the reactor. If passive replenishment of the evaporated water is used, then some kind of valve is needed to ensure that the inflow of fresh culture medium is not simply pushed out through the water replenishment port. On the other hand, if the evaporated water is to be replenished actively (e.g., with a pump), then the evaporation rate must be measured precisely, as any difference between the water replenishment rate and the evaporation rate will result in the dilution or concentration of the culture broth. For continuous culture microbioreactors (chemostat operation, constant reactor volume), the obvious solution is to control the water replenishment rate such that the liquid flow rate in the output equals the feed flow rate.

External syringes or peristaltic pumps are usually used to pump fresh culture medium (see Fig. 2.2 for an example) into the reactor, which then also passively (due to the fixed reactor volume) pushes the same amount of culture broth out of the reactor in the case of a continuous reactor with constant volume (14). This is an easy solution to use in the lab; however, it poses some problems with respect to parallelization. Using one pump for multiple reactors may be a solution, but this will lead to equal flow rates for all reactors unless more elaborate flow-splitting systems are used.

One solution is to use a system of micropumps and microvalves (23) operated by pressurized air (Fig. 2.5). This allows for individual flow rates for each reactor, but also requires a number of air connections (including switching and flow metering circuitry) for each reactor, which adds complexity to each reactor in terms of fabrication requirements and installation difficulty. This type of installation has only been applied in a perfusion reactor system (23), although there is nothing that fundamentally prevents its application to suspension systems.

Onboard micropumps have been investigated by various researchers (23; 34; 35); Lee et al. (11) also proved their applicability to fermentation microbioreactors by injecting minute amounts of acid/base into the reactor chamber. Micropumps can also be used as a driving mechanism for recirculation flow, thus making peristaltic or syringe pumps obsolete. The use of micropumps may on the one hand be an important cost-reducing factor, and on the other hand it also makes the multiplexing of microbioreactors much easier. This in turn would make mixing schemes without stirrer bars more attractive.

Fluidic connections between the macro and the micro world have been investigated in great detail, and these studies have spawned a large number of solutions (36). Though most of these solutions were generally intended to solve macro-to-micro world interfacing issues for microfluidic devices, some of them have been adapted (directly or with slight modification) to microbioreactor systems. For microbioreactors consisting of multiple PMMA-PDMS layers, fluidic connections are typically established on the solid layer (PMMA) of the reactor, as this allows for a defined fluidic interconnect. In the simplest approach, a needle that can be connected directly to a syringe or tubing is glued into a channel in a PMMA layer. Whilst this type of connection is easily established and only

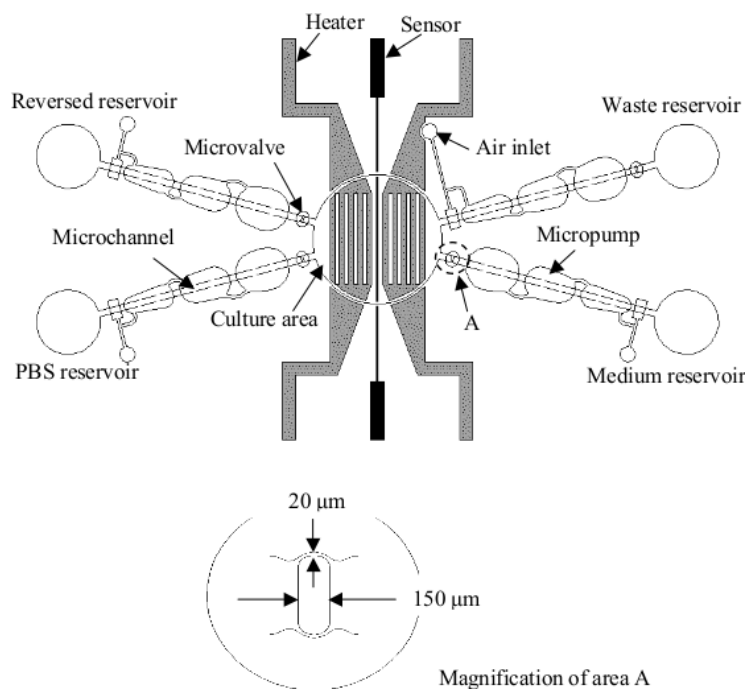


**Figure 2.5:** Schematic illustration of an automatic cell culture system. It consists of a cell culture area, four micropumps, four micro check valves, microchannels, reservoirs, two heaters and a micro temperature sensor (23)

requires material that is typically present in any laboratory, the disadvantage of this approach is that it only allows for connections in the plane of the PMMA layer (in most cases this is horizontal). Additionally, there is a significant risk of glue/epoxy seeping into the needle and thus clogging it.

A more advanced solution uses O rings embedded in a PMMA layer. Rigid tubes can be stuck through these (slightly too small) O rings, thus achieving tightness (37). This method allows for repeated plugging and unplugging of the connection in an easy manner. The connecting tube will then stand normally to the PMMA plane and can reach to any desired depth in the microbio reactor. It requires two sealing interconnects to make it tight: the surface between the tube and the O ring (mostly defined by how oversized the needle is), and that between the O-ring and the device itself (largely defined by the axial or radial space into which the O ring is pressed). This connection type obviously requires precise fabrication of the O rings and the corresponding PMMA layers and thus skilled fabrication personnel. If the reactor is designed to be placed into a holder or docking station, the fluidic tubes can be rigidly mounted on the holder. Surface-contact gaskets then seal between the holder and the clamped reactor (11). This solution is very elegant, although quite inflexible. As such, it is only applicable to systems that have fixed outer dimensions and fluidic connection locations.

A middle path can be pursued by using specialized connectors (e.g., from Lee, Upchurch, and Vici Jour) for a standard tube-nut assembly, as illustrated in Fig. 2.6. This type of connection has a very small and defined dead volume and may even provide a plug-and-play solution for fluidic connections of microbio reactor systems. It is, however, relatively costly.

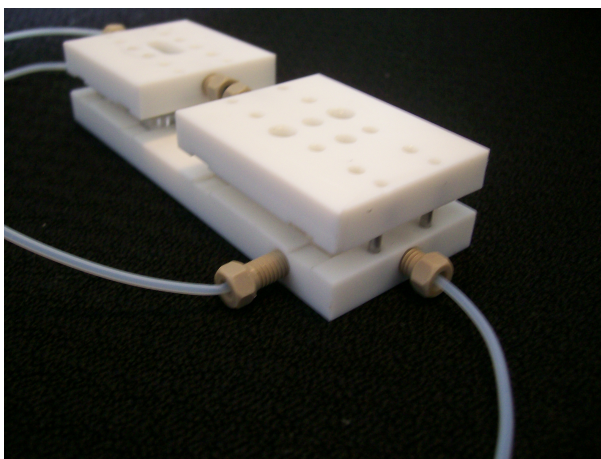


**Figure 2.6:** Fluidic connections with a standard tube-nut assembly mounted on a rigid part of the microbio reactor

Finally, for a PDMS-based reactor, the simplest solution would be to establish a needle-diaphragm interconnect where the needle is pushed through the PDMS itself, so that the contact pressure between the needle exterior and the enclosing PDMS then ensures adequate tightness (Fig. 2.7). This may offer an easy-to-use solution for microbio reactor systems, but misalignment or improper interconnect sealing may compromise the leak-free operation of the reactor. Additionally,

needles are not seen well upon by industry—mostly due to the risk of injury.

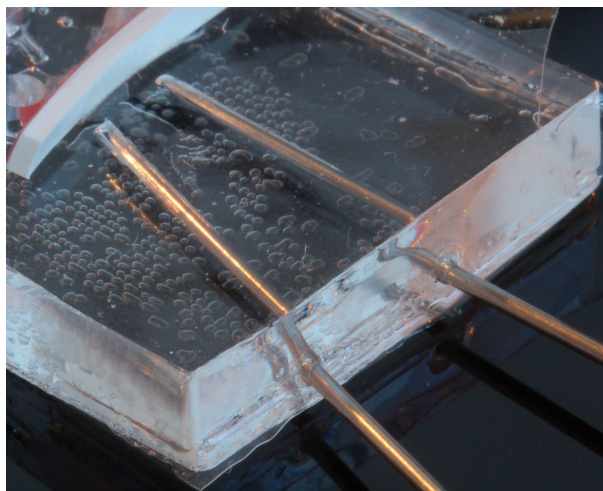


**Figure 2.7:** Needle-diaphragm interconnect where the needle is pushed through the PDMS layer into the reactor chamber

A system with a docking station would also be feasible for a reactor with a finalized design. In this case, the holder would also encompass needles that pierce the reactor material when the reactor is placed in the docking station. This kind of needles however should not pose major problems as the risk of injury is quite a bit smaller than with normal hand-held needles.

These systems all have their specific (dis)advantages and work fine in an appropriate lab environment, but they are seldom applicable to low-cost single-use systems due to either price or integration difficulties. Consequently, as yet there is no single state-of-the-art solution which solves most problems satisfactorily. However, Kortmann et al. (38) have recently proposed a clamping system for lab-on-a-chip devices that focuses primarily on the fluidic and electrical connections. A system of spring elements for each connection allows for precise adjustment of the sealing pressure. This system addresses many of the above-mentioned problems, and in the future it may well become the solution of choice for microbioreactors.

## 2.4 Sensing and control

While mass and heat transfer challenges must be resolved in order to enable fermentations, sensing (39) and control over the fermentation are also crucial to obtaining meaningful results. Indeed, the growth and production rates of the microorganisms usually depend strongly on pH and temperature. Control over these variables is therefore a requirement for performing fermentation experiments under relevant conditions that lead to high productivity. This part of the review therefore focuses on the key fermentation variables—temperature, pH, and dissolved oxygen—whilst also considering some other measurements that could greatly increase the amount of information per experiment.



### 2.4.1 Temperature

In microbioreactors, temperature is typically measured by means of thermistors or resistance temperature detectors (RTDs) (11; 12; 32; 40). Thermocouples are used in some setups (9; 10; 13; 14). RTDs are sensors that have a resistance that varies according to the temperature; RTDs made from platinum are preferably used (e.g., Pt 100 or Pt 1000 sensors; these have nominal resistances of 100 and 1000  $\Omega$  at 0 °C, respectively) (41). RTDs are very cheap and are commercially available in bulk quantities. Since they are mass-fabricated for many industries in relatively small sizes (5x2x1.3 mm), this type of sensor can easily be embedded into a microbioreactor to precisely measure the temperature of the microbioreactor content (40). They are fairly accurate (to 0.1 °C) (42), and are able to operate reliably for long periods of time (40). Moreover, RTDs can also be connected to an external circuit with connecting lead wires or wire bonded onto a printed circuit board for online temperature measurement and control (12; 42).

Such features are crucial to parallel operation at various operating temperatures. Ideally, for precise temperature measurement, the temperature sensor should be located close to the microbioreactor chamber. However, in several cases it was reported that temperature was measured at other parts of the setup. Lee et al. (11) controlled the temperature of the microbioreactor by measuring the temperature of the base plate holding the microbioreactors. Vervliet-Scheebaum et al. (43) integrated the Pt 100 sensor into a flow-through measuring device to measure the temperature of the liquid that was circulating in the microbioreactor system. Zanzotto et al. (9), Szita et al. (13), Boccazzi et al. (10), and Zhang et al. (14) measured the temperature of the circulated heated water that was used to control the temperature of the microbioreactors or that of the enclosing chamber.

Whilst temperature measurement is relatively easy to achieve in microbioreactors, temperature control is a rather challenging task due to the high surface area to working volume ratio ( $S/V$ ). For instance, a conventional bench-scale bioreactor with a height-to-diameter ( $H/D$ ) ratio of 2 would have an  $S/V$  ratio of about 0.9 (44). In contrast, microbioreactors with a chamber diameter of 10 mm and a height of about 2 mm would give a  $S/V$  ratio of about 1500 (14). This implies that heat transfer in microbioreactor systems is large and very rapid compared to conventional systems. One also needs to bear in mind that heat loss by natural convection is significant and inevitable when working at such a small scale. Another factor that affects the efficiency of temperature control in microbioreactors is the location of the heating element. It is necessary to place the heating element in a position where it will not create a large temperature gradient (40). This is particularly important for microbioreactors fabricated from PMMA and PDMS, because these materials have very low thermal conductivities of about 0.2 W·m<sup>-1</sup>·K<sup>-1</sup> (45) and 0.17 W·m<sup>-1</sup>·K<sup>-1</sup> (46), respectively.

Temperature uniformity in the microbioreactor chamber is another critical issue when establishing a good temperature control system for a microbioreactor. There are several techniques that can potentially be used to probe temperature uniformity in the reactor chamber. First, one could place several temperature sensors at different spots within the reactor chamber to evaluate the temperature distribution. Second, thermal distribution patterns in the reactor chamber

can also be examined by monitoring heat images using a thermo or infrared camera (47; 48). Finally, based on a model describing mass and heat transfer in a microbioreactor, one could also opt to simulate a three-dimensional (3D) temperature distribution profile in the reactor chamber using, for example, the finite element method (14; 40), which is now a standard engineering tool implemented in several software packages. As a rule of thumb, however, one should, in our opinion, assume that a mixing system that can keep cells in suspension will also provide for adequate temperature uniformity.

Several alternatives are available to efficiently control the microbioreactor temperature. The simplest method is to conduct the experiment in a temperature-controlled room (43) or in an incubator (49). Vervliet-Scheebaum et al. (43) reported that the temperature variation can be kept to within 1.5 °C of the desired set point in a temperature-controlled room. Although the temperature can be accurately controlled with this method, and allows for the operation of many microbioreactors in the same space at the same temperature, it is of course not feasible for the parallel operation of microbioreactors at different operating temperatures, such as when screening for the optimal growth temperature of a strain.

Another option is to link the device to a water bath and circulate thermostated water through the microbioreactor chamber base (9; 10; 13; 14). The main drawback of this method is the limitation it imposes on the parallel operation of reactors at different temperatures. Also, the additional fluidic system increases the risk of a liquid leak leading to failure of the temperature control system.

Temperature control in microbioreactors can also be accomplished by integrating electrical microheaters (11; 12; 40; 42). Maharbiz et al. (12) and Krommenhoek et al. (42) incorporated a microheater onto a printed circuit board that was adhered to the base of the microbioreactors. The microheater was positioned next to the thermistors such that tight temperature control of the microbioreactor content could be achieved. Lee et al. (11) implemented a commercially available on-off controller (Minco, Fridly, MN, USA, CT325TF1A5) to control the temperature of the base plate that served as the microbioreactor holder. The microbioreactor temperature was controlled by maintaining the temperature of the copper base plate at a constant level using a foil heater. Petronis et al. (40) embedded two electrode heaters into the side walls of the microbioreactor chamber to create an even heat distribution across the chamber.

Having an integrated heater in the microbioreactor setup is by far the most preferable method of temperature control in microbioreactors, as it is simple and cheap and allows for parallel operation at different temperatures, provided that some thermal insulation preventing thermal crosstalk is in place. However, as the reactor chamber is not thermally insulated, the high  $S/V$  ratio makes a well functioning temperature control loop necessary.

### 2.4.2 pH

Standard pH probes are too bulky and are not feasible for use in microbioreactors. The most commonly applied miniature pH sensors are optical sensors based on fluorescence sensor spots (Fig. 2.2) or ‘optodes’ (9; 10; 13; 14; 41; 50; 51) and solid-state, ion-sensitive, field-effect transistor (ISFET) pH sensor chips (12; 17; 42; 52). Many microbioreactor operators seem to prefer the optical sensors due to their noninvasive nature and ease of integration (9–11; 13; 14; 29; 53).



Since optodes do not require any reference element to perform pH measurements and are relatively cheap (EUR 15 per piece), they are good alternatives for disposable microbioreactors (9; 10; 13; 14).

Optical sensing is performed through either fluorescence intensity or fluorescence lifetime measurements (9; 10; 13; 14; 53). However, the fluorescence sensor spots suffer from the photobleaching effect, reducing their lifetimes, and have a rather narrow dynamic pH range, typically 2–4 pH units (53). Lifetime would not be an issue for single-use reactors as the reactor packaging could be light-proof and the cultivation itself typically does not run long enough for this to be an issue.

Optical pH sensors have a measurement accuracy of about 0.01 pH units with a response time ( $t_{90}$ ) of less than 90 s. Furthermore, the operating temperature for optodes ranges from 0 to 50 °C. Most pH sensor spots have a measurement range from pH 4 to 9 and a nonlinear response (53). This nonlinearity is apparent as a low sensitivity of the sensor signal to pH changes at both ends of the measurement range, which makes pH control there very difficult. In the middle of the measuring range, the sensor spots have an almost linear response, with a sensitivity of around 10° phase angle per pH unit.

In contrast, ISFET pH sensors cover a wider pH range (typically from pH 2 to 12 (54)) and have a linear response that is similar to that of a standard pH probe (Nernstian sensitivity of about 58.2 mV per pH unit at 20 °C (54)). ISFET pH sensors have a measurement accuracy of about 0.01 pH units with response time ( $t_{90}$ ) of less than a second. They can also work across a wide temperature range (-45 °C to 120 °C). Though ISFET pH sensors have a broader dynamic measurement range and greater sensitivity than pH sensor spots, the ISFET pH sensors also have some drawbacks. This includes measurement drift (linear and reproducible in due course, thus allowing for data compensation) and sensitivity to surrounding light (12; 17; 54). Moreover, the ISFET pH sensor chip requires a reference electrode (i.e., Ag/AgCl reference electrode) to perform the pH measurement (12; 17; 42), meaning that the microbioreactors have to be designed such that the part with the integrated ISFET pH chip is reusable in order to keep the cost per microbioreactor at an acceptable level. Practically, this is typically done by encapsulating the ISFET pH sensor chip on a printed circuit board before integrating the pH sensors into the microbioreactors (12; 17; 42).

Despite some limitations, both sensors have been shown to provide rapid and precise pH measurements over a long period of time (9–14; 17; 29; 42; 51–53). It can thus be concluded that real-time pH measurement in microbioreactors, similar to the pH monitoring feature of lab-scale bioreactors, is fully feasible.

While a number of reliable pH sensors are available for online monitoring of pH, pH control in microbioreactors is still in the development phase. Early attempts to control pH in microbioreactors were accomplished by either a buffered system (9; 10; 13; 14; 43) or by intermittently injecting base or acid (11; 15; 29; 42). The use of buffer to control pH in microbioreactors is the simplest way of controlling pH. Nevertheless, the use of a buffered system is not always sufficient to maintain a constant pH level: pH buffers have a limited buffering capacity and can only compensate for a certain number of ions before losing their resistance to pH changes. This limitation was apparent in a stirred, membrane-aerated microbioreactor study where the pH dropped by nearly 2 pH units due to acidification during the fermentation process (9). The limit on the buffer capacity

can, however, be extended in a continuous culture microbioreactor system. Wu et al. (55) showed in a perfusion reactor system that continuous feeding of a freshly buffered nutrient medium enabled the reactor pH to be kept constant to within  $\pm 0.02$ . It is expected that a similar effect would be visible in a continuous culture microbioreactor with cells in suspension, assuming that the buffer strength is adapted to the substrate concentration.

Intermittently injecting base or acid is another alternative approach to pH control in microbioreactors. It is a direct adaptation of a bench-scale bioreactor pH control method. Zhang et al. (29) and Lee et al. (11) showed that the decrease in the pH value due to the metabolic activity of the growing microorganisms can be compensated for by intermittently injecting a base solution. Lee et al. (11) managed to reach higher cell densities when the pH was maintained for a longer period at the desired set point. However, this method is limited by the microbioreactor chamber volume. The addition of an excessive volume of acid or base dilutes the culture broth, which leads to uncertainties in concentration measurements (15). A strong base (or acid) can be used to reduce the added volumes, but this may lead to local high (or low) pH values, particularly if mixing is poor. Such pH deviations can locally stress the growing cells, leading to lower average growth rates for the cultivation as a whole.

A solution to this problem would be gaseous pH control, the practical feasibility of which has been proven by Isett et al. (50), and it has been implemented in an industrial system (56) in a 24-well 4–6 mL plate where  $\text{NH}_3/\text{CO}_2$  are sparged through the individual wells. Maharbiz et al. (12) developed an in situ electrolytic gas generation where  $\text{CO}_2$  gas can be precisely dosed from underneath the reactor chamber through a thin, semi-permeable silicone membrane. However, Maharbiz et al. (12) are yet to test the effectiveness of  $\text{CO}_2$  gas generation for pH control with a real culture. The method applied seems promising, but the formation of bubbles due to gas diffusion is not desirable in microbioreactors. De Jong (17) demonstrated that the pH of a *S. cerevisiae* fermentation can be controlled by dosing  $\text{CO}_2$  gas and  $\text{NH}_3$  vapor. However, this method needs further development, as the microbioreactor that was fabricated had poor mixing and the response time with respect to pH control was rather slow (the pH took several hours to return back to its desired set point). Although both Maharbiz et al. (12) and De Jong (17) are yet to optimize their methods, they have certainly underlined the potential of introducing gases through a membrane to control pH in microbioreactors.

### 2.4.3 Cell concentration

In microbioreactor experiments, one typically uses the Lambert-Beer absorption law (57) to estimate the cell density in the microbioreactors online via an optical measurement. The absorbance measured is normally correlated to either the dry weight or the number of cells per volume. This enables the visualization of the cell growth in real time. An online system is necessary because sampling is typically not possible in such small working volumes, and analytical techniques other than optical density (OD) measurements are difficult to apply.

Online monitoring of the cell density in microbioreactors is normally realized via optical probes (Fig. 2.2). Light from light-emitting diodes (LED) is guided into the microbioreactors with optical fibers, sent through the reactor chamber, and then guided to a photodetector (9–14). The wavelength for microorganisms

is normally chosen to lie within the range of visible light (400–700 nm); for example, *S. cerevisiae* has traditionally been measured at 600 nm. Many state-of-the-art microbioreactors implement this technique for OD measurements (9–14). Most devices send in light from the bottom of the reactor and collect the transmitted light at the top (9; 10; 13; 14), although one device works the other way round (11). In either case, the resulting path length is in the range 0.3–2 mm. Optical fibers for OD measurement can also be positioned on the side of the microbioreactor chamber, resulting in a horizontal optical measurement path. This approach can provide a longer optical path length because the lateral dimensions of microbioreactors are normally larger than their heights. This can be useful for improving the measurement accuracy when operating at low biomass concentrations.

The fixation of the optical fibers in the microbioreactor is important as it determines the accuracy and sensitivity of the OD measurement. Misalignment of the fibers will lead to a loss of transmitted light which will hinder the measurement. The OD measurement depends on both the path length and the intensity of the incoming light, where both parameters can be adjusted individually. A shorter path length will allow for the measurement of higher-density broths, as will more intense illumination, and vice versa. Depending on the mixing method chosen, care must be taken to avoid collisions between, for example, the mixing bead(s) and the fibers. In the case of single-use reactors, care must be taken to ensure that the fibers can only be attached to/inside the reactor at one single defined position, as variations here will change the measured absolute values of transmitted light, which in turn will make calibration necessary for every single reactor.

Though OD measurement via optical probes has proven to be the most feasible way of estimating cell density in microbioreactors, gas bubbles in the reactor chamber can interfere with OD measurements. OD measurement via optical probes is also sensitive to ambient light, but this can be circumvented by utilizing modulated light or by filtering the OD signal using a lock-in amplifier. It is also important to mention that the OD measurement measures the total cell concentration, since it cannot distinguish viable cells from dead cells.

Near-infrared technology (NIR) also allows for the online optical measurement of cell concentration (58). As a complete NIR setup is expensive and requires elaborate signal processing, industrial NIR turbidity measurement systems are now available (59) at a reasonable price, although they are still significantly more expensive than a simple transmission measurement system.

Alternatively, cell density can also be estimated in microbioreactors by means of impedance spectroscopy, as proposed by Krommenhoek et al. (42; 54). This method, which is commonly applied to larger-scale reactors, applies an alternating current (AC) electrical field to the culture and measures the cell conductivity as a function of frequency. As only cells with intact membranes are able to polarize charge and hence contribute significantly to the conductivity, this method only measures live cells. Krommenhoek et al. (42; 54) integrated this impedance sensor onto a multi-sensor chip and placed it underneath the microbioreactor chamber to measure biomass concentration. Here, the lowest biomass concentration that can be measured is  $1 \text{ g} \cdot \text{L}^{-1}$ , which corresponds to a relative conductivity change of about 0.1%.

### 2.4.4 Dissolved oxygen concentration

Oxygen is one of the substrates in an aerobic fermentation. Thus, it is crucial that this variable is controlled properly to prevent oxygen-limiting conditions during the fermentation process (5). In industrial-scale fermentations, the dissolved oxygen concentration is normally controlled, often even with dynamic set point profiles during, for example, fed-batch operation. Providing a sufficient oxygen supply in microbioreactors is a challenge due to the low solubility of oxygen in water, which is only worsened by laminar flow and difficult mixing circumstances. To supply sufficient oxygen in a bubble-free system, a high interfacial area is required in order to improve the interfacial mass transfer area to volume ratios of the microbioreactors (9; 11; 60). Luckily, the high  $S/V$  ratios of microsystems can provide a large interfacial area. Still, efficient transport of oxygen-rich fermentation broth away from the membrane is also important, and can be achieved by providing sufficient mixing (see above). Another method of achieving sufficient oxygen supply is to increase the  $O_2$  content in the gas phase, as this will significantly increase the saturation concentration of oxygen in the fermentation broth.

The dissolved oxygen concentration in microbioreactors is typically measured by optical sensors (Fig. 2.2) with the use of fluorescence sensor spots (9; 10; 13; 14; 29; 49). Optodes for dissolved oxygen are based on the quenching of fluorescence by oxygen (61). Even though they can work for the entire range of saturation values, from 0 to 100%, their sensitivity is optimal at low concentrations (61), which is the relevant range for fermentations. Just like the optodes for pH measurement, they can be manufactured in small sizes, are easy to integrate, insensitive to ambient light, relatively cheap, and nonreactive. Using these oxygen optodes, microbioreactors can also be made disposable (9–13).

The dissolved oxygen concentrations in microbioreactors can also be measured by an electrochemical sensor such as the ultra-microelectrode array (UMEA). The UMEA is an amperometric biosensor and measures oxygen concentration based on the electrochemical reduction of oxygen (42). Its working principle is similar to that of the Clark oxygen electrode (5). Such a sensor has been used in a bench-scale reactor cultivation of *Candida utilis* (42). The sensor delivered results that were very similar to those of the reference sensor. It is small enough to fit into a 96-well plate, which clearly makes it a candidate for implementation in a microbioreactor system.

For microbioreactors with a low working volume (e.g., 50–300  $\mu\text{L}$ ), where bubbles are not desirable and bubble sparging is therefore not feasible, oxygen supply is often achieved by membrane aeration. Several strategies have been developed for the oxygenation of microbioreactors. Maharbiz et al. (12) developed in situ electrolytic gas generation to supply oxygen into a microwell-based microbioreactor. Oxygen was allowed to diffuse into the reactor chamber through an orifice that was laminated with a thin gas-permeable membrane. With this method, oxygen transfer rates as high as 40  $\text{mmol } O_2 \cdot \text{L}^{-1} \cdot \text{h}^{-1}$  can be achieved. For comparison, values of up to 200  $\text{mmol } O_2 \cdot \text{L}^{-1} \cdot \text{h}^{-1}$  have been reported for bench-scale reactors (59). However, since the system of Maharbiz et al. (12) was aerated from the bottom of the reactor chamber, the aeration membrane bulged upward due to positive pressure from the electrolysis chamber. Furthermore, there was immense bubble formation in the system because the magnetic beads used for mixing were not strong enough to break the bubbles forming on the

aeration membrane surface. Implementing a mixing system that more efficiently scrapes the bubbles from the membrane surface may in this case alleviate the formation of large bubbles.

Alternatively, aeration in microbioreactors can also be achieved by integrating a gas-permeable membrane into the top side of the microbioreactor chamber (9–11; 13; 14; 29). In this method, the gas stream is typically pushed into a gas chamber which is separated from the reactor contents by a thin PDMS membrane that allows the diffusion of small molecules from the gas phase (e.g., oxygen) into the liquid phase. Since diffusion is merely based on surface aeration, no bubbles were observed in the reactor chamber. The standard measure of the oxygen transfer efficiency is the volumetric oxygen transfer coefficient  $k_La$  [ $\text{h}^{-1}$ ], which is composed of the mass transfer coefficient  $k_L$  [ $\text{m/h}$ ] and the interfacial area  $a$  [ $\text{m}^2/\text{m}^3$ ].

Islam et al. (62) compared the oxygen mass transfer coefficients in five different volumes ranging from microwell plates to 75 L stirred-tank reactors, and then performed cultivations at matching  $k_La$  values. For high  $k_La$  values ( $247 \text{ h}^{-1}$ ), they report very similar fermentation kinetic profiles and yields across scales, and actually identify  $k_La$  as being one of the most important factors during scale-up. Zanzotto et al. (9) developed a microbioreactor with a shallow reactor chamber ( $300 \mu\text{m}$ ) to shorten the diffusion distance (distance from the gas-liquid interface to the bottom of the reactor chamber). In their design, a  $100 \mu\text{m}$  thick PDMS membrane was bonded onto the top of the reactor chamber for oxygenation. The  $k_La$  obtained in the Zanzotto et al. (9) microbioreactor is, however, rather low ( $k_La \approx 72 \text{ h}^{-1}$ ), as a comparison with larger-scale reactors shows (4). This is because no active mixing scheme was realized and oxygen transfer was based merely on the diffusion of air from the atmosphere. On the other hand, Lee et al. (11) demonstrated that, under perfect mixing conditions and tight oxygen control, a  $k_La$  value as high as  $500 \text{ h}^{-1}$  could be achieved in their microbioreactors. They implemented a proportional-integral (PI) control algorithm to control the dissolved oxygen concentration in the microbioreactors. They also showed that oxygenation at various oxygen concentrations or with compressed air coupled to integrated peristaltic mixing tubes can accurately maintain the dissolved concentration at a set point that is up to about 30 to 40% of the saturation value.

### 2.4.5 $\text{CO}_2$

In bench-scale reactors, the  $\text{CO}_2$  content in the off-gas is often measured. However, the amounts of off-gas produced in a microsystem are very small, which makes another type of sensor necessary. Ge et al. (63) and Liebsch et al (64) have implemented an optical and thus noninvasive  $\text{CO}_2$  sensor based on a fluorescent dye applied onto a silicone membrane. Similar sensors spots are also available commercially (PreSens, Germany); these use sensing equipment similar to the above mentioned dissolved oxygen and pH spots.

### 2.4.6 Spectroscopy

Spectroscopy may provide the means to estimate the concentrations of various analytes, such as glucose, acetate, and lactate, with online optical methods. These systems measure a whole wavelength spectrum for one single measure-

ment. Appropriate signal processing and the evaluation of the data with chemometric models then allow the analyte concentrations to be estimated. These basic characteristics make these measurement systems interesting but they also make their application more complicated. Each measurement system, such as near-infrared (NIR) (58; 65) or Raman spectroscopy (66–68), has its own advantages and disadvantages that must be evaluated with the specific application in mind. Raman spectroscopy, for example, is advantageous due to the low interference from water and the flexibility in choice of wavelengths (66), but it is more expensive and more laborious than NIR, which is a more well-developed technique for fermentation (58; 65).

## 2.5 Discussion

The construction and operation of well-controlled microbioreactors have been demonstrated, and there is a great potential for their application within process and strain development labs in the fermentation industry. With the increasing drive towards a bio-based economy where bioresources are replacing hydrocarbons as feedstocks, harnessing microorganisms for chemical and energy production becomes more important. In the US, the market share of bio-based chemicals is expected to grow from 5% in 2002 to 12% in 2010, and this growth is expected to continue at a significant pace (69). Furthermore, a recent vision paper published by the Industrial Biotechnology section of the European Technology Platform for Sustainable Chemistry (70) foresees that up to 30% of the raw materials used by the chemical industry will originate from renewable sources by 2025.

In every industrial biotechnology process, strain improvement programs for increased yields and volumetric productivities are crucial to economical viability. High throughput screening is needed to identify interesting, improved production strain candidates among a large number of mutants. Microbioreactors provide an interesting alternative to the shake flasks or microtiter plates commonly used for screening today. They allow for the continuous measurement and control of various fermentation variables, such as pH or dissolved oxygen, which are not that straightforward in shake flasks or microtiter plates. Thus, establishing suitable control loops on the microbioreactor platform implies that the conditions in the microbioreactor will be much more similar to those in larger-scale operations than they presently are for experiments in standard shake flasks or microtiter plates. Another area of application for microbioreactors could be investigations of process and media optimization, where a range of conditions can be tested in less time and at a lower cost in microbioreactors than in shake flasks or bench-scale reactors.

In order to be able to apply them to the abovementioned applications, microbioreactors must be disposable, cheap, allow for tight control over the fermentation, and give results that are upscalable. If all of these conditions can be fulfilled, microbioreactors will undoubtedly be used as standard experimental platforms for fermentation research in the future. As mentioned before, cost reductions should be obtained on the one hand through the considerable reduction in size and on the other hand through the use of polymer materials and established polymer processing methods to construct disposable reactors.

As shown in this review (Table 1), many enabling technologies for this vision



of a single-use reactor already exist. The most important culture variables—temperature, pH, cell density, and dissolved oxygen content—can be readily measured at the micro scale using methods that are both noninvasive and disposable. One future area of research should be to extend the measurement ranges of sensor systems that already exist; pH is the most obvious example. Most cultivations of yeast and filamentous fungi are currently run at pH 4–6, which corresponds to the range where pH optodes are rather insensitive. pH sensors that can cover the full range needed for cultivations at a cost similar to that of pH optodes would greatly increase their applicability and usage.

It should be emphasized once more that control over the fermentation conditions is of crucial importance to the future acceptance of microbioreactors as a useful and versatile experimental platform. Methods for controlling temperature, pH, and dissolved oxygen in microbioreactors (11; 12; 15; 29; 40; 42; 50) do exist, and it has also been demonstrated that several control loops can be combined in a single microbioreactor (13), such that the experimental work in microbioreactors can be performed under culture conditions that are fully comparable to cultivation conditions in bioreactors that operate at industrially relevant scales. However, in comparison to bench-scale reactors, the limited ability to manipulate essential reactor variables within the small working volume typical of microbioreactors is an engineering challenge, and therefore continued research on the implementation of simple but well-functioning control loops in microbioreactors is a must.

At this point, the capabilities of microbioreactor technology could be extended further by including substrate feeding control strategies (71), such that, for example, advanced feeding strategies typical of fed-batch operation (72; 73)—the most widespread mode of operation for industrial fermentations—could be investigated at the micro scale. It should also be kept in mind that the integration of all these control loops into a limited reactor volume will be a continuous challenge, and typically a tradeoff will have to be made between the ability to control many variables in the microbioreactor and the need to keep the cost per reactor at an acceptable level.

Provided the reactor design is in place, the next important step is to prove that the results are scalable. Only if the results of, for example, a ranking experiment in the microbioreactor can directly be transferred to bench-scale or even full-scale reactors will the system be a valid candidate for industrial applications. A number of articles already report that results obtained in microbioreactors compare well to results obtained at larger scales (9; 74). Future research should maintain its focus on this topic, since the acceptance of microbioreactor technology as a useful and versatile experimental platform will need the support of successful examples where scalability of results has been demonstrated convincingly.

Also interesting from a scalability perspective is the incorporation of additional sensors that provide more information on the metabolism or microorganism performance than achieved with standard sensors. As mentioned above, spectroscopic methods provide an appealing option since biomass, substrate, and product concentrations may be determined. Interestingly, for aerobic fermentations, the implementation of spectroscopic methods may be easier in microbioreactors with bubbleless aeration than in bench-scale reactors, where sparging of gas bubbles disturbs the measurements.

Other interesting sensors are lab-on-a-chip devices for biosensing different bi-

ological molecules such as DNA, proteins, or small molecules (75). Assuming that a few relevant biomarkers that are correlated to the stress level or production level of the cells can be identified for a certain process, the inclusion of a chip analyzing these biomarkers in the microbioreactor design would provide detailed insight into the performance of the strain. This would open up the possibility of gaining in-depth knowledge about the process strain behavior in microbioreactors, and would thus provide valuable information for scaling up.

Clearly, parallelization is also an important issue. In order to be able to run high throughput experiments (e.g., comparing different culture conditions or strains), parallelization is a necessity. This not only requires the potential for parallel sensing, but ideally it also demands an infrastructure that enables the reactors to be run under different conditions (e.g., pH or temperature). Whilst some researchers and companies (12; 13; 50; 56; 68) have proven the basic feasibility of multiplexed reactors, current systems do not actively support full control over different operating conditions. For example, temperature may be the same for all reactors (13), or either pH or DO can be controlled, but not both together (56). Additionally, current systems normally do not allow for continuous operation.

One major criterion here is the separation of ‘fixed machinery’ from ‘single-use reactor’. Or in other words, questions of major importance in microbioreactor design include: how many sensors, actuators, etc., should be included in the reactor itself? What should be included in the supporting machinery? How should the interfaces be established? The answers to these questions greatly impact on the reactor design, as well as on the microbioreactor operating cost per fermentation experiment in particular. Current systems usually solve the sensing question by including fluorescent sensor spots in every single reactor well, and then use one single measurement/evaluation unit for every measurement type (e.g., DO, pH, etc.) (13; 56). This measurement/evaluation unit is then sequentially applied to the individual wells (see Fig. 2.8 for a practical example). This of course calls for some machinery and/or electronics that can precisely position the sensor onto the fiber or switch from well to well in some other manner. However, with modern robotics this is a minor obstacle.

Controlling pH and DO for every individual well calls for either an elaborate system of tubes and valves, or again for a suitable positioning mechanism—in this case for a dosing system—that also ensures adequate tightness. Individual temperature control of every well obviously requires a heating system in every reactor well. Possibly a general minimum temperature could be adjusted atmospherically such that the individual wells only have to be heated to their individual destined temperatures. This necessitates an incubator-type enclosure, but makes the temperature easier to control due to the lower thermal losses.

In order to make the whole microbioreactor system as cheap as possible, the system should be flexible; in other words, it should only seek to satisfy the requirements of each individual application (e.g., to only provide pH control if it is needed), as stripping out unnecessary features significantly reduces the complexity of the system.

Whilst one focus must be the complexity and thus cost of the system, the other should be the ruggedness and ease-of-use required in industrial applications. As current systems (56) prove, it is possible to reduce the complexity enough to allow the fabrication of a convenient system. Further work here may be directed at downsizing and providing more individual control over every reactor.



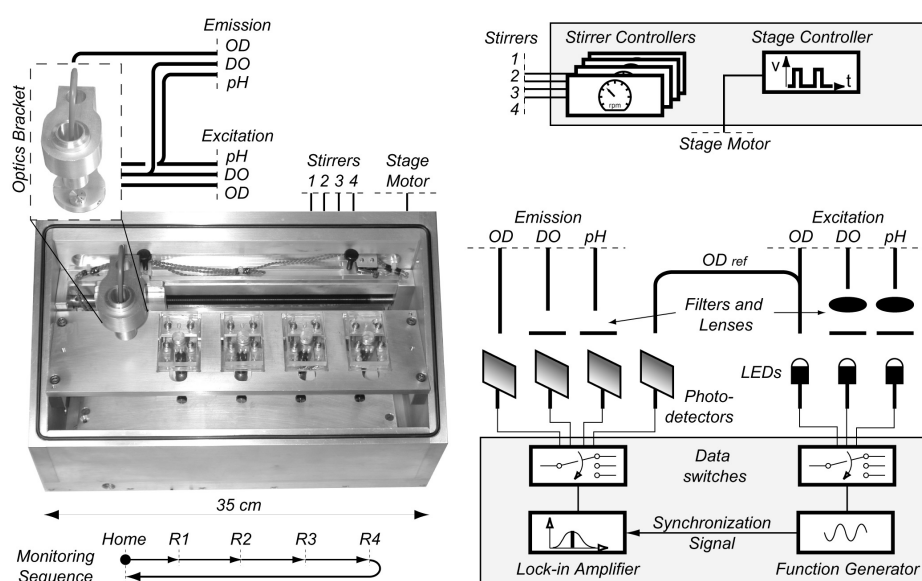


**Figure 2.8:** Multiplexed microbioreactor setup with four stirred microbioreactors, indicating sequential measurements of OD, DO, and pH (13)

Last but not least, the importance of software aspects should not be underestimated. If a microbioreactor platform is employed to acquire real-time experimental data via cheap and high-throughput experimentation under well-controlled conditions, an immense amount of data will be generated. The trend here is for the amount of online data generated for each cultivation to increase in the future; for example, when online spectroscopic methods are implemented on the microbioreactor platform too. Handling such data does not pose any problem in terms of computing power or data storage capacity. It should be emphasized though that manual processing of these data is simply not an option. Instead, microbioreactor platforms should be supported by advanced software for online visualization and interpretation of the online data. Perhaps most importantly, the software will need to allow for the efficient storage, retrieval, and documentation of experimental data so that the user can work efficiently with a microbioreactor setup. This documentation functionality is also especially relevant to process development in the pharmaceutical sector.

In addition, existing algorithms relying on multivariate statistical methods should, for example, be implemented as standard to keep track of the state of the fermentation experiment (76); ideally, abnormal situations should be detected and logged so that this type of information can be presented to the experimentalist in a condensed form for each experiment. Spectroscopic data—which will also be standard microbioreactor measurements sooner or later—will need to be converted to useful estimates of the analytes of interest in an online fashion, meaning that chemometric methods will have to be implemented in the software as well. Last but not least, online data can be further enhanced by making use of software sensors to estimate important cultivation parameters that are otherwise difficult to measure online. For example, a software sensor

application was recently developed to detect physiological stress in the growing cells (77).

## 2.6 Conclusions from the literature review

A review of existing microbioreactor technology confirms that microbioreactors can be applied for fermentation experiments under well-controlled conditions of pH, temperature, and dissolved oxygen concentration. The use of polymer materials to construct microbioreactors results in cheap and disposable (single-use) reactors that are ideally suited to fermentation screening experiments. For microbioreactors to become generally accepted in the fermentation industry, future research should focus on: (1) the further development of cheap and disposable online sensors, including extending the usable range of existing sensors such as pH optodes and extending the number of variables that can be measured online; (2) the implementation and demonstration of controlled substrate feeding strategies in microbioreactors, similar to fed-batch operation at the industrial scale; (3) scalability, in other words, the ability to transfer experimental results obtained in microbioreactors to pilot or production scale for a broad range of microorganisms; (4) parallelization, or more specifically the development of smart technical solutions to perform a series of experiments under different conditions in a range of parallel microbioreactors; (5) software to support the documentation of experiments and to handle the storage, online interpretation, and retrieval of the massive amounts of experimental data generated by parallel cultivations.

## 2.7 Goals of the PhD project

The aforementioned conclusions set the framework for the scope of this PhD thesis—the development of a reactor that can sustain continuous cultivations is the very first step and also the basis for the focus points mentioned above. Thus, the requirements for the microbioreactor (Fig. 2.9) are

- disposable (low price and easy fabrication) microbioreactor with an operating volume of approximately 100  $\mu\text{L}$ ,
- easy handling which results in few operating errors,
- capability to run batch or continuous cultivations, thus longer-term (e.g. 1–2 weeks) operation which requires flow of fluids and also evaporation control,
- efficient mixing which not only equally distributes e.g. nutrition and air, but also keeps nonmotile cells such as *S. cerevisiae* in suspension,
- bubble-less aeration of the culture broth, e.g. through a membrane,
- temperature control of the broth,
- measurement (and possibly control) of dissolved oxygen in the cultivation broth,
- measurement of the cell density in the broth,

- measurement and control of pH,
- automated system for measurement, control and recording of data.

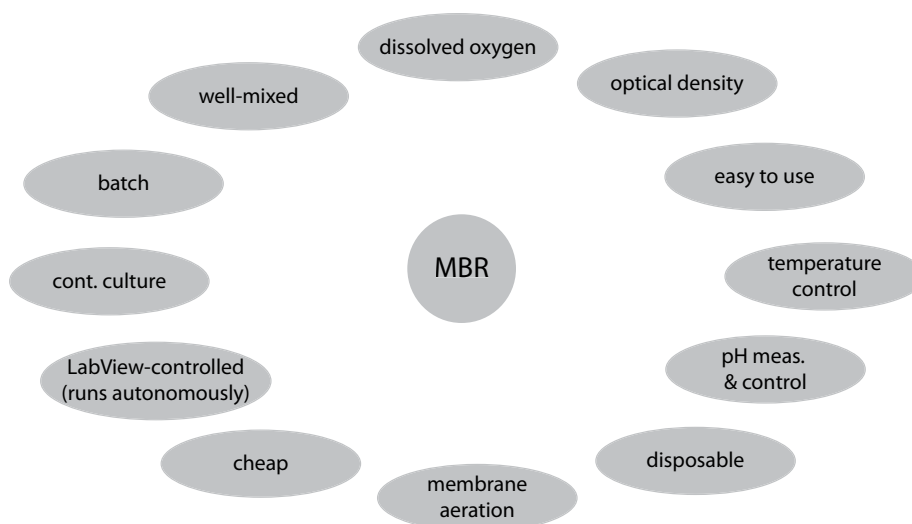


**Figure 2.9:** Components that have to be established in order to be able to reach the goal of the PhD project.

All of the above points have to be fulfilled in order to have a functioning microbioreactor—already one single subsystem which does not work satisfyingly will cripple the operation of the whole reactor. Additionally, the whole handling procedure—such as e.g. ‘how does one inoculate?’—which is well known for larger-scale reactors has to be adapted and tested such that microbioreactor cultivations can be set up reliably and reproducibly.

The correct functioning of the microbioreactor is to be tested by comparing cultivations in the microbioreactor with cultivations in larger scales, e.g. shake flasks or bench-scale reactors. Ideally, the two scales should give the same results e.g. when comparing growth rates; If not then both the reason(s) and the ‘transformation laws’ for the differences have to be known. Comparison of maximal growth rates could e.g. be achieved by creating wash-out curves in the different scales.

The next test is then to run ranking tests where the productivity e.g. of a certain enzyme is tested and ranked for different strains. Ideally, the ranking produced in the microbioreactor cultivations should be the same as that achieved in bench- or industrial scale reactors.

# Microbioreactor Design Considerations and their Implementation

---

As shown in the introduction, the field of microbioreactors is a wide one where the final solution both depends on the requirements to the specific product and the preferences of the designer. There is no single obvious ‘best’ solution—all the implementations of the subsystems have their own inherent advantages and drawbacks which also might influence each other. As in multiparameter optimization theory there is the possibility that several technically different solutions have a similar overall ‘goodness’, but many of the drawbacks of the chosen solution may first manifest themselves in operation. So, one possible candidate design has to be chosen, fabricated and operated in order to be able to evaluate its performance.

This chapter is dedicated to describing the reactor solution that evolved in the course of the past four years along with the considerations and the details of the various sub-solutions chosen. I briefly review what has been done in this specific part of the microbioreactor world before concentrating on my own solution, where I first give an overview over the whole reactor concept and then describe the sub-problems in greater detail.

## 3.1 Current state-of-the-art

Continuous cultivations pose several requirements to the design of a reactor system: The volumetric inflow has to equal the volumetric outflow of the reactor—the reactor volume has to stay constant. This can be achieved rather easily for a lab-scale reactor, but for microbioreactors it means for example that no significant bulging of the membrane—typically used for bubble-free aeration—is allowed. Also, the concentration of cells has to be controlled to a certain

level—most often this is done by setting the dilution rate  $D$  [ $\text{h}^{-1}$ ] to a constant level whilst keeping the nutrient concentration in the inflow constant (chemostat operation). Moreover, bioreactions can only truly be regarded as continuous culture reactions if the culture medium composition of the outflow is the same as that of the reactor content, i.e. if the assumption of an ideally mixed reactor holds. This in turn requires the mixing system to be efficient both in achieving a uniform distribution of for example nutrients and oxygen, but also in keeping the cells in suspension without the formation of dead zones. Finally, bioreactors for continuous culture should operate in parallel to rapidly provide statistically meaningful data and to enable direct comparison between different operating conditions.

Several research projects have addressed these issues (8; 78; 79), two of which are to be presented here. Akgün et al. (80) used specially prepared shake flasks with an outlet melted onto the side of the flask for the continuous cultivation of *S. cerevisiae*. Centrifugal motion caused by an orbital shaker kept the liquid level inside the flask constant as the excess liquid flowed out through the overflow, but no means of control over the cultivation parameters was implemented. Another approach (50; 81) used twenty-four 10 mL cylinders on a 24-well plate format. The individual cylinders are equipped with sensors for pH and DO. The whole system allows for the control of both pH and DO via sparging of the appropriate gases. Whilst this system allows a good degree of control over the fermentation, it does not support continuous cultivations.

Microbioreactors (commonly with volumes below 1 mL) are advantageous for running cultivations: they allow parallel cultivations under well-controlled conditions in disposable reactors (82) with a relatively low consumption of resources (nutrients, power, etc.). However, there definitely still is a need for more specifically designed and machined microbioreactors which enable high-performance cultivations (1). Lee et al. (11) presented a 100  $\mu\text{L}$  reactor fabricated out of PDMS which incorporated a novel mixing and aeration system as well as control over pH, DO and temperature. The supporting holder allows for the simultaneous operation of eight reactors. Batch cultures with *E. coli* showed that the system is able to deliver reproducible results which are comparable to bench-scale reactors. Szita et al. (13) presented a microbioreactor consisting of various layers of PMMA and PDMS. The design mimicked larger bench-scale reactors with cylindrical shape, and also included an impeller for magnetically actuated stirring. They successfully demonstrated both the reproducibility and comparability with larger scale reactors in multiple batch cultivations of *E. coli*. Finally, Zhang et al. (14) have described a polymer-based microbioreactor with integrated measurements of OD, DO and pH which was capable of achieving steady-state in continuous cultivations of *E. coli* at different dilution rates. They additionally also modified the surface of the reactor to reduce the amount of wall growth and included a heat barrier in the inflow channel to prevent the upstream migration of bacteria.

These examples illustrate that microbioreactor technology has reached a development stage where the operation of bench-scale reactors can be mimicked. The feasibility of pH (11; 17; 29) and DO (11) control has been demonstrated and sufficient mixing (30) has been proven for *E. coli*. However, no specifically designed microbioreactor as described above has yet been able to make the step from the laboratory environment to being a de-facto standard in industrial applications as the current microbioreactor systems available on the market build

on microtiter platforms. Additionally, scaling-up at different  $k_La$  values and for different types of organisms still has to be demonstrated. Islam et al., for example, investigated the influence of three different scales of operation on the culture properties of *E. coli* and have suggested that  $k_La$  is a useful scale-up criterion for microbioreactors (62).

Incidentally, most of the work on microbioreactors done to date deals with microbial cultures such as *E. coli*; Only little is concerned with the cultivation of eukaryotic cells such as *S. cerevisiae*. This does not reflect the fact that many industrially relevant cultivations use *S. cerevisiae* as production organism. *S. cerevisiae* has been used in baking and alcoholic brewing for centuries, and lately also to a large extent in heterologous protein production. It is a favorable host in pharmaceutical production as it has obtained GRAS (Generally Regarded As Safe) status by the FDA. Furthermore, it is easy to modify genetically and easy to grow and handle in large-scale processes.

## 3.2 Microbioreactor design and fabrication

### 3.2.1 Overview

The microbioreactor (Fig. 3.1) is 4.2 mm high and has an outer diameter of 14 mm. It comprises a reactor volume of 100  $\mu\text{L}$ , provisions for the measurement of dissolved oxygen, pH and optical density as well as a magnetic stirrer bar for mixing. Additionally, an aeration layer is enclosed in the reactor for the bubble-less supply of oxygen. A specifically fabricated holder plate includes a temperature sensor and resistance wires for the adequate temperature control of the reactor contents.

The reactor consists entirely of PDMS (Sylgard 184, Dow Corning Corp., Midland, MI, USA. Mixing ratio of 10 parts silicone : 1 part curing agent) with the exception of the sensor spots and the magnetic stirrer bar. PDMS is commonly used in microbioreactor design for its favorable properties: It is optically transparent in the wavelengths required, is non-toxic, can easily be shaped with molding techniques and is permeable to gases such as oxygen, carbon dioxide or also water vapor.

Due to the fabrication technique used the reactor consists of 4 layers which are bonded together to form one single block of material in the final product. The lower main layer (Fig. 3.2, brown part) is 2 mm high and contains the actual reactor chamber. It is closed both on top and bottom by a membrane (80  $\mu\text{m}$  thickness). It contains two windows of 1 mm thickness each, onto which optical sensor spots for the measurement of DO and pH are attached. Additionally, two tunnels for the insertion of optical fibers for the measurement of OD are present. These tunnels stop short of the reactor chamber forming a thin (0.5 mm) PDMS window between the broth and the fibers. This helps to ensure both sterility as there is no direct connection of the broth to the outside world and also the reproducibility of the measurements as the distance between fiber tips (and thus the path length of the light) is fixed.

On top of the upper membrane lies the aeration layer (Fig. 3.2, green part). It has a thickness of 2.2 mm and holds the meandering aeration channel (0.75 mm deep x 0.5 mm wide).

The whole setup was controlled via a LabView (National Instruments Corpo-



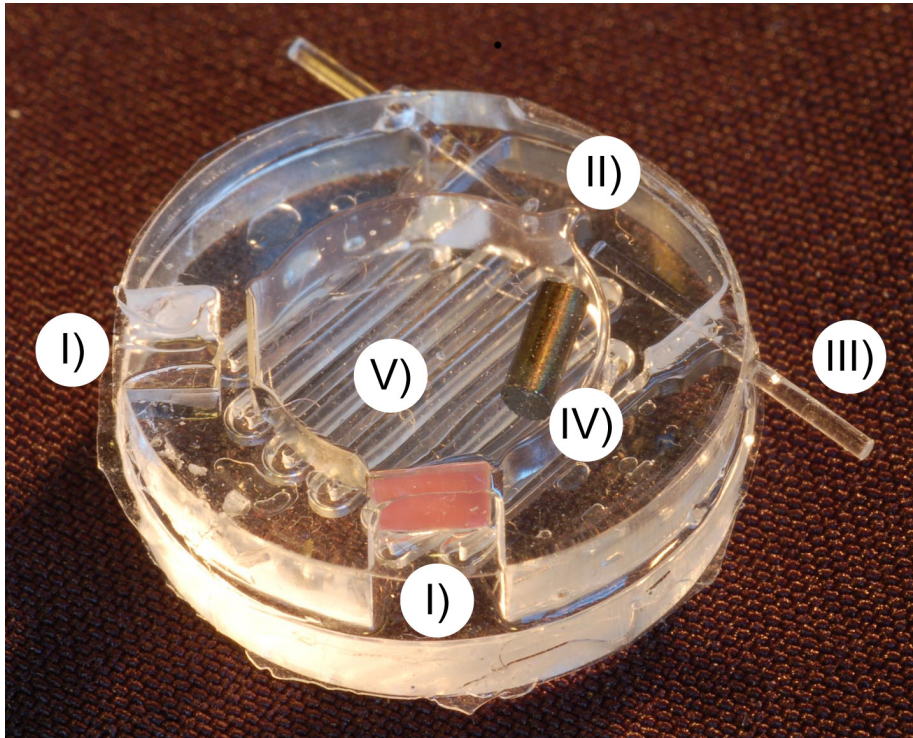


**Figure 3.1:** Photo of the complete microbioreactor seen from the bottom: On the inside of the two windows the optical sensor spots (I, black for DO and white for pH) are attached. The magnetic stirrer bar (IV) lies freely inside the chamber. The two optical fiber stubs (III) show the location of the OD measurement (II). The two holes in the aeration layer are used to connect the aeration tubing to the meandering channel (V).

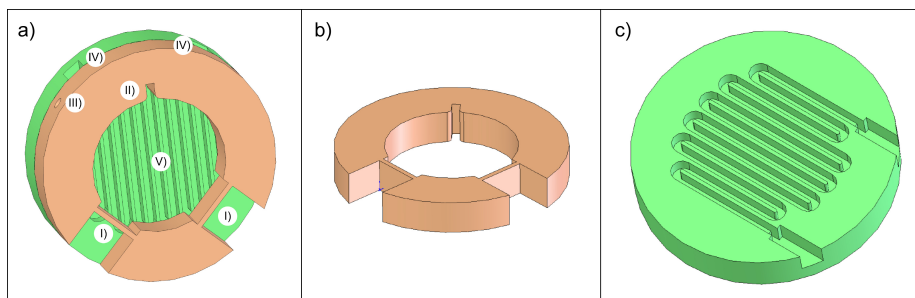


**Figure 3.2:** Sketch of both main reactor layers as seen from below (without membrane layers): The reactor layer (orange) comes to lie on the holder, which leaves the aeration layer (green) on top. The two optical windows for the DO and pH measurements (I), the radial recess (II) for the OD measurement and the tunnels for the OD fibers (III) are located in the reactor layer, whereas the connections (IV) for the gas tubes and the meandering channel (V) are located in the aeration layer.

ration, TX, USA) interface using A/D cards (USB-6229 and PCI-4461, National Instruments Corporation, TX, USA) for in- and output of the signals. OD and DO were measured, whilst temperature and pH were both measured and controlled to the desired levels. All the measurement data are written into text files for further processing with other software, e.g. Matlab (The MathWorks, Inc., MA, USA).

Both the bottom and the upper main layer are fabricated by pouring liquid PDMS into a micromilled (CNC micromill, Minitech MiniMill 3/Pro, Minitech Machinery Corporation, Norcross, GA, USA) PMMA mold and subsequent curing at 70 °C for one hour. Upon removal from the mold the two optical sensor spots were bonded onto their respective windows on the inside of the reactor using PDMS itself as the glue. In this manner no additional glue was used, hence eliminating the risk of chemical contamination of the culture. The PDMS membranes were then spin-coated onto the bottom of both the reactor layer and the aeration layer.

Finally, a magnetic stirrer bar was placed into the bottom (reactor) layer. The reactor layer and the aeration layer were then bonded together by applying liquid PDMS to the contact surface, clamping the two components together and curing for an hour at 70 °C. This resulted in a reactor which has a completely sealed culture chamber, a stirrer bar, two optical sensors and an aeration layer. Additionally, all materials chosen were suitable for irradiation sterilization.

A reactor holder (Fig. 3.3) was fabricated to control the microbioreactor temperature. It includes resistance wires to heat the reactor and a temperature sensor. When the reactor is placed on the holder, the thin membrane on the bottom of the reactor offers virtually no thermal resistance and thus allows for the direct temperature measurement and heating of the reactor contents.

### 3.2.2 Dissolved oxygen

Current lab-scale cultivation techniques have vessels which are only partly filled and have a headspace. They rely on sparging of air (bench-scale reactors) or surface-aeration (shake flasks or microtiterplates) for the aeration of the cultivation. On the contrary, most microbioreactors have well-defined volumes which are completely filled with liquid (no headspace). Also, due to the small size of microbioreactors sparging is not an option. Small air bubbles coalesce and form larger air bubbles which can displace culture liquid or block fluidic ports and disturb optical measurements.

For aeration, this kind of microbioreactors therefore rely on diffusion of oxygen through a membrane (83) which leads to bubble-free aeration. Apart from preventing the formation of bubbles, it also greatly increases the quality of the online measurements. Moreover, the concept has been proven effective earlier (11; 13; 30). Also, PDMS e.g. allows CO<sub>2</sub> to diffuse out of the reactor.

The aeration layer of our reactor (Fig. 3.2, green part) contains a meandering channel through which the aeration gas flows which maximizes the contact area between gas on the one side and liquid on the other side of the membrane (Fig. 3.5). At the same time it supports the membrane in such a manner that it cannot bulge significantly in any direction. This ensures a constant volume of the microbioreactor, even under overpressure, which is for example essential for chemostat operation. The aeration channels support the diffusion of CO<sub>2</sub> out of the reactor as all gas diffusing out of the reactor is transported away



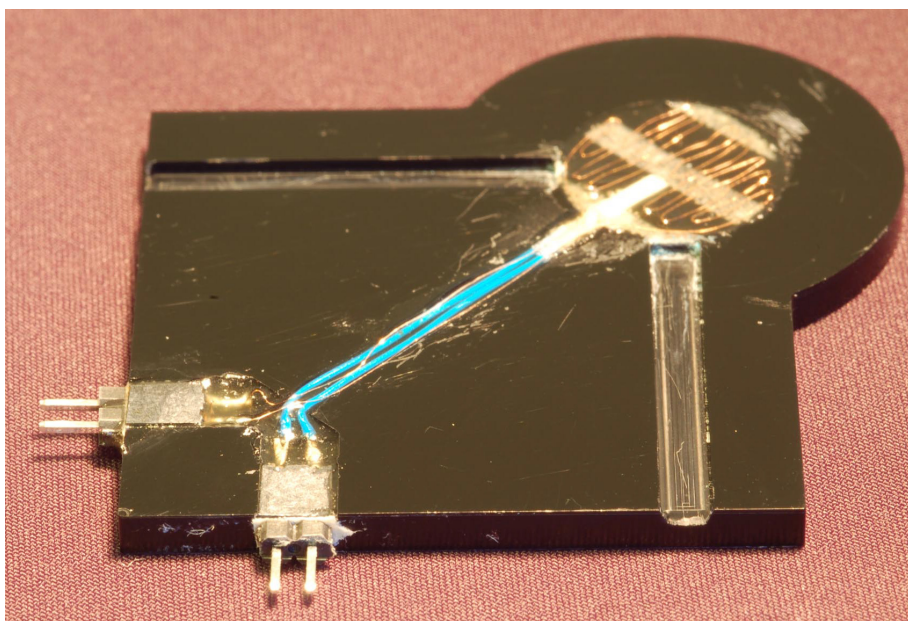


**Figure 3.3:** The holder consists of a temperature sensor (Pt-100) embedded in a thin epoxy layer, surrounded by resistive heating wires. The two channels serve to align the bifurcated fibers used for the DO and pH measurements.

immediately, thus keeping the diffusion driving force high. Naturally, good mixing of the reactor contents is required to prevent concentration gradients in the liquid phase.

The concentration of dissolved oxygen was measured with a fluorescent optical sensor spot (Fig. 3.6, SP-PSt3-NAU-D4-YOP, PreSens - Precision Sensing GmbH, Regensburg, Germany). Sine-modulated light (5 kHz) from a blue-green LED (505 nm, NSPE590S, Nichia Corporation, Tokushima, Japan) shone onto the sensor spot which was mounted on the inside of the reactor in direct contact with the culture broth. This sensor in turn emitted fluorescent light at 652 nm peak wavelength with the same sine frequency as the excitation light but with a certain phase lag. The emitted light was then collected with a silicon detector (Thorlabs PDA36A, Thorlabs Inc., NJ, USA) and the resulting voltage was read by LabView. A lock-in amplifier programmed in LabView then measured the phase shift between the outgoing and the incoming signal; this shift then translated directly to the dissolved oxygen concentration.

The quality of the measurement can be heavily influenced by the modifications of the light: It is possible to use optical filters which either limit the wavelength bandwidth of the excitation or of the emission light. A filter will both decrease the amount of 'noise' the sensor measures, but will also limit the amount of light that reaches the sensor. As the emitted light is very weak, a filter could easily decrease the light intensity below the detection limit of the photodetector. We have done tests with all four different configurations (a filter at both locations, a filter at only one location or no filter at all) which all resulted in different phase

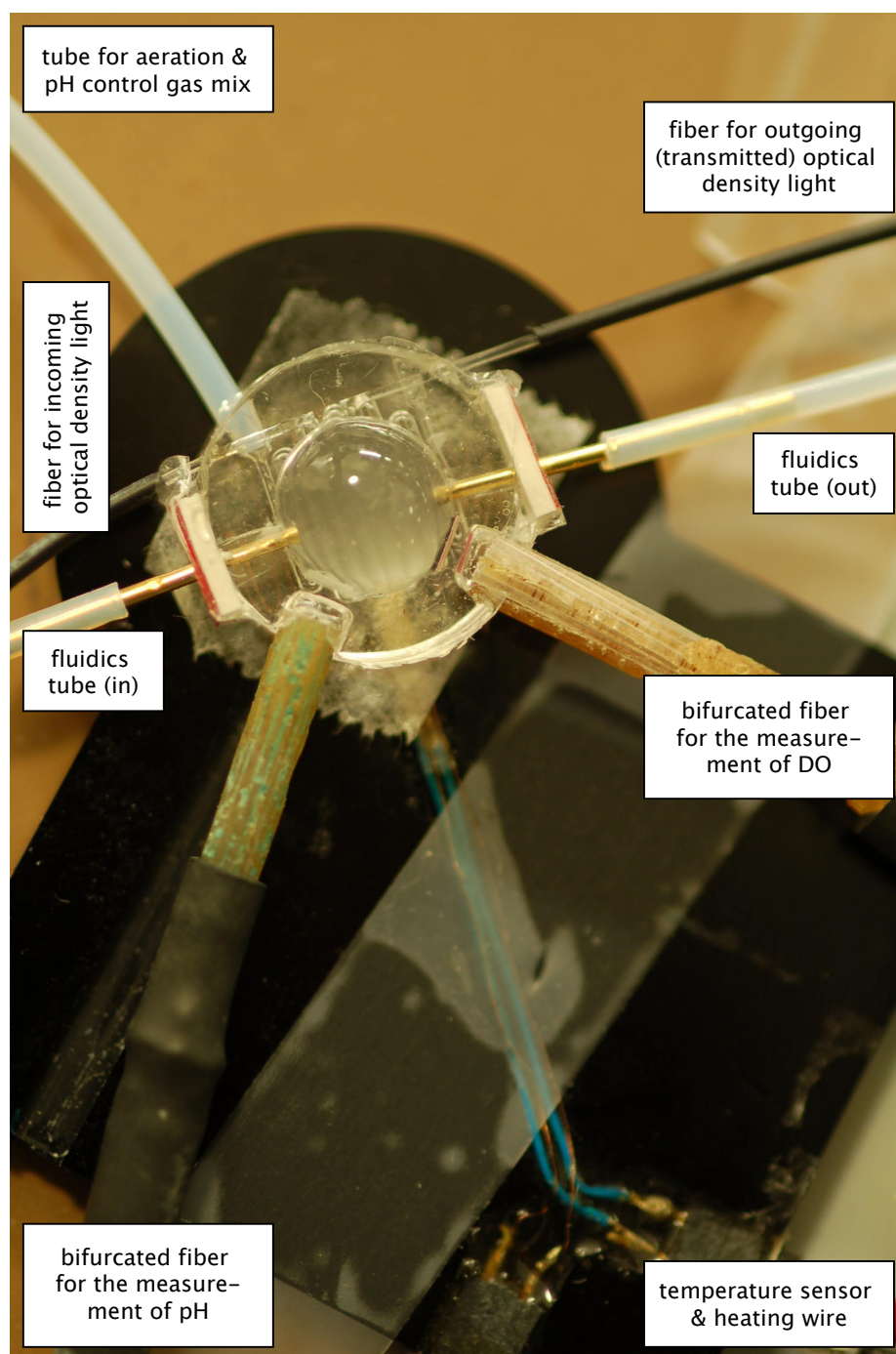


**Figure 3.4:** The microbioreactor (turned upside down) lying on the temperature control plate is filled with a solution of baker's yeast and all the necessary connections have been made. Observe a) the bulging of the membrane due to the pressure created by the elevated (30 cm higher) water reservoir, b) the septum pieces attached to the outer diameter of the reactor to make the fluidic connections more secure.



**Figure 3.5:** The meandering aeration channel (located in the aeration layer, here on the bottom) is only separated from the reactor chamber (side wall visible in the middle of the picture) by a membrane (not visible).

measurements and stabilities. The variant with only a bandpass filter (Bandpass filter XF1016, Omega Optical, Brattleboro, VT, U.S.A.) in the excitation light path gave the best results here.

We have also conducted experiments where the optical DO sensor spot was mounted on the *outside* of the reactor and was only in contact with the culture broth via a thin membrane analogous to the aeration membrane. The transport of oxygen through the membrane obviously reduces the reaction speed of the measurement—however this is negligible compared to the speed with which the oxygen concentration in the culture broth changes. This has the advantage that it would allow for the production of an even cheaper reactor as one sensor spot can be reused. However it has the drawback that it also opens for new errors as the sensor spot itself bleaches out with use and ceases to function after some time. Thus, the quality of this external sensor spot would have to be checked continuously, and if necessary the sensor spot would have to be replaced before the cultivation. In order to achieve more reliable operation we therefore have chosen to integrate the sensor spot into the reactor.

### 3.2.3 pH

pH was measured by means of an optical measurement with the use of a fluorescent sensor spot (Fig. 3.7, SP-pH-HP5-YOP-D4, PreSens - Precision Sensing GmbH, Regensburg, Germany). Sine-modulated light (44 kHz) from a blue LED (465 nm, NSPB500S, Nichia Corporation, Tokushima, Japan) was shone onto an optical sensor spot which was mounted on the inside of the reactor (in direct



**Figure 3.6:** The carrier layer of the DO sensor spot (red) is attached to the inside wall of the reactor chamber whilst the active (fluorescent, black colour) layer is in direct contact with the broth. The measurement is done through the reactor wall (window thickness 1 mm).



contact with the culture broth). This sensor spot in turn emitted fluorescent light at 520 nm peak wavelength, with the same frequency as the incoming light, but with a phase lag. The emitted light was then collected with a silicon detector (Thorlabs PDA36A, Thorlabs Inc., NJ, USA) and the resulting voltage was read by LabView. A lock-in amplifier programmed in LabView then measured the phase shift between the outgoing and the incoming signal; this shift then translated directly to pH values.

Here too (in analogy to the DO measurement), the quality of the measurement can be heavily influenced by the modifications of the light: We have done tests with all four different configurations (a filter at both locations, a filter at only one location or no filter at all) which all resulted in different phase measurements and stabilities. The variant with a bandpass filter (Bandpass filter XF 1072, Omega Optical, Brattleboro, VT, U.S.A.) in the excitation light path and a low pass filter (Optical glass OG-515, Schott Scandinavia, Kgs. Lyngby, Denmark) gave the best results here.

The optical pH sensor used has a measurement accuracy of about 0.01 pH units with a response time ( $t_{90}$ ) of less than 90 s (1). Our calibration data (Fig. 3.8) shows the dynamic measurement range of the sensor spot to lie between pH 5.5 to 8. Within this range, the sensor response is almost linear with a sensitivity of about  $10^\circ$  phase angle per pH unit.



**Figure 3.7:** The carrier layer of the pH sensor spot (white) is attached to the inside wall of the reactor chamber whilst the active (fluorescent, yellowish colour) layer is in direct contact with the broth. The measurement is done through the reactor wall (window thickness 1 mm, located in the right half of the picture).

pH control was accomplished by dosing of either a gas mixture containing 20 000 ppm ammonia gas,  $\text{NH}_3$  (the rest is nitrogen gas) or pure carbon dioxide gas,  $\text{CO}_2$  to respectively increase and decrease the pH of the reactor content (17). Both gases were supplied from pressurized gas bottles equipped with two-

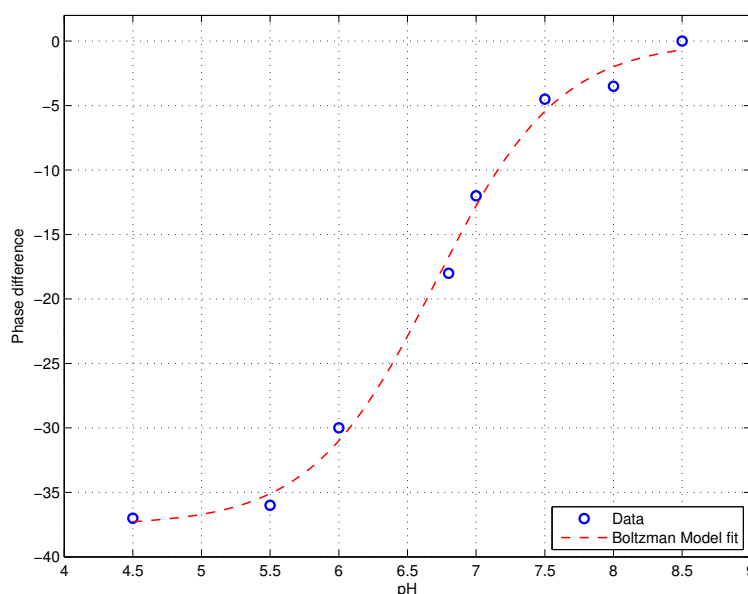


**Figure 3.8:** The calibration curve shows how the pH sensor sensitivity decreases for high/low pH values.

stage gas regulators. A two-stage gas regulator ensures a more constant gas pressure, and therefore provides better stability for the process control than a single stage regulator would. The gas flow from the gas bottles was quantified by using mass flow meters (SHO-RATE, Brooks Instrument, Holland, Model 504-ES-22-F2B). For gas addition, 2-way Polyetheretherketone (PEEK) solenoid valves (Bio-Chem Valve, Cambridge, UK, 038T2B12-32-5) were connected directly to each of the mass flow controllers (one for  $\text{NH}_3$  and one for  $\text{CO}_2$ ). Both valves were connected in parallel and remain closed unless a voltage supply is connected. An additional solenoid valve was installed in each of the gas lines to depressurize the gas line prior to dosing of gas into the reactor. This additional valve is necessary: When the solenoid valves are in the ‘closed-position’, the continuous gas flow from the gas bottle causes the pressure in the tubing to increase until the whole tubing has the pressure which was adjusted at the regulator. Overpressure in the gas connections is not desirable because it may lead to an undesired overshoot in reactor pH.

The  $\text{NH}_3$  and  $\text{CO}_2$  gas lines were then joined together via a T-connector and introduced into the microbioreactor by connecting the gas line to the top layer of the microbioreactor. During pH control, only one gas was dosed at a time. Part of the gas diffuses through the semi-permeable membrane and induces the desired pH changes. The remaining gas flows out through the outlet port and is removed with the ventilation. All gas connections were established by standard perfluoroalkoxy (PFA) tubing with an outer diameter of 3.175 mm using fittings from Upchurch Scientific.

The pH of the reactor content was controlled by an on/off controller. The on/off controller was implemented by using a LabView<sup>TM</sup> v8.5 software (Na-

tional Instruments Corporation, TX, USA) interface using A/D cards (USB-6229 and PCI-4461, National Instruments Corporation, TX, USA).

First, the LabView program (Fig. 3.9) will compute the deviation (error) between the desired set point value,  $pH_{sp}$  and the measured value,  $pH_m$ . The controller was made to include a tolerance limit (dead band) around the set point. The dead band prevents the dosing valves from rapidly or continuously switching because in an on/off controller the measured value never exactly fits the set point value. During pH control, no titration will take place if the pH deviation from the set point is within the tolerance limits. If the error is larger than the tolerance limit and positive ( $pH_{sp} > pH_m$ ),  $NH_3$  gas will be added and if the error is negative ( $pH_{sp} < pH_m$ ),  $CO_2$  gas will be added. A latching relay was used to control the state ('open' or remain 'closed') of the solenoid valve for gas addition. During addition of gas, the controller will first depressurize the gas connection (depressurizing period was set for 1 s) before opening up the dosing valve. Furthermore, the controller will only open the dosing valve for a very short period of time (pulse length of approximately 300 ms) before switching the valve back to its 'closed-position'. Thus the time needed for one dosing cycle is approximately 1.3 s. The period during which the dosing valve is open (pulse length) is one of the parameters that can be tuned. Other settings to be adjusted by the user are the gas bottle pressure (or the inflow gas flow rate via the mass flow controller) which determines the amount of gas diffusing through the membrane, the tolerance limits, and of course the pH set point. In our application, the on/off controller was tuned to give the smallest step change possible in both acidic and basic directions.

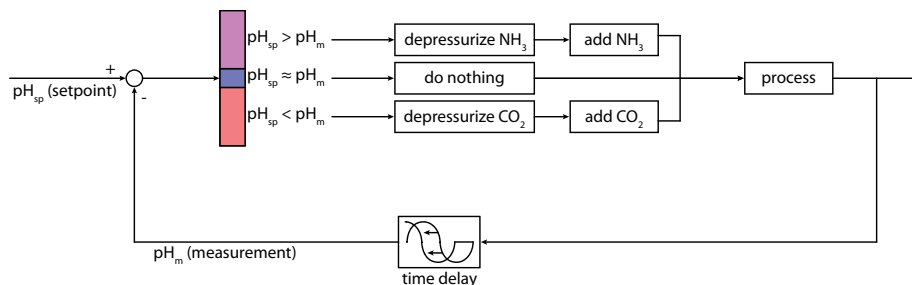


Figure 3.9: pH control scheme.

### 3.2.4 Optical density

One essential culture variable—the biomass concentration—is obtained by the measurement of the cell density in the broth. This is most often done by means of a transmittance measurement where one measures how much light can pass through the broth. This method is easy to set up, works on-line and has been well established (9). However it has the drawback that it measures all cells, both alive and dead. There also exist methods for the measurement of viable cells (e.g. via tryptophan concentration (84; 85) or capacitance measurements (86; 87)), these are however more complex and might be considered in a next version of the reactor. For most cultivation purposes the transmittance measurement is good enough; It is also completely analogous to the measurement method for

larger scales. An additional nice feature of this method is that it allows for continuous online measurements without disturbing the cultivation.

In the system devised here (drawings in Fig. 3.10, mechanical drawings in App. C), a ‘beamsplitter block’ holds the LED and lens needed to generate the measurement light needed. First, light at 600 nm wavelength was generated with a bright yellow LED (L600-10V, Epitex, Kyoto, Japan). This excitation light was first collimated with a lens (NT45-482, Edmund Optics Ltd, York, UK) and was then led onto a 30–70 beamsplitter (NT45-317, Edmund Optics Ltd, York, UK) which diverts 70% of the light intensity away in a 90° angle. Both light paths (70% and 30%) are then bundled (NT45-482, Edmund Optics Ltd, York, UK) and focused into optical fibers (500  $\mu\text{m}$  core fiber, Edmund optics Ltd, York, UK).

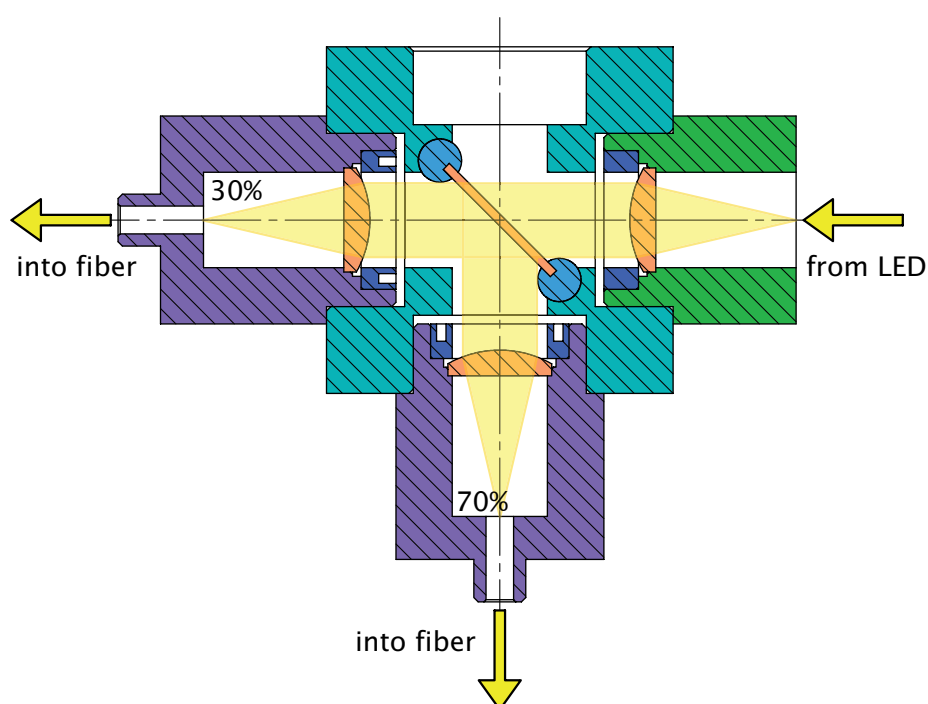


**Figure 3.10:** Detail of the beamsplitter box which splits the light for the optical density measurement into two intensities.

70% of the incoming light was first guided to the microbioreactor for the measurement and was then fed onto a photodiode (IPL 10530, Integrated Photomatrix Ltd., UK) whilst the remaining 30% were directly fed onto a photodiode (IPL 10530, Integrated Photomatrix Ltd., UK) for reference purposes. This slightly more complicated setup was chosen in order to be able to compensate for variations in the light intensity given by the LED—by deviding the intensity of the measurement signal with that of the reference signal any variations will automatically be cancelled out. Naturally, this adds another uncertainty as the two photodiodes used for transforming the incoming light into voltage might also change their behaviour over time. But as photodiodes are required anyway this risk was deemed acceptable.



The part of the light used for the measurement (70%) travelled in a fiber optics cable to the reactor, through the PDMS measurement window (0.5 mm thickness), then through the reactor with a defined path length of 0.5 mm and out through the second window into a second fiber optics cable (Fig. 3.11) and on to a photodiode. With this setup the path length in the culture broth is well-defined and the same for different reactors (as it is a part of the geometry); Also it does not require any direct access to the culture broth as the reactor material is used as ‘window’.



**Figure 3.11:** The tunnels made during fabrication are now filled with the optical fibers. The tunnel ends short of the reactor chamber creating a window through which the light reaches the chamber. The chamber has a protrusion to allow for a defined measurement path length.

In order to eliminate the effect of ambient light, the incoming light source was sine modulated (47 Hz) and the AC component of the measured signal was processed for OD analysis. A more precise measurement would involve a lock-in amplifier which *only* measures the intensity at 47 Hz—with that any possible influence of the electric lighting (50 Hz) would be removed. We have however not been able to observe any significant change in OD measurement with or without electrical light in the lab.

This measurement has a range where the light transmitted (and thus the voltage output) correlates linearly with the cell concentration in the culture broth. As the OD measurement follows the Lambert-Beer law

$$A = -\log_{10} \frac{I}{I_0} = \varepsilon \cdot l \cdot c \quad (3.1)$$

where  $A$  is the absorbance [-],  $I$  the power [W],  $\varepsilon$  is the molar absorptivity of the absorber [ $\text{L}\cdot\text{mol}^{-1}\cdot\text{cm}^{-1}$ ],  $l$  is the path length [cm] and  $c$  is the concentration of the absorbing species [ $\text{mol}\cdot\text{L}^{-1}$ ].

The linear range can be adjusted by manipulating the components of equation 3.1. The incoming light intensity was set to the maximal value deliverable by the LED—this increases the amount of light actually reaching the photodiode and thus increases the signal-to-noise ratio. The density of the broth is the variable which is to be measured, thus it cannot be adjusted. The remaining factor is thus the path length—a shorter path length will allow for measurements in more dense broths whilst a longer path length will allow for measurements in more dilute broths. The path length chosen here (0.5 mm) was based on the experience with previous reactors where the fibers had been pushed directly into the reactor (without windows).

The Lambert-Beer law assumes that every absorbing particle behaves independently with respect to the light. However, in a very dense solution, some particles will lie in the shadow of others. The law therefore loses its linear relationship to the density at very high concentrations as it tends to underestimate the amount of absorption. The law will also become nonlinear if the material is highly scattering as some of the incoming light will be derived out of the measurement beam.

### 3.2.5 Mixing

Thorough mixing of the reactor is essential both for the transport of oxygen and nutrients throughout the reactor and for keeping the cells in suspension. Only if the continuous reactor contents can be considered homogeneously mixed can it also operate properly as a chemostat and generate useful results. In microbioreactors, liquid motion in the reactor becomes predominantly laminar, so mixing in this case has to rely on minimizing diffusion distances (88). An additional problem is that some cell types sediment, for example yeast (89; 90). A homogeneous suspension of yeast cells will quickly sediment if there are any zones without uplift in the reactor.

In the microbioreactor that is presented here, mixing is achieved with a free-floating magnetic stirrer bar, similar as in shake flasks. In contrast to shake flasks it is essential that the stirrer bar does not rotate regularly in the middle of the reactor, since the reactor contents are then forced into a rotating motion which forces the heavier cells out towards the reactor walls where they then sediment into cell heaps on the reactor floor. As the stirrer is actuated slightly eccentrically it rotates both around its vertical axis, but also moves around on the floor of the reactor, ever so often to hit and then ricochet off the side wall.

While testing different types of mixing in the microbioreactor this highly irregular and chaotic motion was observed to be very effective as it does not have any dead zones without mixing and can keep yeast (*S. cerevisiae*) cells in suspension over several days. Also, it does not require any specifically fabricated impellers nor any precisely machined rotation axis, thus simplifying fabrication and reducing the final cost.

### 3.2.6 Evaporation

Evaporation becomes an issue at this reactor scale as it can reach very significant rates (33; 91). Boccazzi et al. (10) measured an evaporation rate of  $4.3 \pm 0.4$   $\mu\text{L}/\text{h}$  through a 100  $\mu\text{m}$  thick PDMS membrane with 10 mm diameter—a reactor with 100  $\mu\text{L}$  volume would thus completely dry out within 24 hours.

There are two obvious solutions to this problem: For batch reactors, it is highly effective to attach a water reservoir which is elevated above the level of the microbioreactor (30). Any water which evaporates is then automatically replenished from the reservoir while keeping the concentrations (e.g. of cells) undisturbed.

Alternatively, evaporation of the reactor content can be minimized with pre-humidified aeration gas. This is particularly useful for continuous culture microbioreactors as it decouples the evaporation control from the flow control and thus permits to minimize the evaporation rate without affecting the dilution rate. In our design, the gas stream used for aeration is sparged through an external water volume before reaching the microbioreactor. This gives a high relative humidity of the gas and therefore minimizes the driving force for evaporation out of the reactor volume. This approach reduces the water losses through evaporation to tolerable amounts; in our reactor, no change in reactor liquid volume could be observed over the course of several days for a microbioreactor operated in batch mode.

### 3.2.7 Fluidics

The necessary fluidic connections are currently made by first piercing the side walls of the reactor at the designated locations with a needle with 0.6 mm outer diameter (BD Microlance 3, Becton Dickinson, NJ, USA) in order to create a tunnel. The needle was then removed and a small copper tube (Spring spade terminal, beryllium copper, RS Components Ltd., Corby, UK, part no. 261-5238) is inserted in its place. Unlike the needle, the copper tube has the advantage of having a flat end which allows it to be mounted flush with the inner wall of the reactor and thus does not disturb the spinning bar. As the tube is tightly enclosed by the surrounding PDMS, the connection is leak-free at the pressures required for the cultivation of yeast. In order to make the connection more leak-proof, a self-sealing septum (Waters, MA, USA) can either be embedded in the PDMS or be attached to the outside of the reactor.

When a needle is pulled out of the material, the material closes the hole so that no liquid can seep out. During the tests a reactor had been pierced several times before leakage started to occur. With this configuration, a continuous culture reactor can be constantly pierced by two tubes (one for the inflow of fresh culture medium and one for the outflow of the same amount of cultivation broth including cells). When the broth has to be inoculated or when direct access to the broth is needed for other reasons, a needle can be inserted into the reactor and removed again after use. This obviously makes handling very easy.

### 3.2.8 Temperature

In microbioreactors, several technical and heat transfer-related issues have to be tackled before a tight temperature control scheme can be realized. First

of all, only limited space is available for insertion of temperature sensors and integration of heating elements as actuators for temperature control. As a consequence, the temperature sensor and the micro-heater have to be positioned within a reasonable thermal distance from each other, such that the temperature measurement—and thus also the heater that usually functions as an actuator in a feedback loop for temperature control—responds according to the change of the temperature of the reactor content (the object being heated) and not the change of the temperature of the heating element. Secondly, microbioreactors have a very high surface area to working volume ratio ( $S/V$ ) compared to bench scale reactors. Since microbioreactors are typically not thermally insulated, the high  $S/V$  ratio leads to significant and inevitable heat dissipation to the surroundings by natural convection; typically at a rate of  $20 \text{ W} \cdot \text{m}^{-2} \cdot ^\circ\text{C}^{-1}$  (40). On the one hand, this might impose some technical challenges because heat losses to the surroundings need to be compensated with a corresponding heating of the reactor such that the temperature of the reactor contents can be maintained at a desired set point. One also has to ensure adequate heater power such that sufficient heat can be transferred to induce desired temperature changes. On the other hand, the high  $S/V$  ratio is also advantageous because it implies that this type of reactor has a very fast thermal response. This means that only a small amount of heating power is required to raise the temperature of the reactor significantly (48). Note also that typically only a heating element is required to regulate the microbioreactor temperature. Indeed, the optimal temperature of most fermentations, for example, is typically above room temperature. Finally, another point that needs to be taken into account is the uniformity of the local heating of the microbioreactor. It is critically important that the heating element is placed such that an even heat distribution in the reactor chamber is achieved. Uniform temperature of the microbioreactor contents can also be promoted by guaranteeing sufficient mixing in the reactor and by appropriate design of the reactor.

In previous reactor designs, both the temperature sensor and the heating wire had been embedded in the reactor material (PDMS) itself. This naturally is very good for temperature control as it (a) allows the heating wire to be very close to the broth and (b) opens up the possibility to mount the temperature sensor in the floor or even the wall of the reactor. So, in theory, even more than one sensor could be installed. It also has, however, some drawbacks which would have taken too much time in the current project to be solved. The main problem is that both the sensor and the heating wire have to be electrically contacted, which is quite problematic as the heating wire is very thin and the connections tend to break. Kortmann et al. (38) have devised a system with battery contacts which might make this feasible, however integrated elements both bring increased cost and fabrication effort with them, so it was chosen to locate these elements outside of the reactor. With this setup no electrical connections to the single-use part have to be established which greatly decreases the risk of handling errors. For this purpose a reusable external holder (Fig. 3.3) was constructed which contains both the heating wire and the temperature sensor. As the floor of the reactor is very thin ( $< 100 \mu\text{m}$ ), the thermal resistance is virtually zero.

Temperature was measured with a Pt 100 sensor (JUMO PCA 1.1505.1M, JUMO GmbH & Co.KG, Germany) with outer dimensions of  $5 \times 1.5 \times 1 \text{ mm}$ , located in the reusable holder underneath the reactor. The sensor was connected

to LabView via a transmitter (JUMO dTRANS 04) which linearized and scaled the sensor signal. Also located in the holder was a meandering copper wire with 0.1 mm diameter. An electrical current flowing through the wire heated it up and with it the reactor contents. Temperature was then kept at the desired set point with an on/off controller switching the heating on and off (3).

The LabView program computed the deviation (error) between the desired set point value  $T_{sp}$  [°C] and the measured value  $T_m$  [°C]. If the error is positive ( $T_{sp} > T_m$ ), the heater is activated. In any other situation ( $T_{sp} \leq T_m$ ) the heater will remain off (Fig. 3.12). To ensure a stable operation and prevent rapid switching of the relay output, a time delay of 1 second was introduced before every temperature measurement. For example, if the heater is on (with pulse length set for 4 s) total cycle time would be 5s and when the heater is off, the total cycle time would only be 1 s.

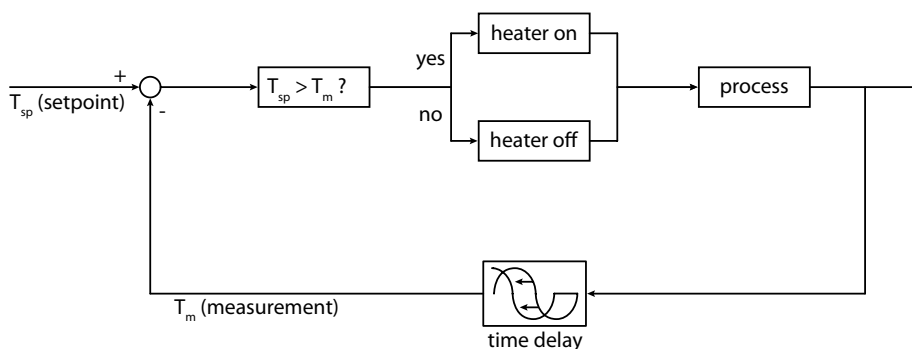


**Figure 3.12:** Temperature control scheme.

The on/off controller was tuned to generate sufficient heat input via the resistance wire for a satisfactory performance over the temperature range of interest. In our application, the operating temperature range of interest is between 30 °C and 50 °C, as this is a highly relevant range for cultivation of mesophilic microorganisms (e.g. *Escherichia coli*, 37–42 °C (5) and *S. cerevisiae*, 30–37 °C (92)) and mammalian cells ( $\approx 37$  °C) (93), and for most enzymatic reactions as well (5).

### 3.3 LabView control program

One of the requirements for the microbioreactor setup is ‘automatic measurement and control’ of the essential culture variables. Sampling is not an option, thus there is no need for a human operator to be present. In the current setup, four different measurements (DO, OD, pH and temperature) were implemented and two of these (pH and temperature) were also controlled.

The whole setup is controlled via a LabView (National Instruments Corporation, TX, USA) interface using National Instruments A/D cards (USB-6229 and PCI-4461, National Instruments Corporation, TX, USA) for in- and output of the signals. All the measurement data is written into text files for further processing with other software, e.g. Matlab (The MathWorks, Inc., MA, USA).

In an effort to not only build a small reactor but also keep the surrounding

machinery as small as possible, we opted for replacing commercially available lock-in amplifiers with such programmed in software (LabView). This saves space and increases flexibility, but calls for a A/D card with certain specifications: The pH measurement uses a sine wave of 44 kHz, thus the sampling frequency must—according to the Nyquist theorem—be at least 2-3 times higher (in practice preferably 5-6 times). Also, it must have two input and two output channels and must have a digitizer for every single channel in order to allow for the precise measurement of phase/time. The National Instruments PCI-4461 is one possible solution as it offers 204 kHz total sampling frequency and thus can cover the DO and the pH measurements. On the other hand a ‘slower’ card is also required which can handle the other measurements (T and OD) and can give out analog and digital signals to control the system. The National Instruments USB-6229 offers a wealth of input/output channels and thus was the card of choice.

The functioning scheme of the program orients itself very much around the two A/D cards (Figure 3.13): One loop runs on the fast (PCI) card and does the DO and the pH measurements, another loop runs on the slow (USB) card and handles the temperature and OD measurements. A third part is concerned with the digital in-/output on the USB card. This separation was necessary as it is not possible to have two different processes access the same analogue part of a card. Therefore it was not possible to have the DO and pH measurements to run as an individual loop each; Instead they had to be placed into the same looping sequence. The same is also valid for the temperature and OD measurements on the slow card.

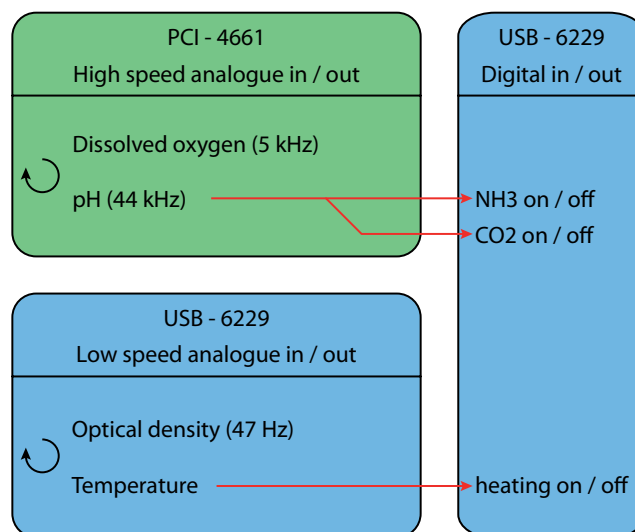


**Figure 3.13:** Overview over the LabView program

In the high speed part the DO and pH measurements are handled where the two measurements are done sequentially in a continuous loop (Fig. 3.14). First, for DO, a sine voltage is given out through the AO/0 port which excites the LED according to the specifications described earlier. As the LED does not draw much power the PCI card can directly act as a power source. This output

signal is looped internally back as a virtual input channel serving as the reference signal. In parallel, the fluorescent light coming from the sensor spot is recorded by the photodiode and transformed to voltage by AI/0. These two input signals, the 'real' input signal (AI/0) and the internally looped reference signal are then fed into the 'lock-in amplifier' section in LabView which determines the phase shift averaged over a period of time. The resulting phase lag value is then both displayed on the screen and written to file (meas\_data\_do.lvm) together with the current time stamp.

After a brief pause, the system does the same with the pH measurement where the channels AO/1 and AI/1 are used. The phase lag value determined here is (a) displayed on the screen, (b) is written to file (meas\_data\_ph.lvm) together with the time stamp and (c) sent to the digital part of the program to be used for the *control* of pH.

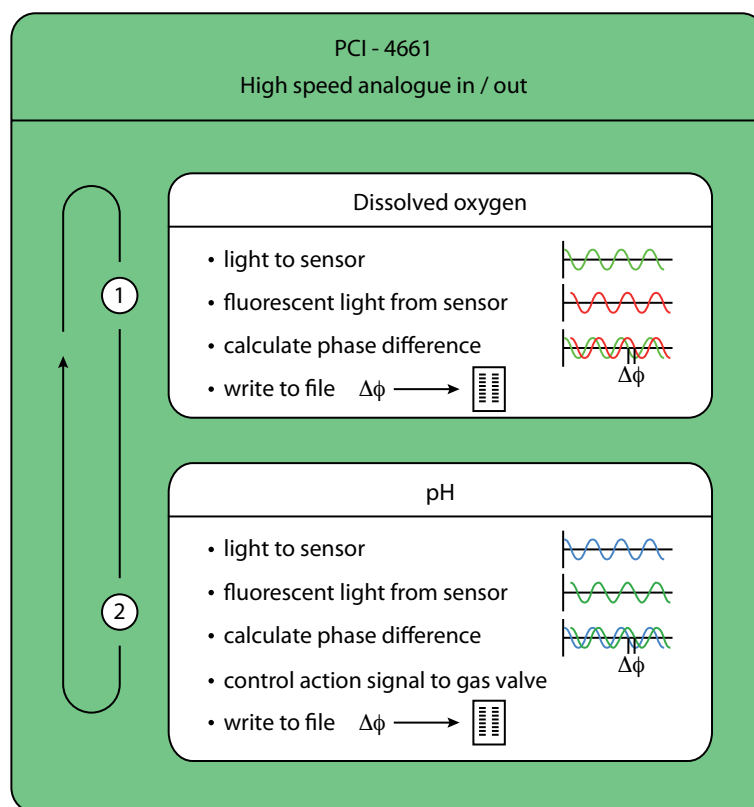


**Figure 3.14:** Schematic of the LabView program: high-speed part

The low-speed analogue part (Fig. 3.15) sequentially works on the optical density and the temperature measurements. This loop is independent of the high-speed loop described above. First the optical density LED is excited with a sine wave (via AO/0) according to the specifications described earlier. Here too, the power from the A/D card is sufficient to feed the LED. This light is then split into two parts which are led to their respective destinations. Finally, the two light beams are fed onto a photodiode each which transforms light



into voltage. These two voltage signals are digitized (AI/3 and AI/4), the AC component of each is determined and the ratio is formed. All these values are written to file (meas\_data\_od.lvm) together with the according timestamp whereas only the resulting OD value is displayed on the screen.

For the temperature measurement the temperature sensor is probed and the resulting value is fed to the digital part of the program for the temperature control part. In addition, the measured temperature value is displayed on screen and written to file (meas\_data\_temp.lvm) together with the time stamp.

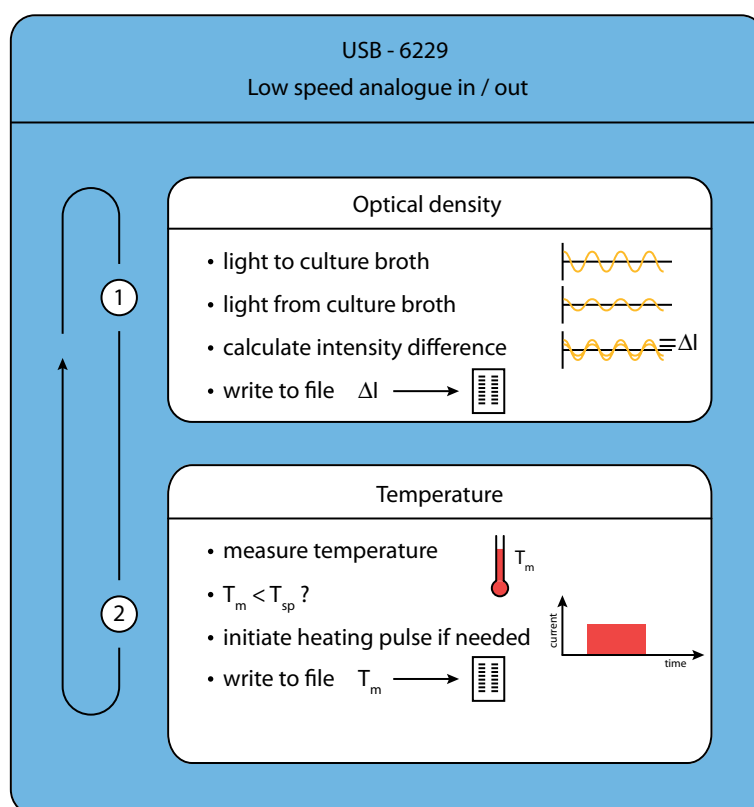


**Figure 3.15:** Schematic of the LabView program: low-speed part

Both analogue parts communicate with the digital part (Fig. 3.16 of the USB card). This is needed to interact with valves (to open/close the gas flow for pH control) or relays (switch on electricity for heating). Specifically the temperature loop switches the heating current on/off and the pH control loop opens and closes the appropriate gas valves if needed.

The LabView program as displayed in Appendix H has not been operating reliably: Occasionally the software crashed ('blue screen')—a problem which could not be solved neither by KT computer support nor by National Instruments themselves. After two months of testing different operating systems and hardware setups the program is running again—the underlying reason however is still unknown. As 100% explainable and reliable behaviour is required for any 'productive' system this is not acceptable.



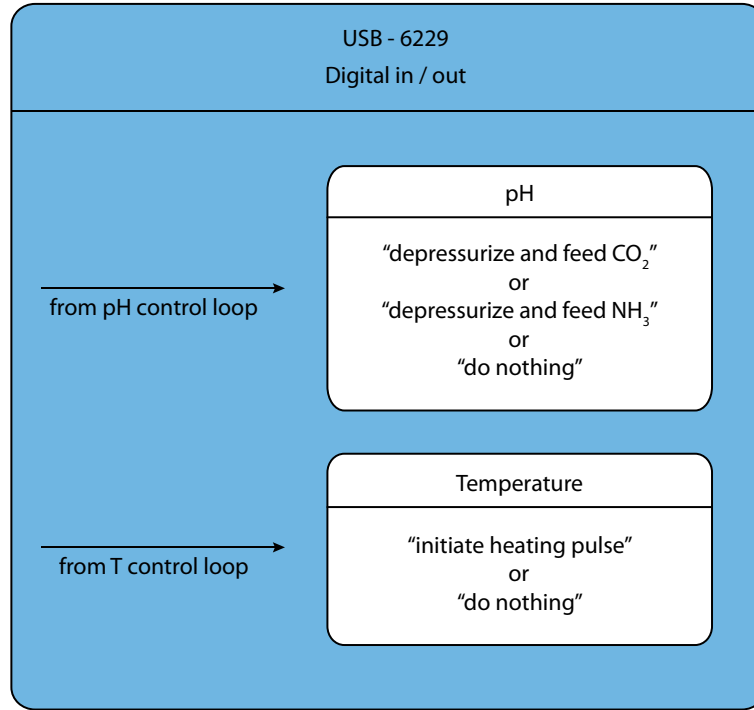


**Figure 3.16:** Schematic of the LabView program: Digital part

### 3.3.1 Lock-in Amplifiers

Many measurement methods suffer from a bad signal/noise ratio—the phase measurement used here is no exception. The fluorescent light coming from the sensor is very weak, and there are many potential disturbances, such as e.g. ambient light. In our specific case we have the advantage that our signal is located at a fixed frequency (4779 Hz for DO and 44 kHz for pH measurement) so that we can ‘tune in’ our measurement system to specifically look at that frequency. A lock-in detector does exactly what we want: It takes a periodic reference signal (the voltage we send to the LED) and a noisy input signal (the signal we get back from the fluorescent sensor) and uses a phase-sensitive detector (PSD) to extract only that part of the input signal which lies at the reference frequency (Fig. ). In order to fully understand how this works some mathematics are necessary (94; 95):

A prerequisite are the cosine (Eqs. 3.2–3.4) and the sine (Eqs. 3.5–3.7) rules which state that

$$\begin{aligned}\cos(a + b) &= \cos(a) \cos(b) - \sin(a) \sin(b) \\ \cos(a - b) &= \cos(a) \cos(b) + \sin(a) \sin(b)\end{aligned}\tag{3.2}$$

which added together give

$$\cos(a + b) + \cos(a - b) = 2 \cos(a) \cos(b)\tag{3.3}$$

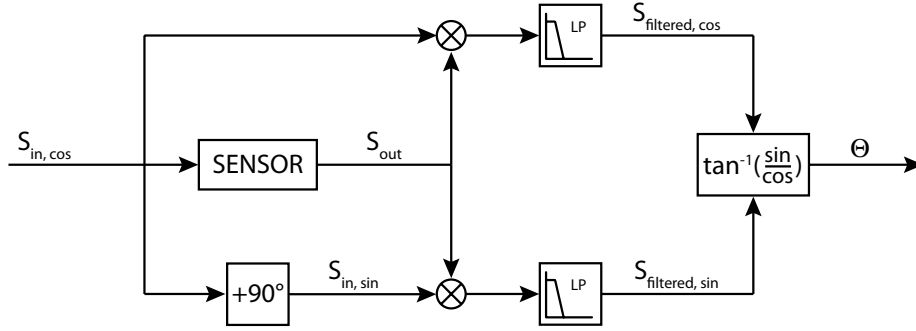


**Figure 3.17:** Schematic depicting the operating mode of the lock-in amplifier.

or equivalently

$$\cos(a) \cos(b) = \frac{1}{2} [\cos(a+b) + \cos(a-b)] \quad (3.4)$$

and

$$\begin{aligned} \sin(a+b) &= \sin(a) \cos(b) + \cos(a) \sin(b) \\ \sin(a-b) &= \sin(a) \cos(b) - \cos(a) \sin(b) \end{aligned} \quad (3.5)$$

which added together give

$$\sin(a+b) + \sin(a-b) = 2 \sin(a) \cos(b) \quad (3.6)$$

or equivalently

$$\sin(a) \cos(b) = \frac{1}{2} [\sin(a+b) + \sin(a-b)]. \quad (3.7)$$

Now consider an input signal sent to the sensor spot

$$S_{in} = A_{in} \cos(\omega_{ref} \cdot t) \quad (3.8)$$

The second signal to the PSD (which is the output signal we get back from the fluorescence sensor) has the same frequency as the reference signal but comes with a phase shift:

$$S_{out} = A_{out} \cos(\omega_{ref} \cdot t + \delta_{out}) \quad (3.9)$$

Unfortunately this output signal is covered with uniform broadband noise which itself consists of cosine waves at every possible frequency and every possible phase:

$$S_{out} = A_{out} \cos(\omega_{ref} \cdot t + \delta_{out}) + \sum_{\omega_{noise}} A_{noise} \cos(\omega_{noise} \cdot t + \delta_{noise}) \quad (3.10)$$

Multiplication of the input with the output signal gives

$$\begin{aligned}
S_{mult,cos} &= 2 \cdot S_{in} \cdot S_{out} \\
&= 2 \cdot A_{in} \cos(\omega_{ref} \cdot t) \cdot \left[ A_{out} \cos(\omega_{ref} \cdot t + \delta_{out}) \right. \\
&\quad \left. + \sum_{\omega_{noise}} A_{noise} \cos(\omega_{noise} \cdot t + \delta_{noise}) \right] \\
&= 2 \cdot A_{out} A_{in} \cos(\omega_{ref} \cdot t) \cos(\omega_{ref} \cdot t + \delta_{out}) + \\
&\quad 2 \cdot \cos(\omega_{ref} \cdot t) \sum_{\omega_{ref}} A_{noise} A_{in} \cos(\omega_{noise} \cdot t + \delta_{noise}) \\
&= A_{out} A_{in} \cos(\omega_{ref} \cdot t - \omega_{ref} \cdot t + \delta_{out}) \\
&\quad + A_{out} A_{in} \cos(\omega_{ref} \cdot t + \omega_{ref} \cdot t + \delta_{out}) \\
&\quad + \sum_{\omega_{noise}} A_{noise} A_{in} \cos((\omega_{ref} + \omega_{noise}) \cdot t + \delta_{noise}) \\
&\quad + \sum_{\omega_{noise}} A_{noise} A_{in} \cos((\omega_{ref} - \omega_{noise}) \cdot t - \delta_{noise}) \\
&= A_{out} A_{in} \cos(0 \cdot t + \delta_{out}) + A_{out} A_{in} \cos(2 \cdot \omega_{ref} \cdot t + \delta_{out}) \\
&\quad + \sum_{\omega_{noise}} A_{noise} A_{in} \cos((\omega_{ref} + \omega_{noise}) \cdot t + \delta_{noise}) \\
&\quad + \sum_{\omega_{noise}} A_{noise} A_{in} \cos((\omega_{ref} - \omega_{noise}) \cdot t - \delta_{noise})
\end{aligned} \tag{3.11}$$

Low pass filtering the signal then gives

$$S_{filtered} = A_{in} A_{out} \cos(\delta_{out}) + A_{noise@ref} \cos(\delta_{noise@ref}) \tag{3.12}$$

As the phase of the noise will vary randomly, this leaves us with

$$S_{filtered,cos} = A_{in} A_{out} \cos(\delta_{out}). \tag{3.13}$$

If the input signal additionally is phase shifted by  $90^\circ$  to

$$S_{in,shifted} = A_{in} \cos(\omega_{ref} \cdot t + 90^\circ) = A_{in} \sin(\omega_{ref} \cdot t) \tag{3.14}$$

then the multiplied and filtered signal will give

$$S_{filtered,sin} = A_{in} A_{out} \sin(\delta_{out}). \tag{3.15}$$

These two signals can then finally be used to calculate the magnitude

$$R = (S_{filtered,sin}^2 + S_{filtered,cos}^2)^{1/2} \tag{3.16}$$

and the phase

$$\Theta = \tan^{-1} \left( \frac{S_{filtered,sin}}{S_{filtered,cos}} \right) \tag{3.17}$$

where the phase is the value we are most interested in here. The amplitude of the signal also depends on other influences, e.g. the bending radius of the fiber or the fluorescent intensity of the sensor spot. The phase however stays the same no matter what (for a given system—a change of e.g. the fiber length might change the phase too).

# Results

---

## 4.1 Dissolved Oxygen

A good measure for the quality of the oxygen supply is the  $k_La$  which describes the transfer of oxygen (or another gas) into the reactor per unit volume. This is best measured with the dynamic gassing out method (9) where the culture liquid first is stripped of oxygen by e.g. flushing the aeration side of the membrane with nitrogen gas. Then, the aeration flow is changed to contain oxygen (e.g. pure oxygen or ambient air) and the rise of DO in the liquid is measured.

Out of this data the  $k_La$  is extracted as a first-order rate constant with

$$\frac{dC}{dt} = k_La \cdot (C_s - C) \quad (4.1)$$

where  $C_s$  is the saturation concentration (which depends on the temperature and on the composition of the aeration gas mixture used) and  $C$  is the concentration of oxygen. With the current system we estimated (using the least-squares method in Matlab) the average (over nine different measurements)  $k_La \approx 63 \pm 7 \text{ h}^{-1}$  which is in line with other microbioreactor systems (9) and the values measured in shake flasks, while still being below the values for bench-scale reactors which can be as high as  $247 \text{ h}^{-1}$  (62). This result averages measurements in different reactors and at different operating conditions (mixing speed and aeration flow rate & pressure). Thus the relatively high standard deviation of 11% can be seen as a worst case variation which can be significantly reduced by standardizing mixing and aeration conditions.

When running cultivations of *S. cerevisiae* at maximum growth rates with ambient air, this level of  $k_La$  is not enough to keep the oxygen level sufficiently high. However, we have also observed that the amount of gas transferred into the reactor can significantly exceed the uptake rate of the liquid: When flushing the aeration channel at significantly higher gas flow rates so much air was seen to diffuse into the reactor that the liquid was displaced. Also, this mechanism has been used actively for pumping (96; 97) or bubble-removal (97) purposes. We

thus expect that a careful step-wise increase of the aeration force will allow the  $k_L a$  to be increased significantly before liquid displacement takes place. This is in line with Zanzotto et al. who have shown that the transfer of oxygen into the system is primarily dependent on the oxygen uptake rate of the liquid phase and not on the diffusion through the membrane (9).

## 4.2 pH

We first evaluated the system behavior by conducting two different sets of titration experiments. In the first titration experiment,  $\text{CO}_2$  gas was dosed into a solution with a starting pH of 8 at a constant dosing pulse length of 1 s until the solution reached a final pH of about 6. In the second titration experiment, a reverse titration was made in which  $\text{NH}_3$  gas was dosed into the reactor (initial pH of the solution is 6) at a constant dosing pulse length of 1 s until the solution pH reached an end value of about pH 8.2. For both experiments, the tolerance limits of the controller were set to  $\pm 0.1$  of  $pH_{sp}$ , and the pressures of the  $\text{NH}_3$  and  $\text{CO}_2$  gas bottles were regulated to 1 bar and 2 bar, respectively. At given operating pressures, the  $\text{NH}_3$  and  $\text{CO}_2$  gas flow rates were measured to be 18 L/hr and 24 L/hr, respectively. The limited viable measuring range of the pH sensor spot does not permit us to perform experiments beyond pH 5.5 and 8. This is because beyond this pH range (lower than pH 5.5 and higher than pH 8) the sensitivity of the sensor spot levels out. The titration experiments were conducted in YPD medium (a common rich medium for *S. cerevisiae* cultivation) consisting of 10 g/L yeast extract, 20 g/L peptone and 20 g/L glucose monohydrate at room temperature. 1M hydrochloric acid (HCL) and 1M sodium hydroxide (NaOH) were used to adjust the pH of the solution to its desired starting pH value. By performing the experiment in YPD medium instead of distilled water, a more realistic and stable pH response from the process can be obtained due to the mild buffering capacity offered by the medium. This makes pH change slightly slower, thus large fluctuations in pH after the addition of base or acid are avoided.

From the response obtained, it is seen that upon dosing of  $\text{CO}_2$  gas the pH of the reactor content drops significantly at a very fast rate (indicated by a steeper slope of the curve,  $-dpH/dt_1$ ) until the solution pH reaches a pH value of about 6.5. From this point onward, the solution pH decreases slowly (indicated by the second slope of the curve,  $-dpH/dt_2$ ) until it reaches a final pH value of about 6.2 to 6.3. This behavior is explained from the acid-base equilibrium of the system and the reactions that took place when  $\text{CO}_2$  gas dissolved in the water: When  $\text{CO}_2$  dissolves in water, it instantly reacts with  $\text{OH}^-$  ions from the water to produce hydrogen ions,  $\text{H}^+$  and forms carbonic acid,  $\text{H}_2\text{CO}_3$  which then rapidly dissociates into bicarbonate,  $\text{HCO}_3^-$  ( $pK_{a(1)}$  at  $25^\circ\text{C} = 6.36$ ) and also into carbonate,  $\text{CO}_3^{2-}$  ( $pK_{a(2)}$  at  $25^\circ\text{C} = 10.32$ ) (98) which lowers the solution pH ( $\text{pH} = \log [\text{H}^+]$ ). In the mild basic region of pH 7.5–8, due to the excess of hydroxyl ions ( $\text{OH}^-$ ), and since the solution is not buffered (pH is nowhere near  $\text{CO}_2$   $pK_a$  values), a sharp reduction in solution pH upon the addition of  $\text{CO}_2$  was observed. However, in the slightly acidic region ( $\approx$  pH 6–6.5), the solution pH is very close to the  $pK_a$  of the first dissociation of  $\text{H}_2\text{CO}_3$  ( $pK_{a(1)}$  at  $25^\circ\text{C} = 6.36$ ). Around this pH the solution will be buffered and thus the rate of change of the pH decreases.

On the contrary,  $\text{NH}_3$  gas undergoes a much more straightforward reaction when it dissolves in water. It will react with the hydrogen ( $\text{H}^+$ ) ions from the water forming ammonium ions,  $\text{NH}_4^+$  and hydroxyl ions ( $\text{OH}^-$ ) (99). Further addition of  $\text{NH}_3$  gas will consume more hydrogen ( $\text{H}^+$ ) ions and thus, increase pH of the solution. Also, during the whole experiment, the working pH range (pH 6 to pH 8) was far away from the dissociation constant of ammonia ( $\text{p}K_a$  ( $\text{NH}_3$ ) at  $25^\circ\text{C} = 9.25$ ). This explains why increasing of solution pH following the dosage of  $\text{NH}_3$  gas into the reactor is indicated by only one slope,  $\text{dpH}/\text{dt}_3$ .

Based on the results of the titration experiment, we then tuned the on/off controller and performed a set-point tracking experiment to evaluate the controller performance in terms of its accuracy, and response time. Since the values of  $\text{pH}_{sp}$ , the tolerance limits and the gas bottle pressures have already been set, the tuning steps required were simplified, leaving dosing pulse length of each gas as the only controller parameter to be tuned. In our application, we adjusted the dosing pulse lengths of both gases to induce pH changes with the smallest magnitude possible. This may prolong the time needed to achieve the desired setpoint especially if the pH set point is changed significantly. However, small step changes ensure a more stable operation in the sense that large pH fluctuation around the set point can be avoided. Also, in cultivations the pH will seldom change very quickly, thus a slower but more precise control is to be preferred.

We adjusted the dosing pulse length of both gases manually depending on the working pH region of interest. In the mild basic region ( $\approx$  pH 7.5–8), the dosing pulse lengths of  $\text{CO}_2$  and  $\text{NH}_3$  gases were set to 250 ms and 100 ms, respectively. The dosing pulse length of  $\text{NH}_3$  gas was deliberately chosen to be a bit longer in order to counteract the sharp pH drop induced by the addition of  $\text{CO}_2$  gas in this pH range. In the near neutral region ( $6.5 < \text{pH} < 7.5$ ), dosing pulse lengths of both gases were set at 100 ms. For pH control around or below pH 6.5,  $\text{NH}_3$  gas dosing pulse length was retained at 100 ms but  $\text{CO}_2$  dosage pulse length was prolonged to 1000 ms. This is necessary in order to dissolve more  $\text{CO}_2$  such that the reaction equilibrium can be shifted to produce more carbonic acid,  $\text{H}_2\text{CO}_3$  instead of bicarbonate,  $\text{HCO}_3^-$  ions. By implementing these settings, we performed the set point tracking experiment by adjusting the pH of the reactor content at three different pH set point values ( $\text{pH}_{sp} = 7.5, 6.8$ , and  $6.3$ , respectively).

The results of the set point tracking experiment (Fig. 4.1) demonstrate that the pH on/off controller has a fast set point tracking capability for a series of downward (pH 6.8 to pH 6.3) and upward (pH 6.8 to pH 7.5) step changes in the pH set point. The results also show that by only adjusting the gas dosing pulse length accordingly, a controller accuracy as high as  $\pm 0.1$  of  $\text{pH}_{sp}$  can be achieved. The largest pH step change made was from a pH set point of 6.3 to a pH set point of 7.5, and in this case the rising time was approximately 6.5 minutes. During the pH step changes, only a short delay (less than a minute) was recorded. This is probably due to a high gas transport rate through the PDMS membrane and good mixing via the micro-impeller incorporated in the reactor which allow for a fast response. In the current setup, adjustment of the dosing pulse lengths has to be done manually. However, optimal settings for the pulse length can be programmed in the software controlling the setup, such that the settings are changed automatically when the pH set point value is altered.

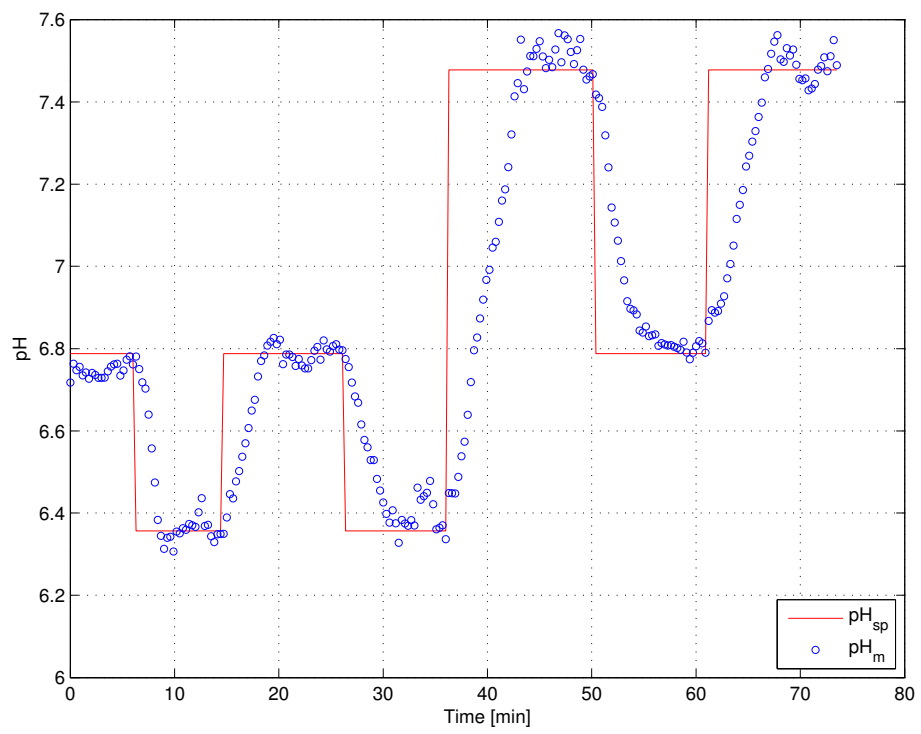


**Figure 4.1:** Set point tracking experiment for the pH control algorithm.

### 4.3 Optical Density

Two measurements are done to properly determine OD in the microbioreactor. Both the intensity of the reference light beam  $I_{ref}$  and that of the measurement light beam  $I_{meas}$  are measured with photodetectors and give voltage values. The effective intensity of the light passing through the broth is then

$$I_{eff} = \frac{I_{ref}}{I_{meas}}$$

which increases for decreasing values of  $I_{meas}$  which corresponds to a denser broth. The voltage ratio then behaves proportionally to the concentration of cells in the broth (Fig. 4.2) within a certain density range. The linear range is determined by the intensity of the incoming light, the sensitivity of the photodetector and the light path length in the broth. With the setup described here the linear range lies between 0–20 g<sub>DW</sub>/L.

Care has to be taken to eliminate both the influence of ambient light (day vs. night) and electrical lighting sources (50 Hz influence). For this purpose the measurement light was modulated with a sine of 47 Hz—with this the real signal can be separated from both disturbances by the appropriate filtering.

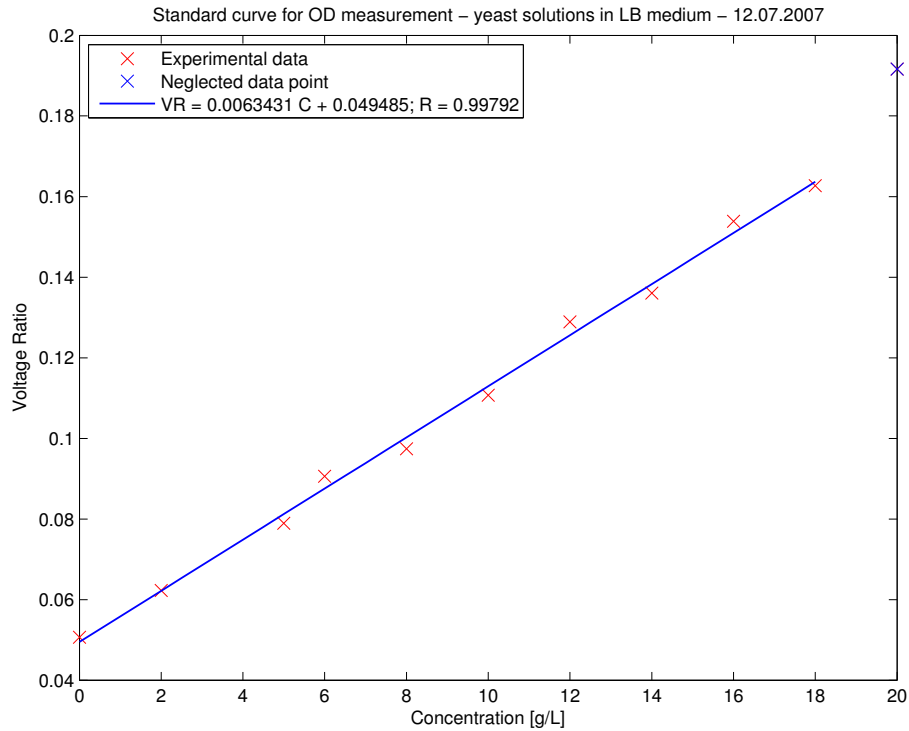


**Figure 4.2:** Calibration curve for the OD of yeast cells suspended in LB medium. OD correlates linearly with the measured voltage ratio.



## 4.4 Mixing

We have currently used three indirect indications to quantify the quality of the mixing system: a) the continuous measurement of OD, b) mixing tests with dye and c) visual inspection of the reactor for sedimented cells. For a), baker yeast was dissolved in pure water (without substrate) and the optical density of the broth measured over time. These measurements showed that the measured optical density stays constant over a period of several hours, which is long enough to prove that no sedimentation of cells is taking place.

In addition, specific mixing tests (b) were performed with bromothymol blue solution (Bromothymol Blue solution, Sigma-Aldrich, St. Louis, MO, USA). With this method mixing can easily be observed as an addition of base induces a color change from yellow to blue; Addition of acid then reverses the color change. After the addition of base at 500 rpm, the solution again has a uniform color after approximately 1.2 sec (Fig. 4.3). This forms a clear indication that the reactor contents is well-mixed.

Finally, the reactor was inspected for the presence of sedimented cells (c) after a cultivation with baker's yeast that lasted several days and was mixed with 600 rpm. After the cultivation the membrane on top of the reactor was cut away and the liquid was slowly removed. No sedimented cells could be observed in the reactor, proving that mixing in the reactor is sufficient.

## 4.5 Temperature

When a voltage is applied to the embedded wire, a current will flow through the wire and thus increase its temperature (100). The power input by the heater,  $P$  [W] is a function of the voltage supplied,  $V$  [V] and the current,  $I$  [A]. Heat supplied to the system (reactor content) is measured as the energy generated (or dissipated) by the flowing current over a certain period of time. It is a function of heater power input,  $P$  [W] and the total heating time,  $t$  [s] and was calculated as  $E = V \cdot I \cdot t$  [J].

Fig. 4.4 illustrates the response of the on/off controller at set point value of  $T_{sp} = 50$  °C, when the power input was increased gradually from 0.32 W to 1.43 W. An increase of the heater power input accelerates the heating process (the rise time,  $t_r$  shortened from 5 min to 2.55 min when the power input was increased from 0.73 W to 1.43 W), as expected, and thus the temperature of the reactor content rises faster. It was also found that sufficient heating was not provided when the heater power input was set at 0.32 W. This behavior is explained because the heater (resistance wire) will only provide a fixed rate of heat input during each pulse (on/off controller), while the rate of heat loss from the system increases as the temperature rises. In order to compensate for the heat loss at a higher operating temperature, it is necessary to increase the heat input,  $E$  (either by prolonging the heater pulse length,  $PL$  or by supplying a higher voltage,  $V$ ). Any combinations of voltage and time should in the end yield similar total amounts of heat input (Fig. 4.5). Regardless of the power input supplied (0.73 W or 1.43W) or the total heating time needed to reach the temperature setpoint of 50 °C, the same amount of heat input,  $E$  was provided which was 176.8 J (area under curve).

A practical constraint is that the maximal power input is limited according

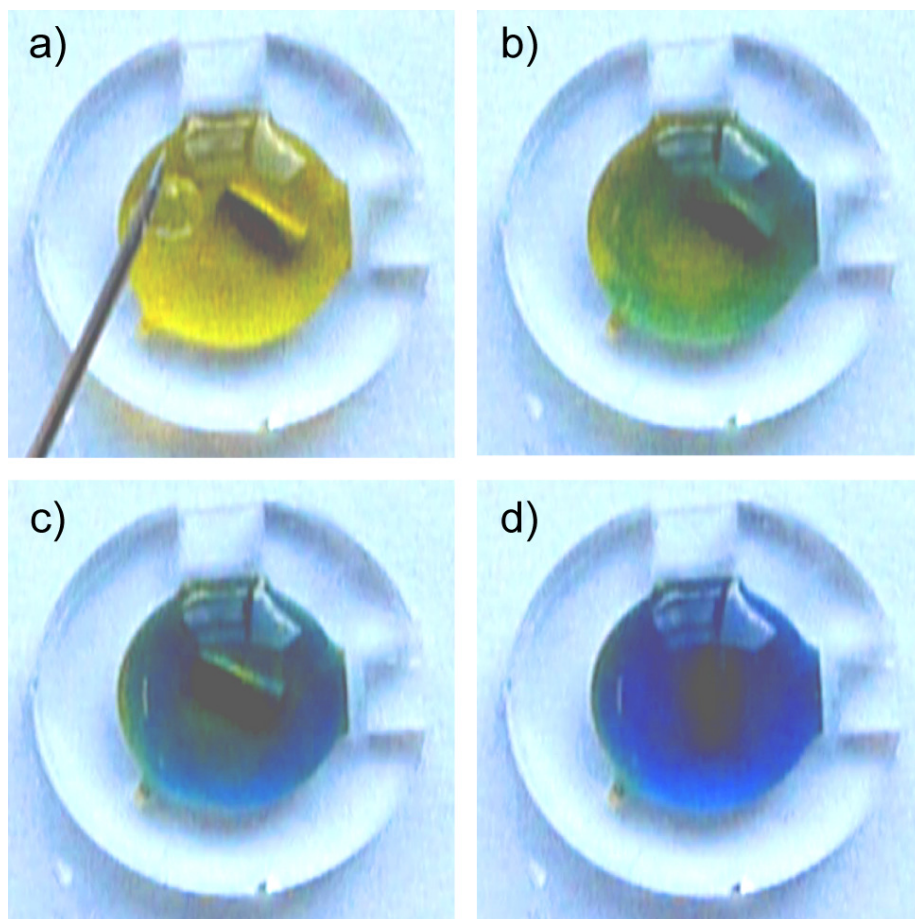


**Figure 4.3:** Mixing in the microbioreactor at 500 rpm visualized with bromothymol blue solution. In a) at time  $t = 0$  a drop of base is added, in b) and c) pictures were taken 0.4 sec and 0.8 sec, respectively, after the addition of base, and mixing is proceeding. Finally, in d) at  $t = 1.2$  sec the reactor contents are thoroughly mixed.

to the type of resistance wire as too large a current will overheat the wire. The wire current handling capacity depends on its length,  $L$ , cross-sectional area,  $A$ , wire resistivity,  $r$  and the heating time. Also, care has to be taken at high heating powers as the controller reacts much more sharply which can lead to overshoot.

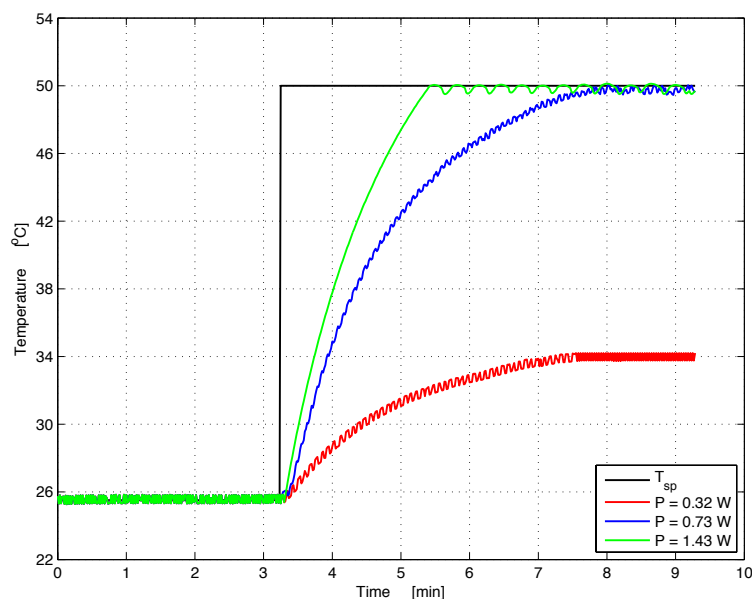


**Figure 4.4:** Faster temperature rise with increasing heating power

When controlling temperature, several aspects are important: Firstly a certain set point has to be held with sufficient accuracy; Secondly the system has to be able to quickly change the temperature of the broth and thirdly the system has to be robust with respect to disturbances. Depending on the characteristics of the controller chosen (power input, heater pulse length and the desired temperature set point), the temperature can be controlled to within  $\pm 0.1$  °C of the set point value. The results (4.6) demonstrate the fast set point tracking capability of the controller for a series of upward step changes in the temperature set point. Almost no delay was observed when temperature was regulated from one set point to another, which is probably due to the high surface area to volume ratio,  $S/V$  ( $1500 \text{ m}^{-1}$ ) in the microbioreactor allowing for a fast thermal response. The largest temperature step from room temperature ( $\approx 23$  °C) to 50 °C only takes about 2.4 minutes. Whilst the heating process is fairly rapid (heating rate  $\approx 0.25$  °C/s), the cooling of the reactor is rather slow. This is due to the fact that there is no active cooling foreseen on the reactor, cooling thus merely depends on convective heat transfer to the surroundings. Room temperature is only reached asymptotically as the driving force is the temperature difference itself.

The disturbance rejection capability of the controller was evaluated by deliberately perturbing the system from its steady-state at  $T_{sp} = 50$  °C. The perturbation was induced by injecting a pulse of distilled water at room tem-

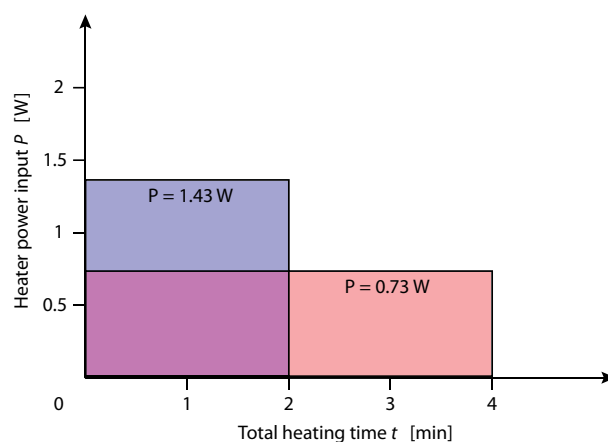


**Figure 4.5:** The total heating energy applied (derived through the measurement of voltage and current) at different voltages is constant.

perature ( $\approx 23\text{ }^{\circ}\text{C}$ ) at 15 mL/hr for 6 s. This disturbance (in which 25% of the reactor content was flushed out) creates a sudden cooling of the reactor content, and a transient response is obtained when the controller drives the system back to the temperature set point (Fig. 4.7). At a temperature set point of  $50\text{ }^{\circ}\text{C}$ , the reactor temperature drops by  $2.5\text{ }^{\circ}\text{C}$  and it took less than 30 s to recover from this disturbance. The results obtained show good disturbance rejection capability of the proposed on/off temperature controller. The temperature sensor is also positioned close enough to detect any rapid temperature change of the reactor content with a minimal time lag.

Another requirement is an equal temperature distribution in the microbioreactor. The temperature gradient in the reactor chamber itself was checked by measuring the temperature difference between the top and the bottom of the reactor chamber upon continuous heating at constant voltage supply of 0.6 V by additionally inserting a temperature sensor into the broth. A slightly lower temperature ( $\Delta T < 0.5\text{ }^{\circ}\text{C}$ , Fig. 4.8) between the bottom and the top surface of the reactor chamber was due to the direct exposure to the surroundings and probably represents a worst case. When the membrane covers the reactor the cooling effect is bound to be lower. If this temperature difference should prove to be a problem, then the aeration air could be preheated, e.g. with a second set of heating wires in the air inflow channel.

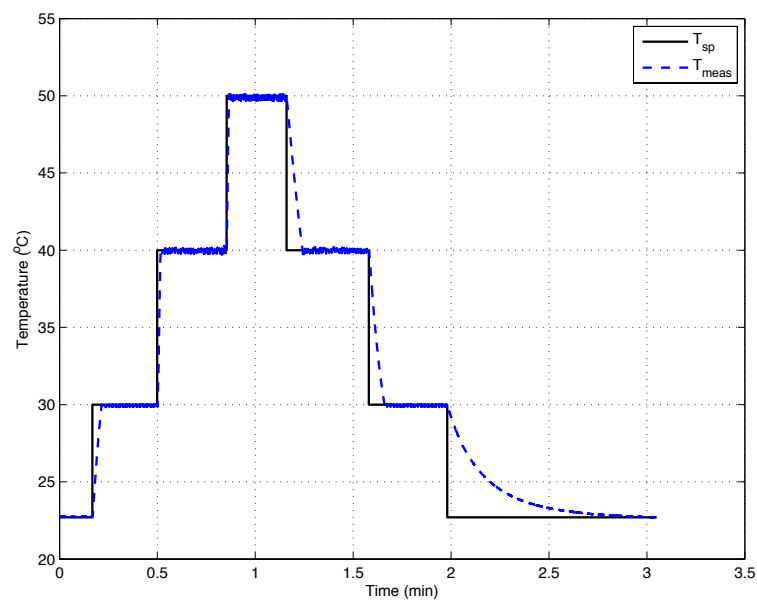


Figure 4.6: Stepping up/down of the reactor temperature

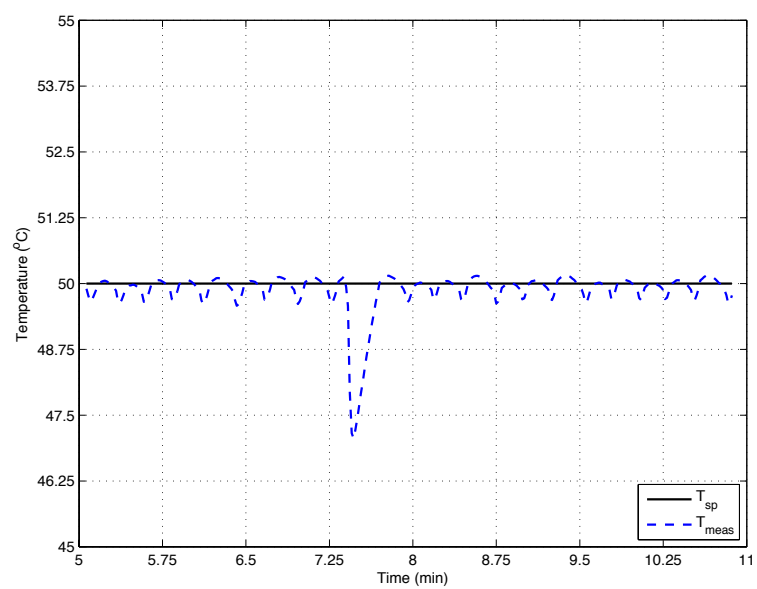
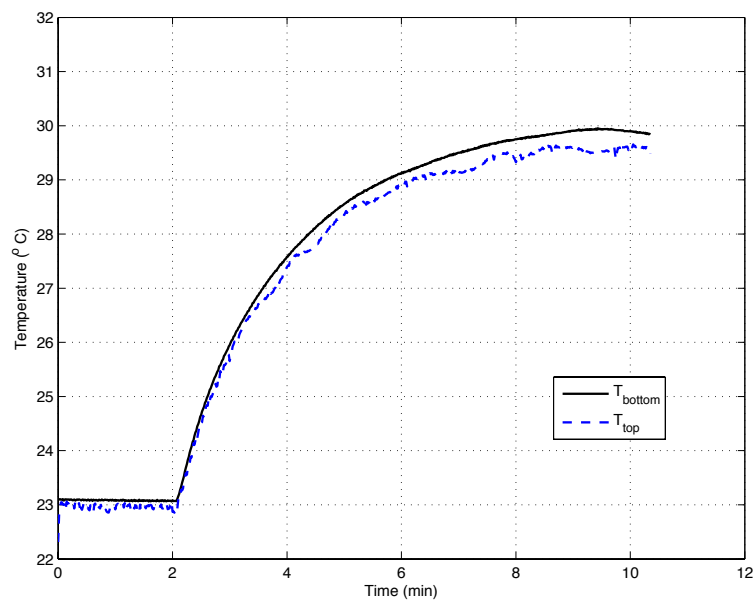


Figure 4.7: Control system response to a disturbance in temperature



**Figure 4.8:** Temperature difference between different locations inside the reactor volume



# Cultivations

---

Once the microscale reactor is physically fabricated and all the measurement & control algorithms are established the time is ripe for cultivations of microbial cells. As the thesis should also be readable by people without a biological background, I briefly describe the basics of cultivation technology (operation modes, equations etc.). Readers with a biological background might want to proceed directly to chapter 5.3. After the introduction, I give some information about the organism chosen followed by the results for shake flask & bench-scale cultivations. Finally, the microbioreactor results are compared to the larger-scale cultivations and the difficulties connected with cultivations in microbioreactors are discussed.

## 5.1 Cultivations of microorganisms

There are three basic modes of operation when cultivating microorganisms:

- In a batch process, all the components needed (apart from oxygen and the reagent(s) needed for pH control) are filled into the reactor which is then sealed. No further substrate is added or removed from the reactor for the duration of the cultivation. If needed additional substances as e.g. an inducer for the production of protein can be added during the cultivation.
- A fed-batch process allows for the addition of material (most often nutrients) but no product stream removal.
- Continuous cultivations have both in- and outflow of material—if the flow rates are the same then the process could (at least in theory) be operated indefinitely (chemostat). Problems here are the risk of contamination as well as the chance of developing mutations.

The ability to run continuous cultivations in the microbioreactor is very enticing as it would allow for



- running of steady-state cultivation (chemostat),
- quick and controlled changes in operating conditions (e.g. pH). Together with online monitoring this offers the possibility of observing the cell metabolism change.
- running of multiple step changes without having to set up a new cultivation.
- simulating the conditions a cell might experience in a production scale reactor where some cycling between different operating conditions is common (due to the gradients present in such reactors) .

### 5.1.1 Batch operation

Batch processes work in a closed system. In the beginning of the process nutrients are added and the products are harvested in the end of the process. During operation, no nutrients are added and no products are removed. However, in a typical aerobic batch fermentation oxygen has to be introduced continuously for aeration while carbon dioxide and other off-gases are removed. For pH control acid or base is added.

In a batch cultivation the inoculated culture will pass through four phases of cell growth (Fig. 5.1). Immediately after inoculation there is a period during which no apparent cell growth takes place. This phase is referred to as the *lag phase* where the cells adapt to the new surroundings.

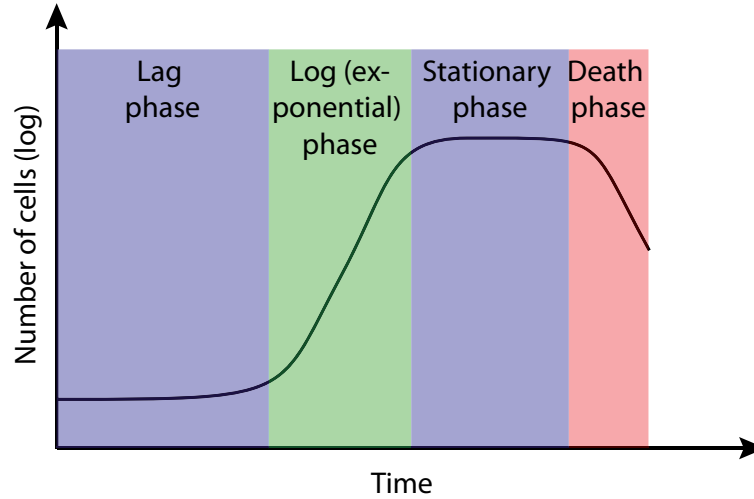


**Figure 5.1:** Growth of a typical microbial culture in batch conditions.

Following the lag phase the growth phase, also called the *log* or *exponential phase*, starts. This second phase is characterised by the exponential increase in the number of cells due to a higher, but constant specific growth rate.

$$\frac{dx}{dt} = \mu x \quad (5.1)$$

where  $x$  is the concentration of viable biomass [g/L],  $t$  is the time [h] and  $\mu$  is the specific growth rate [h<sup>-1</sup>].

Integration of equation 5.1 gives:

$$x_{(t)} = x_0 \cdot e^{\mu t} \quad (5.2)$$

where

$x_0$  is the original biomass concentration at the start of the exponential growth phase [g/L],  
 $x_t$  is the biomass concentration after the time interval  $t$  [g/L].

Applying the natural logarithm to equation 5.2 gives:

$$\ln x_t = \ln x_0 + \mu t. \quad (5.3)$$

Thus, during the exponential phase a plot of the natural logarithm of biomass concentration against time should yield a straight line; the slope of the line being equal to  $\mu$ . Here the cells are growing at the maximal specific growth rate unless limited by e.g. a lack of nutrients.

The doubling time is calculated by:

$$t_d = \frac{\ln 2}{\mu} \quad (5.4)$$

where

$t_d$  is the doubling time [h],  
 $\mu$  is the specific growth rate [h<sup>-1</sup>].

As soon as essential nutrients in the culture medium become depleted or inhibitory products accumulate, the growth rate of the cells slows down and the cells enter the third phase, the stationary phase. In stationary phase no further cell growth occurs. However, the stationary phase in a batch culture is a misnomer concerning the physiology of the organism. The reason for this is that the population is still metabolically active during this phase and consequently the cells may produce products called secondary metabolites. These secondary products are usually not produced during the exponential phase.

The decrease of the growth rate and the cessation of growth due to the depletion of substrate may be described by the relationship between  $\mu$  and the residual growth-limiting substrate. Equation 5.5 is known as the Monod equation, and is one of the most often used explanations to represent the dependence of  $\mu$  on a limiting substrate. More complex explanations are needed in case of substrate or product inhibition, or in case multiple limiting substrates need to be considered.

$$\mu = \frac{\mu_{max} \cdot s}{(K_s + s)} \quad (5.5)$$

where

$s$  the residual substrate concentration [g/L],  
 $\mu_{max}$  is the maximum specific growth rate [h<sup>-1</sup>],  
 $K_s$  is the substrate utilization constant [g/L].

$K_s$  is numerically equal to the substrate concentration for which  $\mu = \frac{1}{2}\mu_{max}$  and is a measure of the affinity of the organism for its substrate. If the organism has a very high affinity for the limiting substrate ( $K_s$  is low), the growth rate will not be affected until the substrate concentration has declined to a very low level. Therefore the growth deceleration phase would be quite short. On the other hand, if the organism has a low affinity for the substrate ( $K_s$  is high), the growth rate will already be negatively affected at a relatively high substrate concentration; The deceleration phase for such a culture would be relatively long.

In the end of the fermentation the biomass concentration is at its highest and therefore, the decline in substrate concentration will be very rapid. Thus, the time period during which substrate concentration is close to  $K_s$  is usually very short.

Reactants are converted to products; the extent to which reactants are converted is expressed by the reaction yield. The term *yield* describes the amount of product formed or accumulated per amount of substrate consumed. The yield coefficient is generally expressed as:

$$Y_{GF} = \frac{\Delta F}{\Delta G} \quad (5.6)$$

where

$Y_{GF}$  is the yield factor,  
 $\Delta F$  is the mass or moles of F produced,  
 $\Delta G$  is the mass or moles of G consumed.

## 5.2 Model system *S. cerevisiae*

The model system chosen for this work is the yeast *Saccharomyces cerevisiae*, which is to be grown under aerobic culture conditions. *S. cerevisiae* cells are unicellular organisms that have an ellipsoidal shape, ranging from 5 to 10  $\mu\text{m}$  at the large diameter and 1 to 7  $\mu\text{m}$  at the small diameter (101). Yeast cells show most of the structural and functional features which are also observed in higher eukaryotic cells. Therefore, yeast is an ideal model for eukaryotic cell biology. Furthermore, yeast is widely applied in industrial biotech processes both in traditional processes such as beer and baker's yeast production and in more modern pharmaceutical processes e.g. for heterologous insulin production. The main difference of yeast cells to mammalian cells concerns the cell wall. Yeast cells are surrounded by a rigid cell wall and develop bud scars during cell division. The vacuole, which is one of the compartments of a yeast cell, corresponds to lysosomes in higher eukaryotic cells (102).

The inherent advantages of the yeast expression system include its high efficiency in terms of short doubling times, high cell densities, high yields and low fermentation costs. Yeast cells can be grown in large scale with simple nutritional demands. Additionally, yeast cells can express correctly folded proteins directly into the medium, which brings several conveniences for the protein purification. Yeast cells are surrounded by a very rigid cell wall which makes it possible to use any kind of bioreactor regardless of stirring and shaking mechanisms. In addition, the yeast is regarded as one of the most safe and simple

expression systems in use. In conclusion it can be said that the yeast expression system combines the advantages of a eukaryotic expression system with those of a bacterial one. Therefore, it is a very convenient system for industrial applications.

The two important physiological phenomena (103) in yeast are the Crabtree effect and glucose repression.

**Glucose repression** (also denoted carbon catabolite repression) is when glucose or other rapidly metabolized carbon sources represses the expression of genes responsible for utilization of other carbon sources. In practice, this means that *S. cerevisiae* in a sugar mixture preferentially will utilize glucose and thereafter other sugars in a sequential order, with a lag phase in between. From an industrial point of view, this is an unwanted phenomenon as the consumption time of the medium is prolonged—a simultaneous use of sugars would be preferential as industrial media usually are composed of sugar mixtures.

**Crabtree effect:** Baker's yeast is produced by aerobic cultivation of *S. cerevisiae*. At these growth conditions the yeast may express a mixed metabolism, with both respiration (breakdown of glucose oxidatively to cells and carbon dioxide) and fermentation (breakdown of glucose oxido-reductively to cells, ethanol and carbon dioxide) being active. At high glucose uptake rates there is a limitation in the respiratory pathway, which results in an overflow metabolism towards ethanol. This is referred to as the Crabtree effect. The exact location of the limitation has not been identified, but it is probably at the pyruvate node, and, additionally, repression of the oxidative metabolism when the glucose concentration is increased also plays a role. In other words, the effect of increasing glucose beyond a certain critical concentration/flux results in a diminished ability of the yeast to oxidize glucose. Hence in a aerobic batch cultivation of *S. cerevisiae* with glucose one sees two phases: First a phase with growth on glucose where ethanol is produced in addition to biomass and then after glucose depletion a phase with growth on ethanol (as also described in chapter 5.3).

The glucose uptake rate, which results in initiation of fermentative metabolism is often referred to as the critical glucose uptake rate, and the critical glucose uptake rate is found to be dependent of the oxygen concentration. Thus, at low dissolved oxygen concentrations the critical glucose uptake rate is lower than at high dissolved oxygen concentrations (and clearly at anaerobic conditions there is only fermentative metabolism corresponding to the critical glucose uptake rate being zero).

### 5.3 Bench-scale and shake flask cultivations: data for benchmarking with microscale

Whilst the goal of running reproducible cultivations in the microbioreactor is important, the results have to be put into context with cultivations done at larger scales. For benchmarking purposes we have therefore run cultivations both in shake flasks and in bench-scale reactors which provide data for cultivations under the same conditions (such as medium, pH, temperature) as they were run in the microbioreactor. It is then interesting to see how the results can

be transferred between scales, and what the limiting factors are.

**Preparation of inoculum:** The inoculum for the bench-scale reactors, the shake flasks and the microbioreactor were all prepared as follows: A colony of wild type yeast strain (CEN.PK 113-7D) was taken from the agar plate and was added to 100 mL of YPD media (20 g/L glucose, 10 g/L peptone and 5 g/L yeast extract) supplemented with 50  $\mu\text{g/L}$  Streptomycin (Streptomycin solution, 1 mg/mL in 1mM EDTA 85886, Sigma-Aldrich) and 50  $\mu\text{g/L}$  of antifoam (Antifoam 204, A6426, Sigma-Aldrich). This was then incubated overnight in a shake flask (30 °C, 700 rpm) until the cells reached  $\text{OD}_{600} = 10$ . The broth was then diluted with medium to get a starting OD of 0.1 accordingly.

Contrary to normal practice the medium had been supplemented with streptomycin to significantly reduce the risk of contamination, especially in the microbioreactor. Tests with and without streptomycin were carried out in shake flasks (data not shown) and did show, as was to be expected, that streptomycin did not affect the growth of the yeast cells. Thus, fermentations with and without streptomycin can for our purposes be considered to be identical.

**Batch cultivations in bench-scale reactors:** Bench-scale cultivations currently are those that offer the most information about the cultivation due to the fact that a) more measurements are available per default and b) the large volume allows HPLC analyses to be run on samples during the cultivation. The cultivations were run in Biostat B fermentors present at the Department of Systems Biology, with a starting volume of 1 L. The broth was stirred at 600 rpm, and the aeration rate was set to 1 vvm.

The cells started to grow immediately after inoculation; The lag phase was virtually inexistent. In the first 8 hours the cells consumed all the glucose (Fig. 5.2) leading to an increase in  $\text{CO}_2$  (Fig. 5.3) and ethanol concentration. Accordingly, the concentration of dissolved oxygen in the reactor dropped steadily until  $t = 8$  hours where the cells shifted metabolism and started consuming the ethanol they had produced earlier. This short break in growth allowed the dissolved oxygen level to increase slightly before it again started decreasing until it was completely depleted at 13 hours. After 20 hours the cells had consumed all the ethanol present and thus stopped growing. Due to the large number of cells present in the system, ethanol depletion took place very suddenly which corresponds to the sharp rise in dissolved oxygen concentration at 20 hours. The average growth rate on glucose was  $0.47 \text{ h}^{-1}$ .

**Shake flask cultivations:** Shake flasks generally have less instrumentation than bench-scale reactors, and their aeration characteristics are much more unspecified. Therefore no  $\text{O}_2$  and  $\text{CO}_2$  measurements could be done. Also, as the maximal growth rate of  $0.41 \text{ h}^{-1}$  (Fig. 5.4) is significantly smaller than that in the bench-scale reactor it has to be assumed that the cells are not being aerated optimally. The underlying fundamental mechanisms however are the same: In a first phase glucose is being consumed and ethanol produced, when all the glucose has been used the cells shift metabolism and start using ethanol (Fig. 5.5). A comparison with the bench-scale data supports the lower growth rate measured: Whilst glucose is depleted in the bench-scale reactor around  $t = 8$  hours, it takes approximately 4 hours longer in the shake flask. The same observation

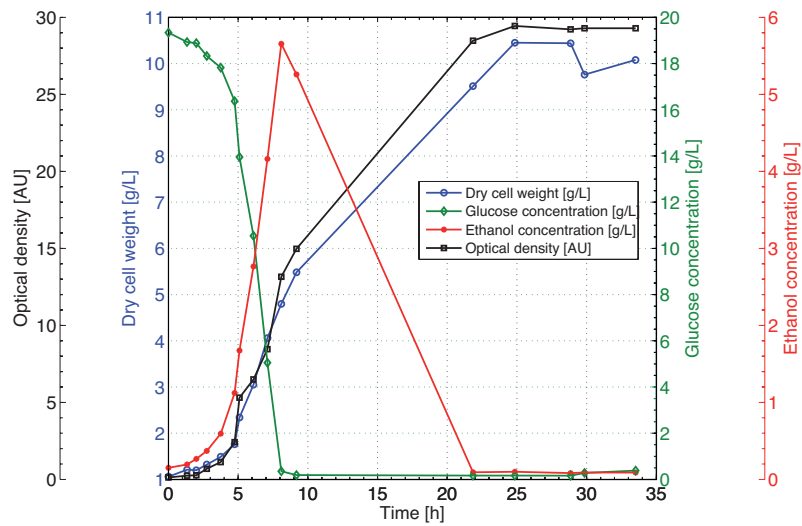


**Figure 5.2:** Biomass, glucose and ethanol concentrations during a batch cultivation of *S. cerevisiae* in a bench-scale reactor.

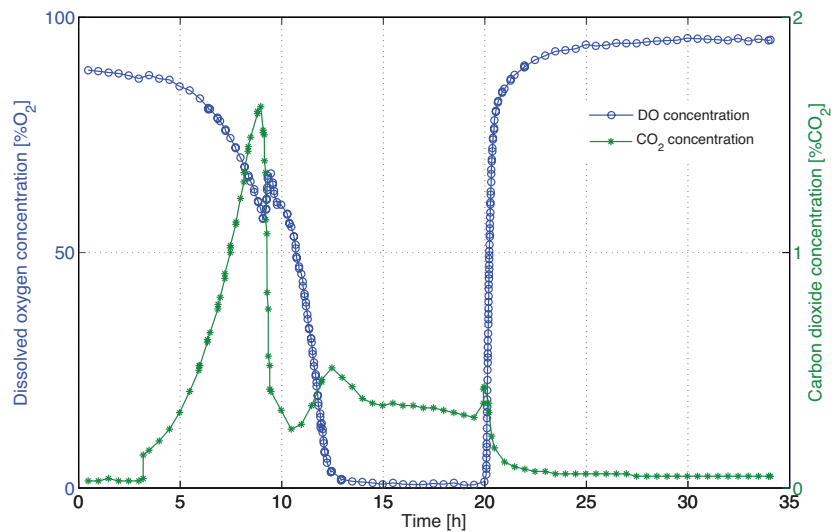


**Figure 5.3:** Oxygen and CO<sub>2</sub> concentrations during a batch cultivation of *S. cerevisiae* in a bench-scale reactor.

can be made with the production of ethanol.

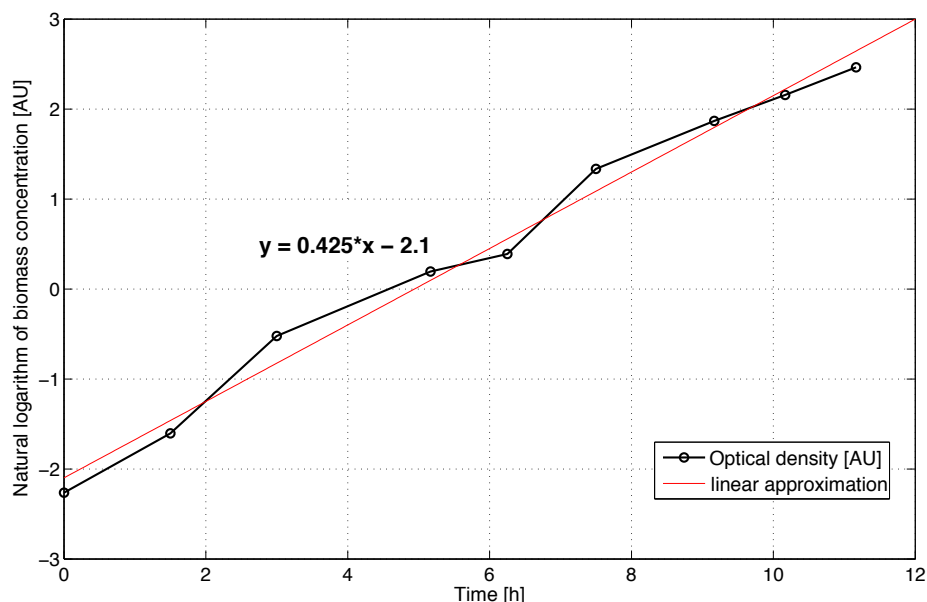


**Figure 5.4:** Biomass concentration during a shake flask cultivation of *S. cerevisiae*.

## 5.4 Cultivations in the microbioreactor and their comparison with the larger scale cultivations

Cultivations corresponding to those in the shake flasks and the bench-scale reactors were also performed in the microbioreactor. The resulting profiles of growth and DO over time were similar to those seen for lab/bench-scale reactors. A representative time course is shown in Fig. 5.6. After a short lag phase the cells started to grow exponentially until approximately 13 hours, when they enter stationary phase, most likely due to glucose depletion. A drastic decrease was seen for the DO level already around  $t = 7$  h, where  $OD_{600} \approx 8$ , which deviates from bench-scale cultivations where oxygen first is depleted at higher cell densities. After several hours (here approximately 20 hours) of reduced oxygen concentration the cells have used both the glucose and the ethanol and thus stop growing. Their oxygen demand stopped radically which led to a subsequent increase of the dissolved oxygen concentration in the broth (here at 28 hours).

It has to be assumed that the aeration is insufficient for aerobic growth, this can be seen in the reduced maximal growth rates: Calculations based on three independent batch cultivations gave a maximum specific growth rate of  $0.3 \text{ h}^{-1}$  (104) for growth on glucose. This is roughly 36% lower than the bench-scale reactor and 27% lower than the shake flasks. A calculation of a ‘fake’ biomass yield, in this case (due to the lack of cell mass measurements in the microbioreactor) described as ‘end OD [AU]’ per glucose for the three scales

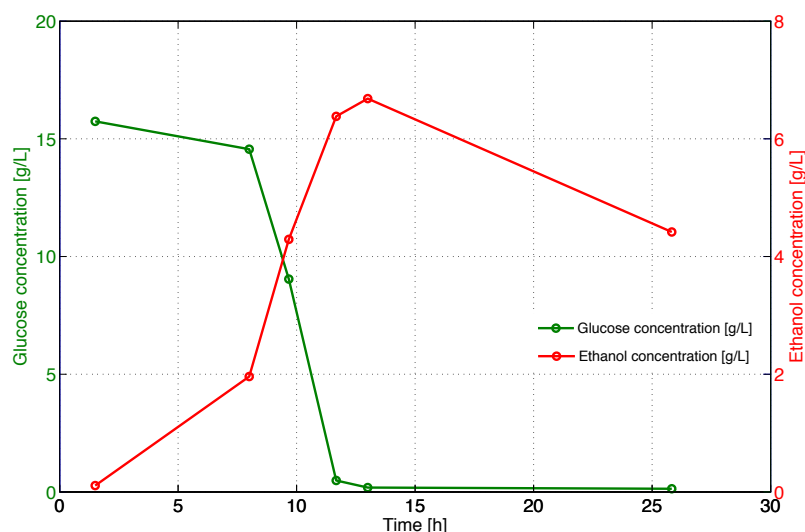


**Figure 5.5:** Glucose and ethanol concentrations during a shake flask cultivation of *S. cerevisiae*.

gives 0.62, 0.65 and 0.42 for the bench-scale reactors, the shake flasks and the microbioreactor respectively.

Oxygen supply may be improved either by exchanging the air with oxygen-air mixtures as discussed in the oxygen transfer section (Ch. 4.1) or by increasing the gas flow rate. Actually, the cultivations presented here were done with an earlier version of the reactor which did not have an aeration layer. Therefore, only the static atmosphere around the reactor was available for aeration. With the present aeration channel, gas can actively be flushed over the membrane which will obviously increase the diffusion rate into the reactor. This had become apparent *in extremis* when the gas flow rate over the membrane was so high that the diffusion pressure actually forced liquid out of the reactor; As a result the reactor become partly filled with an air bubble. Finding the flow rate which is ‘just right’ is one of the next steps which have to be taken—recent experiments show that a rate of around 5 mL/min (which would correspond to flushing the whole reactor chamber 50 times per minute, or nearly once per second) does not produce bubbles in the reactor.

Overall, the system gives reasonable readings; temperature control kept the broth within  $\pm 0.2$  °C of the set point and the mixing system obviously kept the cells in suspension throughout the whole cultivation as no sedimented cells could be observed at the end of the cultivation. This shows that the basic traits of the reactor function as they are supposed to. Whilst wall-growth of the organism may be an issue for certain organisms, no significant growth could be observed while running cultivations with yeast (*S. cerevisiae*) that lasted for several days; thus no specific precautions have been taken. However, techniques to modify the surface properties of PDMS exist (105), so it should be possible to also adapt this reactor design to more adherent organisms.



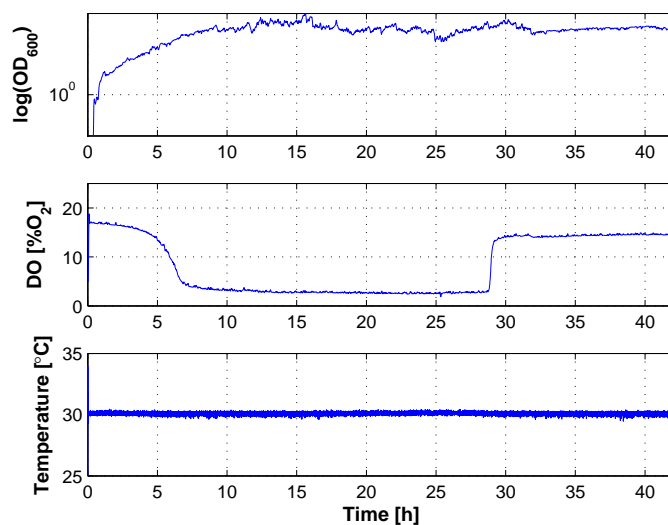


**Figure 5.6:** Optical density, dissolved oxygen and temperature during a batch cultivation of *S. cerevisiae* in the microbioreactor.

A comparison between the bench-scale reactor, the shake flasks and the microbioreactor reveals the slightly better growth conditions in the standard lab-scale reactors (Table 5.1) than in the microbioreactor.

**Table 5.1:** Comparison between the different reactor scales

	Bench-scale	Shake flask	Microbio- reactor
Time for glucose depletion [h]	8	12	-
Time for max. ethanol conc. [h]	8	13	-
Time for oxygen depletion [h]	13	-	7
Time for oxygen recovery [h]	20	-	28
Fake 'biomass yield'	0.62	0.65	0.42
Maximal growth rate [ $h^{-1}$ ]	$0.47 \pm 0.0$	$0.41 \pm 0.01$	$0.30 \pm 0.08$

#### 5.4.1 Standardization of microscale cultivations

It is here that one of the major difficulties in the application of the microbioreactor becomes apparent: Whilst the standard operation procedures for both bench-scale reactors and shake flasks are well known they are virtually in-existent for microbioreactors. This lack of well-validated standardization makes the results of different cultivations difficult, if not impossible to compare. This is illustrated in Fig. 5.7 where the 'official' starting conditions for the individual cultivations had only differed in starting OD. It can be seen that the time during which oxygen is depleted varies a lot between cultivations. Also, these

time points do not correlate with the starting OD of the cultivation and thus cannot be attributed to the varying number of cells present. This shows that the standard operation procedure is not yet good enough.

One example to illustrate this question of ‘optimal standard operation procedure’ is the question of ‘how to inoculate the reactor?’. One could imagine several approaches to this problem:

- a) Fill the reactor with medium, and then inject a very small quantity of inoculum, analogous to inoculation in a bench-scale reactor,
- b) fill the reactor with medium, and then inject cultivation broth of the desired starting OD to completely fill the reactor and replace the liquid present in the reactor before or
- c) fill the empty reactor with cultivation broth of the desired starting OD to completely fill the reactor.

All three methods have their advantages and drawbacks: For a) the very small quantity of the inoculum itself is the problem: How can one be sure to really precisely inject the amount needed? And, as the inoculum is injected into the reactor, some liquid has to leave the reactor (constant volume)—which composition does this liquid have? The problem of the small amount of liquid is addressed by b), however the question of ‘what leaves the reactor’ is accentuated. The third possibility solves both of these problems, however it adds a new one: How does one reliably fill a dry reactor with liquid such that *no* bubbles are present?

The cultivations shown in Fig. 5.7 were inoculated according to procedure b), so, probably, the starting OD was a bit lower than what had been planned. This explains why the duration of oxygen depletion does not correlate with starting OD. Newer cultivation attempts (done in the newest reactor design presented here) were done according to procedure c) as this, with ample experience of filling reactors, promises to give the least variation in starting conditions.

Obviously, this is only one aspect of the whole microbioreactor operation which has to be tested and standardized. Others are e.g. the preparation of the inoculum/starting broth, when to connect the elevated water reservoir (for batch cultivations) or how to prevent the formation of bubbles. All of these factors can potentially influence the quality of the results and therefore have to be evaluated carefully.

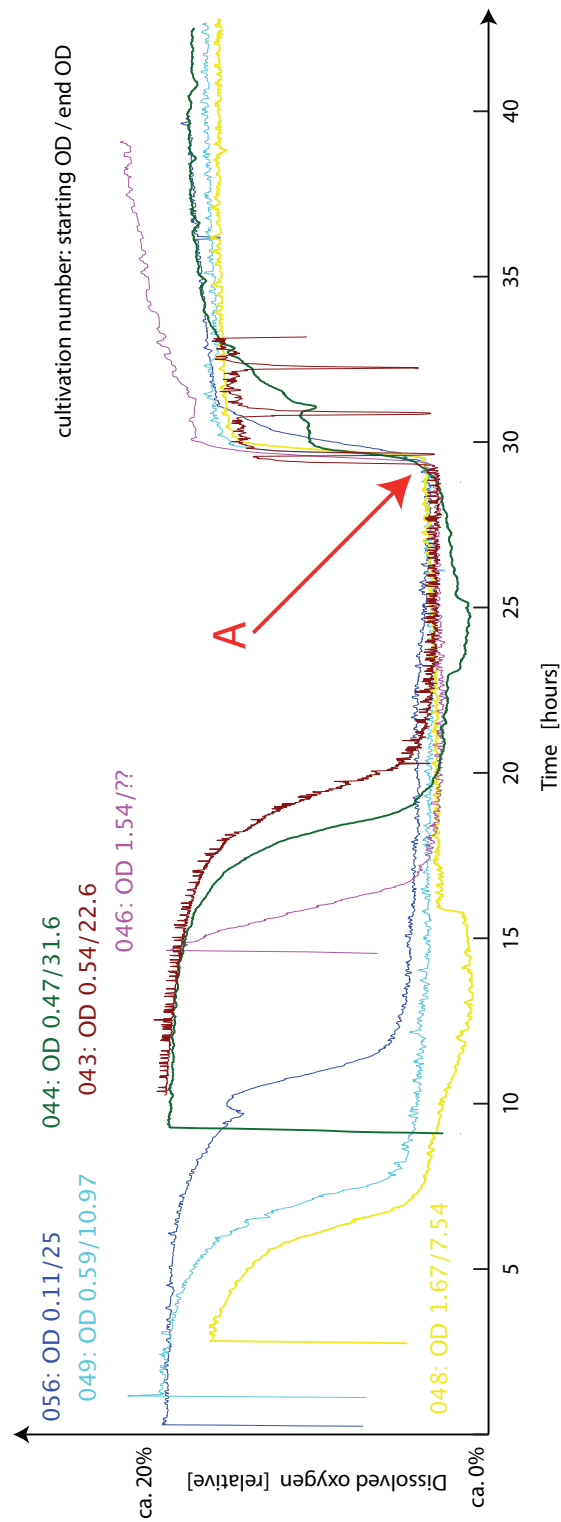


**Figure 5.7:** The dissolved oxygen measurements illustrate the differences between cultivations that should have been at least 'similar'. The curves were shifted such as to be aligned in point A.

# Topology Optimization

---

In bioprocesses for industrial applications, genetically engineered microorganisms are used for the production of cell products of commercial interest, e.g. enzymes or antibiotics. A part of the bioprocess design is then concerned with *optimizing the growth* of a chosen strain according to criteria such as productivity, outlet product concentration or substrate conversion efficiency. This optimization is normally done by adjusting process variables such as temperature or pH, by adjusting the feed profile or by modifying the strain. Another aspect of bioprocess design concerns *reactor design*, where focus is on obtaining sufficient agitation and aeration. Industrially, the most commonly used design is the stirred tank where baffles and agitator types are typically the elements considered for altering a reactor configuration. At lab-scale, where experiments typically are performed using bench-scale reactors, shake flasks or microtiter-plates, the number of different reactor configurations that can be realized is also rather limited. Mass transfer limitations resulting from reactor design constraints will often put a constraint on the process productivity that can be achieved.

There has recently been considerable interest in development of microbioreactors that allow experimentation with microorganisms at microscale under well-controlled conditions (1). The increased design flexibility offered by microfluidic systems enables a wide range of reactor configurations with regards to microbioreactors with volumes  $< 1$  mL, eventually leading to higher productivities compared to traditional reactor designs. In fact, the incorporation of solid structures in the reactor, resulting in a more complex flow pattern, has been shown to result in a significant metabolic rate increase for a simplified model of a bioprocess (106). When performing experiments in microbioreactors, the issue of scaling-up results to pilot or production scale is extremely important: Islam et al. (62) showed that  $k_La$  is a good criterion for translation between different scales. However, this work was done for conventional reactors; Further research is necessary to determine whether optimized microbioreactors can show the same characteristics.

*Topology optimization*, a mathematical tool which allows for the determination of the optimal distribution of such structures, enhances the engineering design process through the use of mathematical optimization techniques. The methodology was first applied to the field of structural mechanics (107; 108), and has been recently implemented to the field of microfluidic systems (109; 110). Further the method has been successfully applied to design optimal catalytic micro-reactors (111), which are very analogous to simplified models of metabolic bio-reactors.

Topology optimization puts the traditional design process upside down: Instead of actively, by using the ingenuity of the engineer, changing the design of the structure as to achieve the best results, the engineer now states the problem formulation and lets the computer iteratively design the most optimal solution. It is then up to the engineer to simplify the computer-generated design such that it can be fabricated and is economically viable. A wealth of methodologies for topology optimization have emerged (112; 113). All methods have in common an iterative calculation process which optimizes a system according to certain requirements (e.g. carry a certain weight for a bridge or achieve a maximal concentration of a product in a biological system) and constraints (e.g. only a certain amount of material or space available, production of a toxic product) formulated in an appropriate objective function. They all take advantage of the vast computing power available to apply the user-given rules and so come to a solution, even if it might not be intuitively understandable.

In the present work all three of the disciplines discussed above—reactor design, optimizing the growth and topology optimization—were combined, resulting in a microbioreactor design where an immobilized microorganism is optimally distributed in order to maximize the amount produced of a product of interest, in our case study a soluble recombinant protein. The final computed distribution of the immobilized biomass corresponds to the highest possible product mass flow rate (defined as product concentration at the outlet times outflow flow rate) at the reactor outlet.

As this, to the best of our knowledge, is the first time topology optimization is applied to a real biological problem, the main question we wanted to answer was: Using a reactor with homogeneously distributed immobilized biomass as a reference point, would it be possible, by means of topology optimization of the reactor shape and configuration, to significantly enhance the volumetric productivity of a given cultivation for an identical substrate feed concentration? Topology optimization is in this case the design tool used, microbioreactors the enabling technology and the bioprocess itself the optimization object.

In the following we first present the motivation for this work and discuss possible gains with a structurally optimized reactor. The topology optimization methodology is then explained in more detail followed by a section about the original biological model and its adaptation to the topology optimization routine. The simulated reactor layouts are then presented and their performance is compared to a benchmark. Finally, we give an outlook over the possibilities and challenges presented by this combination of technologies.

## 6.1 Biological motivation

There is a constant need for both strain and process improvement within the biotechnology industry to maintain competitiveness. Mechanistic models describing the different phenomena taking place in the (bio)reactor are important tools for optimization and control of the process (114). Microbial kinetics is typically used to describe the metabolic process of microorganisms contained in the bioreactor. The interplay between different metabolic pathways, regulation mechanisms, inhibition by substrates and products, and formation of intermediate substrates and products result in complex kinetic models. When it comes to modeling of the mass flow, the commonly used stirred-tank bioreactors are most often assumed as ideal, and thus the existence of gradients throughout the reactor is neglected. However, in large scale production bioreactors concentration gradients of substrates and products are present as demonstrated by experimental work in combination with computational fluid dynamics (CFD) and may have a significant influence on the resulting yields and productivities of a process (115; 116).

Topology optimization might allow for higher productivities by optimizing the spatial distribution of the immobilized microorganisms within the reactor (and thus controlling and optimizing the gradients present in the reactor). This might, at least hypothetically, minimize the negative effects on the process due to lack of substrate or excessive amounts of substrate (substrate inhibition), or accumulation of a metabolite or a product (product inhibition).

Heterologous protein production by the yeast *Saccharomyces cerevisiae* was chosen as a model system since it has high relevance and *S. cerevisiae* is one of the microorganisms most commonly used in the biotech industry. Furthermore, production of the protein will be negatively affected by e.g. too high substrate concentration (described more in detail in section 6.2.2 below). Although typical yeast cultivations consist of suspended cells, yeast can also grow adsorbed onto to a carrier (immobilization support). The use of immobilized yeast has been exploited in biotechnological processes offering advantages such as increased process flow rates (117).

Due to the high design flexibility offered by microfluidic systems, microbioreactors are interesting systems for simulating gradients in larger systems and for evaluating the effect of spatial optimization. In microbioreactors where biomass is immobilized inside the reactor the culture medium flows laminarly throughout the reactor, and consequently a gradient of substrate and product is established from the reactor inlet towards the outlet. In a traditional approach, maximization of the product mass flow rate at the outlet would be achieved by a compromise of the reactor length, total amount of immobilized biomass used and substrate feed concentration. However, the laminar flow in the microbioreactor allows for strikingly different shapes in addition to the traditional plug flow configuration, which in essence consists of a single channel in which the cells flow and also grow. It is in such a situation where a non-obvious compromise has to be reached, that the topology optimization methodology can be successfully applied for obtaining an innovative solution.

## 6.2 Microfluidics modeling and optimization

In the model used for optimizing the distribution of cells immobilized onto a carrier within a microbioreactor, two parts had to be considered: A first part is concerned with the modeling of the flow of the culture broth (consisting of culture medium and suspended cells) and how it is affected by the presence of solid structures such as immobilized cells. The second part models the reaction kinetics describing cell growth, substrate consumption and product formation. In the following we describe the flow model with the influence of immobilized cells, and relate it to a general optimization problem.

### 6.2.1 Fluid dynamic modeling of the flow

The flow dynamics of a liquid of density  $\rho$  [kg·m<sup>-3</sup>] and viscosity  $\eta$  [Pa·s] were modeled by the steady-state Navier-Stokes equation relating the flow velocity  $\vec{u}$  [m·s<sup>-1</sup>] and the pressure  $p$  [Pa]. Moreover, we modeled the increase of the flow resistance due to the presence of the cells and their carrier by a simple damping of the fluid, the so-called Darcy friction. There, the influence of cells and carrier on the fluid was described as the distribution of a porous, sponge-like material, where the positioning of the spatial structures, found by the optimization method, corresponds to varying the local porosity inside the reactor.

The Darcy friction is inversely proportional to the local velocity (e.g. pointing in the opposite direction) with proportionality factor  $\alpha(\vec{r})$  [-], which depends on the local porosity of the cell agglomeration and its porous support at position  $\vec{r}$ . If no cells are present in some point  $\vec{r}_0$  in space then  $\alpha(\vec{r}_0) = 0$  and the flow is unhindered at that point, while a large and dense concentration of cells results in a high flow resistance in that point brought about by a local high value of  $\alpha$  e.g. in the range of  $10^5$  -  $10^8$ .

The steady-state Navier-Stokes equation, extended with the Darcy friction term  $-\alpha(\vec{r}) \cdot \vec{u}$  becomes

$$\rho \cdot (\vec{u} \cdot \nabla) \vec{u} = -\nabla p + \eta \cdot \nabla^2 \vec{u} - \alpha(r) \cdot \vec{u} \quad (6.1)$$

This equation must be supplemented with the continuity equation that expresses the incompressibility of the cultivation broth,

$$\nabla \cdot \vec{u} = 0. \quad (6.2)$$

In traditional numerical aided design processes, the geometrical structure of the system is defined a priori, and based on the governing equations of the dynamics, simulations are conducted to evaluate the performance of the system. In optimization problems this process is reversed. Initially, the geometrical structure is not known, but gradually forms through an iterative optimization process within a design region, denoted  $\Omega$ . To guide this process, a pre-defined objective function  $\Phi$  which, by convention, has to be minimized during the optimization process, evaluates the different candidate geometries. This function can depend both on the shape and performance of a candidate geometry, and the optimization problem is solved once a geometrical structure has been found that globally minimizes  $\Phi$ .

In order to search among all possible structures, each candidate geometry has to be uniquely defined by a set of design variables  $\gamma$ . Similarly, unique solutions

of the model system must exist for each choice of  $\gamma$ , such that the performance of each candidate geometry can be evaluated by  $\Phi$ .

In the method of topology optimization, the complexity of the candidate geometries is unlimited, as the design variable is a spatially varying indicator field, bounded between zero and unity,  $0 < \gamma(\vec{r}) < 1$ . The geometries are defined by the value of  $\gamma$  in each point of the design region  $\Omega$ .

In our case the value of  $\gamma$  is directly linked to the presence of the carrier (i.e. the immobilized cells), where  $\gamma = 1$  indicates the presence of only liquid cultivation medium (itself containing suspended cells) in open channels, while  $\gamma = 0$  indicates the presence of a cell saturated carrier, seen as the limit of vanishing small pores in the carrier material. Or put differently, in our case, the value of  $\gamma(\vec{r})$  corresponds to the local volume fraction occupied by the liquid cultivation medium (118).

The effect of the design variable  $\gamma(\vec{r})$  on the flow of the abiotic phase was described by a linear correlation of this variable to the Darcy friction coefficient  $\alpha(\vec{r})$

$$\alpha(\vec{r}) = (\alpha_{min} - \alpha_{max}) \cdot \gamma(\vec{r}) + \alpha_{max} \quad (6.3)$$

where  $\alpha_{max}$  is the maximal value of the friction coefficient. For simple flow problems, this linear correlation turns out to ensure a sharp transition in space between buffer regions and solid or densely porous material region (109). This property seems to hold for the optimized solutions of many simple reactor models (111).

In the present model, the distributed material was assumed to be a dense porous carrier with immobilized cells, which consume substrate in order to grow and produce a soluble recombinant protein. We were interested in the product characterized by the product concentration  $P(\vec{r})$  [units  $L^{-1}$ ]. Although, the ultimate optimization goal we aimed for was the maximization of the product mass flow rate at the reactor outlet (the total output of product per time), the optimization algorithm can deliver a better solution if the optimization function is more closely linked to the design variable,  $\gamma(\vec{r})$ , at any point in the reactor. Therefore, the optimization function was formulated in terms of the product formation rate which is specified for every point in the reactor. Since optimization methods by default minimize the objective function, we introduce a minus sign, and thus define the objective function  $\Phi(\gamma)$  as minus the volume integral of the product formation rate,

$$\Phi(\gamma) = - \int_{\Omega} R(P) dV. \quad (6.4)$$

Besides defining an objective function  $\Phi(\gamma)$  in optimization problems, additional constraints on the design variable  $\gamma$  or on other variables of the system often have to be defined to avoid non-physical or trivial solutions to the problem. In this work both extreme cases of a completely filled or a completely emptied reactor are unfavorable. In the first case the material will act as a plug, blocking the pressure-driven flow, and only a minimal amount of end-product will leave through the outlet channel, while the absence of active material in the second case naturally will be worse, as no reaction will happen at all.



### 6.2.2 Implementation of the biological model

In this section we address the mathematical description of the cell reaction kinetics consisting of a growing cell population of recombinant *S. cerevisiae*. In this system, the cells are both attached onto a carrier and freely suspended in the culture medium. The dynamics of immobilization of brewing yeast cells by adsorption onto a carrier (spent grain particles) have earlier been modeled by Branyik et al (117).

In this model a certain fraction of the yeast cells were assumed to possess a plasmid which encodes for a recombinant protein, the product we aimed to obtain from the cultivation. Glucose was fed to the reactor, and was assumed to be the preferential substrate. The yeast metabolism was simplified to a 3-pathway model suggested by Zhang et al. (119) and schematized in Figure 6.1. A new model, based both on the work of Branyik et al. and Zhang et al, was required in order to perform the topology optimization routine. The new model aims at simulating a cultivation in a microbioreactor where brewing yeast, both immobilized onto a support (carrier) and suspended in the cultivation medium, grows and produces an extracellular soluble recombinant protein *P*.

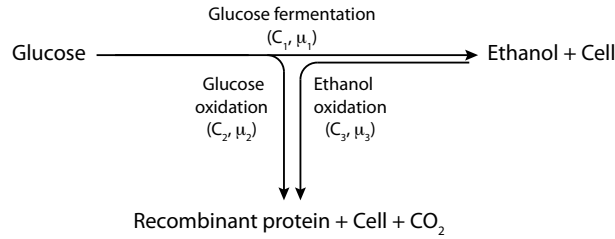


**Figure 6.1:** 3 pathway model for the yeast metabolism where  $C_i$  is a pool of enzymes and  $\mu_i$  is the specific growth rate [-]

**Growth kinetics** The model describes three metabolic events: glucose fermentation, glucose oxidation and ethanol oxidation (Fig. 6.1). In aerobic conditions, glucose is oxidized to carbon dioxide along the respiratory metabolic pathways. However, in case the glucose flow becomes too large for the respiratory capacity of the cell, excess glucose is fermented to ethanol and the activity of the enzymes in the glucose oxidative pathway is attenuated. This phenomenon is typically referred to as the Crabtree effect and is schematically represented by pathways 1 and 2. When glucose approaches depletion, ethanol begins to be metabolized by pathway 3 in the presence of oxygen. The cells grow exclusively on ethanol when glucose is exhausted.

The recombinant protein production is connected to growth and is exclusively associated to the oxidative metabolism (pathways 2 & 3) in yeast cells (suspended or immobilized) carrying the plasmid. The fraction of plasmid bearing cells of the total immobilized cell population, which was set manually, was assumed to be constant.

Additionally, the three pathways were considered quantitatively additive, and were described by modified Monod equations (Eq. 6.5 to 6.7). Although formulated differently, the proposed expressions for growth rates are mathematically

equivalent to the implicitly defined functions proposed by Zhang et al. (119). The use of explicit and continuous functions, rather than implicit, step-change equations, is required in order to integrate this metabolism model into a topology optimization routine. In comparison to the original model (119), a second simplification was introduced: it was assumed that the consumption of substrate for microorganism maintenance was negligible, thus the maintenance coefficient becomes zero.

$$\mu_1 = \mu_{1,max} \cdot \frac{G}{K_{1'} + G} \cdot \frac{1 + k_{a'}G}{k_{b'} + k_{a'}G} \quad (6.5)$$

$$\mu_2 = \mu_{2,max} \cdot \frac{G}{K_{2'} + G} \cdot \frac{1 + k_{c'}G}{1 + k_{c'}k_{d'}G} \quad (6.6)$$

$$\mu_3 = \mu_{3,max} \cdot \frac{E}{K_3 + E} \cdot (1 - \tanh(G)) \quad (6.7)$$

**Immobilization kinetics** Cells can attach onto and detach from the immobilization support (carrier). Branyik et al. (117) have argued that the deposition rate is proportional to the dilution rate and the detachment rate is a function of the glucose concentration. As mentioned in section 6.2, the calculations concerning the flow of the liquid cultivation medium are performed separately from the ones concerning cell metabolism—thus a dilution rate dependent term describing the deposition of cells onto the carrier is problematic. However, as the deposition coefficient determined by Branyik et al. was of a considerably lower order of magnitude than the detachment and growth rates, the deposition was disregarded in the formulation of the new model.

In addition, it was assumed that only a constant fraction of the immobilized biomass,  $X_{im}^{act}$ , is actively growing, as observed experimentally by Branyik et al. Therefore, in the model, the growth rate equals the detachment rate. Thus, by setting  $X_{im}$  we define *which* steady-state should be run. Also, if the number of immobilized cells was not constant, then the biological part of the model would change the parameter the optimization routine uses to define the structure. In this case the routine would have no control over the design parameter.

Concerning the release of cells from the support as a result of the flow of the culture broth, the detachment kinetics are mathematically described by Eq. 6.8, where  $C_3$  reflects a switch to growth on ethanol (pathway 3) caused by glucose depletion (I). It was assumed that the saturation constant was the same for both substrates.

$$k_{det}^* = K_{det}^{sst} \cdot \frac{G}{G + K_s} + C_3 \cdot \frac{E}{E + K_s} \quad (6.8)$$

### 6.2.3 Model for topology optimization: spatial dependency

In typical bioprocess models for continuously stirred reactors (CSTR), the reactors are considered perfectly mixed, and, therefore, state variables are not dependent of their location within the reactor. Due to the heterogeneity in the reactor space resulting from the unequal distribution of immobilized cells, spatial dependency now has to be taken into account. In this case, the reactor can be considered to be a collection of local, infinitesimally small CSTRs, where the

transport across the interfaces is described by diffusion, and the fluid transport in the reactor is described by convection. Assuming steady state conditions at each position, the total variation of a general state variable  $A$  is given by Eq. 6.9 where  $\vec{u}$  represents the velocity vector [ $\text{m}\cdot\text{s}^{-1}$ ] and  $D_A$  [ $\text{m}^2/\text{s}$ ] is the diffusion coefficient for the variable  $A$ . Similar equations were written for the following model state variables: glucose concentration  $G$  [ $\text{g}\cdot\text{L}^{-1}$ ], ethanol concentration  $E$  [ $\text{g}\cdot\text{L}^{-1}$ ], total free (suspended) biomass  $X_f$  [ $\text{g}\cdot\text{L}^{-1}$ ], plasmid bearing freely suspended biomass  $X_f^+$  [ $\text{g}\cdot\text{L}^{-1}$ ], and protein concentration  $P$  [ $\text{units}\cdot\text{L}^{-1}$ ].

$$\vec{u} \cdot \nabla A = \text{Sources} - \text{Sinks} + D_A \cdot \nabla^2 A \quad (6.9)$$

It is important to note that the terms *Sources* and *Sinks* in Eq. 6.9 stand for the production or the consumption of the given component but do not include any terms related to the transport into or out from the infinitesimally small reactors as these are accounted for in the convective term on the lefthand side of Eq. 6.9. These convective terms are taken care of by the calculations for the flow of the culture broth that is considered to be a 1-phase flow (liquid only). The cells in suspension are assumed not to significantly influence the flow characteristics of the liquid. Consequently, when referring to the suspended biomass, the sources are the detachment of immobilized cells, as well as the growth of the suspended population. As cell deposition is disregarded, there are no sinks. In the case of the substrate, glucose, there are no sources to be considered, whereas the sinks are the consumption of glucose by immobilized and suspended cells by glucose oxidation and glucose fermentation. Finally, with regard to ethanol, the sources are the production of this component by glucose fermentation and the sink corresponds to the ethanol consumption by the ethanol oxidation pathway. The corresponding equations are presented in Appendix I.

As the immobilized biomass is not transported in the flow, different considerations have to be made for the variables  $X_{im}$  and  $X_{im}^+$ . The former can be called an actuator variable, as it is imposed in the beginning of each iteration of the optimization routine when the distribution of the carrier material (and with it the distribution of the immobilized cells) is determined, until the optimal spatial distribution of immobilized biomass is found, and the other state variables are calculated based on it. The latter,  $X_{im}^+$ , is directly proportional to  $X_{im}$  as the fraction of plasmid bearing cells in the immobilized population is assumed to be constant.

Thus, in summary, the overall optimization procedure (Fig. 6.2) is such that:

1. A certain initial distribution of carrier material and immobilized cells is assumed. Most often the initial assumption is that biomass is just homogeneously distributed, but in theory the starting point for the optimization can also be a completely different situation.
2. The steady-state flow of the culture broth (liquid with suspended cells) through the structure is calculated. This e.g. defines how much glucose moves from one infinitesimally small CSTR to the other.
3. Based on these results the cell kinetic model is run. The results here are e.g. the product concentrations in every small CSTR.

4. The optimization procedure determines if the solution is good enough. If it is not, a new direction (resulting in a new distribution of material) is determined.
5. The process restarts at step (1) and runs until the resulting solution fulfills the stop criterion for the optimization.

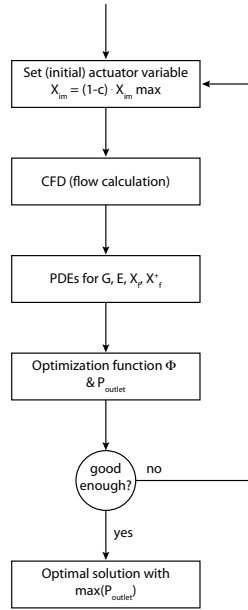


**Figure 6.2:** Scheme depicting the optimization procedure.

## 6.3 Simulation results

The topology optimization routine was implemented and solved using the commercially available software COMSOL®. Simulations were carried out for a microbio reactor with dimensions 1.2x1.2x1 mm. Although the reactor height was taken into account in the fluid damping calculations, it was assumed that the flow is two-dimensional. Therefore, the state variables were considered constant along the z-axis and vary only along the x- and y-axes. The pressure drop, diffusion coefficients and other parameters used in the simulation are listed in Appendix I.

The structures that result out of different glucose concentrations in the feed can be very different—for illustration purposes the results for a glucose feed concentration of 0.1 g/L (Figs. 6.3 - 6.4) and 0.5 g/L (Figs. 6.5 - 6.6) are presented. Figs. 6.3 and 6.5 show the resulting structure and the corresponding concentrations in the reactor, while Figs. 6.4 and 6.6 show some of the rates (growth, consumption, production).

Some immediate observations can be done here:

1. Apparently the formation of islands of immobilized yeast allows for a better distribution of glucose, thus maximizing the production of the desired protein.
2. The effect of the glucose concentration can be seen as larger islands of cells for higher glucose concentrations. With higher glucose concentrations, the diffusion pressure into the islands is larger and thus allows for larger islands before the cells suffer from nutrition limitation.
3. The specific growth rate for glucose fermentation follows a similar pattern to the glucose distribution, whereas glucose oxidation was predominant in the regions where glucose is available in lower concentrations, and therefore, the respiratory metabolism is not subject to overflow metabolism.
4. A complementary pattern to the glucose distribution is obtained for the ethanol oxidation, which only takes place when glucose is depleted.

## 6.4 Benchmarking

In order to assess the gains in protein concentration obtained by using structurally optimized reactors rather than reactors where the immobilized biomass is homogeneously distributed throughout the microbio reactor, the protein concentrations at the reactor outlet were determined for the spatially optimized reactors for different glucose feed concentrations (0.001 up to 1 g/L). These concentrations were compared to the maximum protein concentrations obtained, using the same glucose feed concentrations, at the outlet for microbio reactors where the immobilized yeast is homogeneously distributed at the maximal concentration possible. All the optimized reactors have a cell concentration which is lower than that of the corresponding homogeneous reactor.

As observed in Table 6.1, an increase of the protein mass flow rate at the outlet of at least 5 times was observed for all the simulated glucose feed concentrations. The increase in protein concentration at the outlet was more than 8 fold for glucose feed concentrations between 0.005 and 0.5 g/L. In this range of concentrations, the significant gain in protein concentration can be explained by the fact that a structurally optimized distribution where flow is distributed and islands of biomass are surrounded by streams of liquid flow, allows for a balanced distribution of glucose across the reactor leading to higher local protein production rates.

## 6.5 Outlook

This first investigation of the potential of topology optimization for improvement of microbial cultivation processes at micro scale has clearly shown that the use of this methodology can lead to microbio reactors with a significantly higher productivity than conventional reactor designs where immobilized biomass is homogeneously distributed. If we assume that results can be extrapolated to larger scales, topology optimization thus holds the promise of significant increase in the productivity compared to existing stirred tanks. However, it also poses a number of questions and areas for further investigation as discussed below.

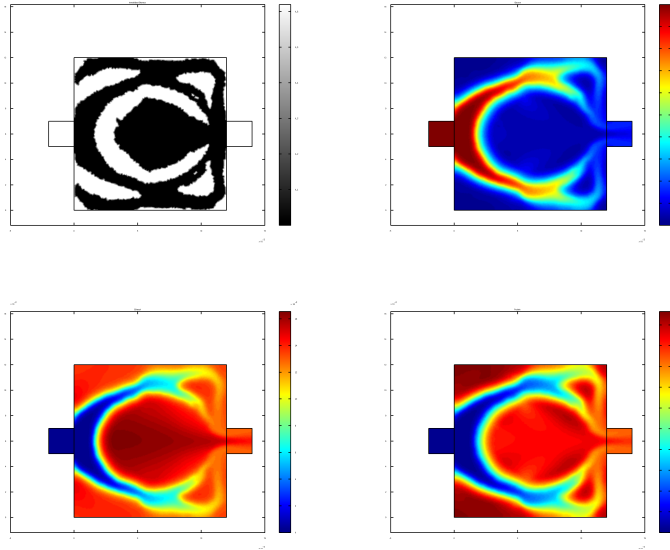


**Figure 6.3:** Resulting structure and concentrations for a glucose flow concentration of 0.1 g/L. (a) Distribution of biomass where white = cells and black = fluid, (b) glucose concentration [g/L], (c) ethanol concentration [g/L] and (d) protein concentration [units/L].

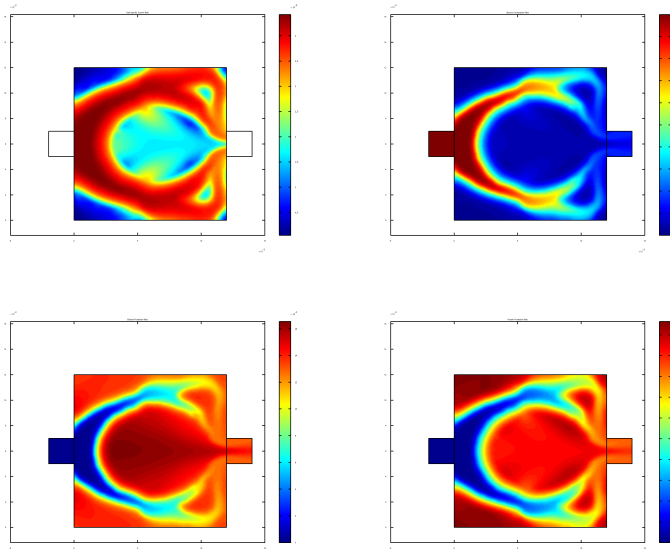


**Figure 6.4:** Rates in the optimized design for a glucose flow concentration of 0.1 g/L. (a) Total specific growth rate [-], (b) glucose consumption rate [g/(L·s)], (c) ethanol production rate [g/(L·s)] and (d) protein production rate [units/(L·s)].

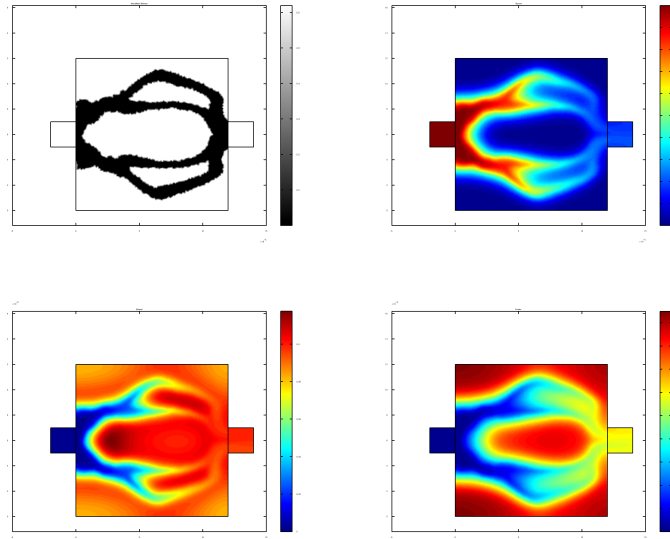


**Figure 6.5:** Resulting structure and concentrations for a glucose flow concentration of 0.5 g/L. (a) Distribution of biomass where white = cells and black = fluid, (b) glucose concentration [g/L], (c) ethanol concentration [g/L] and (d) protein concentration [units/L].

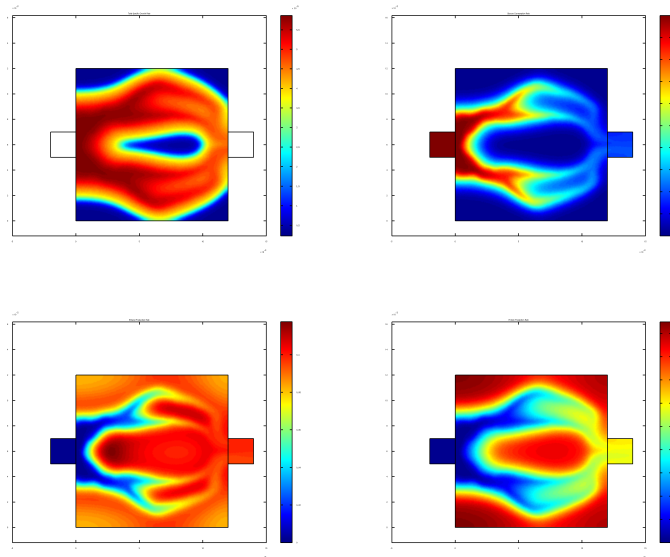


**Figure 6.6:** Rates in the optimized design for a glucose flow concentration of 0.1 g/L. (a) Total specific growth rate [-], (b) glucose consumption rate [g/(L·s)], (c) ethanol production rate [g/(L·s)] and (d) protein production rate [units/(L·s)].

**Table 6.1:** Comparison of the total protein outputs for the homogenous and the structurally optimized reactor designs at different glucose feed concentrations.

Glucose feed concentration [g/L]	Homogeneous reactor [g/h]	Optimized reactor [g/h]	Increase [fold]
0.001	0.0003	0.0027	5.8
0.005	0.0014	0.0129	9.1
0.01	0.0027	0.0231	8.4
0.03	0.0072	0.0574	8.0
0.05	0.0107	0.0917	8.5
0.1	0.0176	0.1703	9.7
0.2	0.0252	0.2295	9.1
0.5	0.0390	0.3252	8.3
1	0.0638	0.3804	6.0

In this study we focused on one single strain under specific operating conditions. It would be very interesting to see if the general results also hold for other cell types, e.g. mammalian cells or filamentous fungi. Another interesting question is the shape of the reactor itself. We considered here a very simple rectangular reactor with one inflow and one outflow. Is a rectangle the best shape? Or might a design with several in- and outflows perform better?

Last but not least, the question of practical applicability is of utmost importance. To perform an experimental validation of the simulation outcome first the necessary techniques to transfer these theoretical results into the laboratory have to be established. This includes the fabrication of the spongelike structure and inoculation of the structure with cells. Then, a comparison between the effective cultivations and the corresponding simulations have to be done in order to prove that the simulations can reliably predict laboratory results. Finally, the methodology has to be applied to relevant industrial problems which justify the additional effort in moving from the laboratory to industrial settings.





## Conclusion and perspectives

---

### 7.1 Conclusions on the final microbioreactor design

As our aim was to develop a reactor with relatively low complexity which is suited for both batch and continuous operation of a fermentation with suspended microorganisms, the reactor has been designed such that complicated fabrication steps as e.g. clean-room work are omitted. Furthermore, material properties were exploited to enable fabrication of the whole reactor out of one material, and fluidic, optical and electrical connections were designed to be easy to handle providing consistent results. The reactor itself consists entirely of PDMS and only contains two optical sensor spots and one stirrer bar. In this form the reactor is gamma-sterilizable and can be delivered prepackaged similar to other single-use laboratory equipment such as syringes. Also, as the cost of PDMS is negligible, the most expensive part of the reactor actually are the optical sensor spots. Here, reducing the size of the sensor spot will lower the price. All in all, a complete reactor ought to have production costs in the range of EUR 10–15 apiece.

The requirements for continuous culture and batch operation are being met with an appropriate mixing system which can also keep cells in suspension, an aeration membrane which cannot bulge and thus ensures a defined culture volume and the surrounding apparatus which enables the measurement and partly also the control of the most essential culture variables in addition to enabling different well controlled flows in and out of the reactor. As shown in the thesis, the various components of the reactor work fine and allow the broth to be held within tight specification limits. From the experiments carried out so far, it can be concluded that the reactor shows a performance which resembles that of previously presented similar, but considerably more complex reactors. Also, it provides significantly more instrumentation than shake flask cultivations, and does so without the need for sampling (which is time consuming and increases

the risk of contamination). This inline measuring setup finally also allows for automatization of the whole system which can run cultivations with a minimum of human intervention.

As stated in the introduction, microbioreactors yet have to find their way into industrial applications. The proposed single-use microbioreactor should be a step towards increased miniaturization of well-controlled fermentation experiments, both in a research / development (screening) environment and in a production environment. The proposed design fits fine also with recent requirements from industry, where there for example is an increasing interest for the production of pharmaceuticals in single-use equipment, mostly to reduce cleaning efforts and to reduce contamination from one production batch or one product to the next one. The proposed microbioreactors could fit well in such a production facility, for example to grow an inoculum under well-controlled conditions or to perform tests with microorganisms sampled from the full-scale fermentor. In addition, the proposed microbioreactors are ideally suited for process development studies, where the small size and the ability to control essential reactor variables form the key to cheap experimentation generating relevant experimental results that can be extrapolated to larger scales. In this context it is also important to emphasize that the volume of the proposed reactor design can be adjusted easily (e.g. increase to 1 mL), while technical solutions developed for mixing, aeration, sensing and control should not have to be modified significantly.

## 7.2 Perspectives and future work

Design and development of a new product is an iterative process—microbioreactor design is no exception. Many of the problems that had appeared in the early reactor designs have been addressed in the current design presented here. Some improvements are still waiting to be implemented; Use of the current reactor design will both prove the efficacy of the design improvements implemented and also show new deficiencies. Some of the next steps for improving the reactor which can be seen already now are

- In the current version of the reactor, the fluidic tubes are manually inserted into the reactor. Obviously, this procedure is not error-free neither during insertion nor during reactor operation. A future version of the holder would therefore also include a guiding and clamping tunnel for the fluidic connections which would define position, direction and insertion length of the tubes. This would then facilitate a reproducible installation of the reactor and the ease of use.
- Currently, the reactor is only being laid onto the holder and sticky tape is being used for fixation. This has the advantage of being very flexible which is important, especially as long as the design is changing. However, a (more or less) final design will need some clamping and alignment mechanism as the flexibility mentioned before also might lead to problems e.g. with the measurements if the fibers shift.
- Currently cultivations are run with a fixed concentration of oxygen in the aeration gas. In a next step closed-loop DO-concentration control will

be implemented using similar control algorithms and devices as for pH control. This will for example also allow to investigate how a cultivation reacts to stress due to lack of oxygen, by controlling the DO-concentration at a low set point.

- The pH range which can be controlled now will not suit all kinds of organisms. Many will require a more acidic pH (e.g. *S. cerevisiae*) which requires a different kind of sensor spot. PreSens is working on a sensor spot which has exactly the same operating principles and conditions, but measures lower pH values. The availability of such a sensor spot measuring low pH values is a necessity for many bioprocesses.
- As mentioned earlier, the LabView program has not been entirely stable. It is not clear where the cause is to be found (driver conflict, 'bad' programming, faulty hardware etc.), and nobody (neither KT computer support nor National Instruments) seems to be able to solve the problem. The program is running right now, but the problem might reappear anytime. Apparently Matlab (Data Acquisition Toolbox) is capable of doing the same, so this is a possibility which will have to be examined. This route would also offer the possibility of creating stand-alone applications which do not require Matlab to be installed on the computer.

Another part of the future work is more concerned with the operation of the whole system and its comparison with other, larger systems. Here some obvious items are:

- Once the reactor design is fixed and a holding plate with clamping mechanism has been created, it would make sense to recalibrate all the measurements. Fundamental changes are not to be expected (e.g. the OD measurement is still expected to be linear), but the numbers might have changed due to the different structure of the light path.
- It would be interesting to know the influence of the aeration gas flow: How does the flow rate for a certain gas composition influence  $k_La$ ? At which flow rates does the diffusion pressure become larger than the hydrostatic pressure from the elevated water reservoir? What is the maximal  $k_La$  that can be achieved?
- As mentioned earlier, it is of utmost importance to create a standardized microbioreactor fermentation protocol where all the minute steps for the preparation and running of a cultivation have to be fixed. This starts with the preparation of the inoculum in the shake flasks, includes the sterilization procedure for the reactor (necessary as long as it is not produced and sterilized industrially) and ends with the problem of reactor inoculation/filling and the prevention of bubbles.
- A comparison of cultivation results over different scales where the influence of aeration is removed would provide some information about the quality of the reactor operation. For this purpose, anaerobic fermentations (flushing with nitrogen gas) in both the bench-scale reactor and the microbioreactor should be done.

- As soon as optimal aeration is established comparisons of the maximal achievable growth rates should be done. This could be achieved by means of wash-out curves in continuous chemostat operations both in the bench-scale reactor and the microbioreactor.
- Finally, in order to really test the scalability from the microbioreactor size to bench-scale or even pilot-scale fermentations, a ranking test (preferably in close collaboration with an industrial partner) would make sense. Here the productivity of different strains should give the same ‘goodness’ (ranking) in all scales. This would be a huge improvement over the pre-study capabilities available today and might well promote the use of microbioreactors in industry.
- These previous points will open the field of the application of the microbioreactor in e.g. kinetic studies where the chemostat operation could be disturbed in a defined manner in order to e.g. simulate the cycling of cells in a production scale reactor. This kind of application is already being envisaged e.g. in international projects headed by Anna Eliasson Lantz and Krist V. Gernaey (<http://www.foesu.biobeast.dk>, website in preparation, due to be online in April).
- Last but not least, the microbioreactor offers enough potential to include some more online measurements, such as NIR or Raman Spectroscopy. This would be very welcome as it would greatly increase the amount of online data gained from the experiments. It should be possible to include the optical probes needed directly into the reactor, similar to the probes for the other optical measurements done now, so that much of the current instruments can be re-used.

With the work presented here, a basis has been laid for the further steps outlined above. The system is functional, and many of the inherent problems of microsystems (leakage, bubbles, alignment etc) have been solved. It is now necessary to push the whole system a step further, away from an experimental setup to an industry-near product which works reliably and repeatedly. From here, the above points are some ideas on how one might proceed with the development of microbioreactors.

Another line of thought goes into multiplication of reactors: Obviously, when microbioreactors have proven their worth, there will immediately be great demand for multiplexing of these systems. One obvious possibility is having a ‘rack’ where several microbioreactors are mounted. This rack then moves relatively to the measurement fibers, so that the whole measurement setup can be used for several reactors sequentially as has been shown by Szita et al. (13). For continuous systems where a constant flow of liquid is required, it would be advantageous to work with on-board micropumps (23; 35) in order to be independent of the large and expensive syringe pumps. It might even be advantageous to have one ‘chip’ containing a number of microbioreactors, complete with micropumps and microvalves which can be inserted into a holder as a whole.

In the end, the final product depends very much on the requirements—microbioreactor technology as such is very flexible, with many of the component being under active development. However, as with probably most new technologies, the starting hurdles are significant and require quite an amount of work

before a system that works satisfactorily can be presented. A starting point has been laid here, it is now up to the ingenuity of others to push the system further.



# Bibliography

---

- [1] D. Schäpper, M. N. H. Z. Alam, N. Szita, A. E. Lantz, and K. V. Gernaey, "Application of microbioreactors in fermentation process development: a review," *Analytical and Bioanalytical Chemistry*, vol. 395, pp. 679–695, 2009.
- [2] D. Schäpper, S. M. Stocks, N. Szita, A. E. Lantz, and K. V. Gernaey, "Development of a single-use microbioreactor for cultivation of microorganisms," *Chemical Engineering Journal*, vol. published online, doi 10.1016/j.cej.2010.02.038, 2010.
- [3] M. N. H. Z. Alam, D. Schäpper, and K. V. Gernaey, "Resistance wire as heating element for temperature control in microbioreactors," *Journal of Micromechanics and Microengineering*, vol. accepted for publication, 2010.
- [4] D. Weuster-Botz, D. Hekmat, R. Puskeiler, and E. Franco-Lara, "Enabling technologies: Fermentation and downstream processing," *White Biotechnology*, vol. 105, pp. 205–247, 2007.
- [5] M. Shuler and F. Kargi, *Bioprocess Engineering: Basic Concepts*. Prentice Hall, New Jersey, 2002.
- [6] G. Lye, P. Ayazi-Shamlou, F. Baganz, P. Dalby, and J. Woodley, "Accelerated design of bioconversion processes using automated microscale processing techniques," *Trends in Biotechnology*, vol. 21, no. 1, pp. 29–37, 2003.
- [7] S. Kumar, C. Wittmann, and E. Heinzle, "Minibioreactors," *Biotechnology Letters*, vol. 26, pp. 1–10, 2004.
- [8] J. Betts and F. Baganz, "Miniature bioreactors: current practices and future opportunities," *Microbial Cell Factories*, vol. 5, no. 1, 2006.
- [9] A. Zanzotto, N. Szita, P. Boccazzi, P. Lessard, A. J. Sinskey, and K. F. Jensen, "Membrane-aerated microbioreactor for high-throughput bioprocessing," *Biotechnology and Bioengineering*, vol. 87, no. 2, pp. 243–254, 2004.



- [10] P. Boccazzi, Z. Zhang, K. Kurosawa, N. Szita, S. Bhattacharya, K. F. Jensen, and A. J. Sinskey, "Differential gene expression profiles and real-time measurements of growth parameters in *saccharomyces cerevisiae* grown in microliter-scale bioreactors equipped with internal stirring," *Biotechnology Progress*, vol. 22, pp. 710–717, 2006.
- [11] H. L. Lee, P. Boccazzi, R. Ram, and A. J. Sinskey, "Microbioreactor arrays with integrated mixers and fluid injectors for high-throughput experimentation with pH and dissolved oxygen control," *Lab on a chip*, vol. 6, pp. 1229–1235, 2006.
- [12] M. M. Maharbiz, W. J. Holtz, R. T. Howe, and J. D. Keasling, "Microbioreactor arrays with parametric control for high-throughput experimentation," *Biotechnology and Bioengineering*, vol. 85, no. 4, pp. 376–381, 2004.
- [13] N. Szita, P. Boccazzi, Z. Zhang, P. Boyle, A. J. Sinskey, and K. F. Jensen, "Development of a multiplexed microbioreactor system for high-throughput bioprocessing," *Lab Chip*, vol. 5, no. 8, pp. 819–826, 2005.
- [14] Z. Zhang, P. Boccazzi, H. Choi, G. Perozziello, A. Sinskey, and K. Jensen, "Microchemostat - microbial continuous culture in a polymer-based, instrumented microbioreactor," *Lab on a Chip*, vol. 6, no. 7, pp. 906–913, 2006.
- [15] A. Buchenauer, M. Hofmann, M. Funke, J. Büchs, W. Mokwa, and U. Schnakenberg, "Micro-bioreactors for fed-batch fermentations with integrated online monitoring and microfluidic devices," *Biosensors and Bioelectronics*, vol. 24, no. 5, pp. 1411–1416, 2009.
- [16] M. Micheletti and G. Lye, "Microscale bioprocess optimisation," *Current Opinion in Biotechnology*, vol. 17, no. 6, pp. 611–618, 2006.
- [17] J. de Jong, *Application of Membrane Technology in Microfluidic Devices*. PhD thesis, University of Twente, Netherlands, 2008.
- [18] Y. Zhao, W. Lu, Y. Ma, S. Kim, S. Ho, and T. Marks, "Polymer waveguides useful over a very wide wavelength range from the ultraviolet to infrared," *Applied Physics Letters*, vol. 77, no. 19, pp. 2961–2963, 2000.
- [19] M. Fleger and A. Neyer, "PDMS microfluidic chip with integrated waveguides for optical detection," *Microelectronic Engineering*, vol. 83, pp. 1291–1293, 2006.
- [20] H. Becker and C. Gärtner, "Polymer microfabrication technologies for microfluidic systems," *Analytical and Bioanalytical Chemistry*, vol. 390, no. 1, pp. 89–111, 2008.
- [21] C. Tsao and D. DeVoe, "Bonding of thermoplastic polymer microfluidics," *Microfluidics and Nanofluidics*, vol. 6, no. 1, pp. 1–16, 2009.
- [22] J. C. McDonald and G. M. Whitesides, "Poly(dimethylsiloxane) as a material for fabricating microfluidic devices," *Accounts of Chemical Research*, vol. 35, no. 7, pp. 491–499, 2002.

- [23] C. Huang and G. Lee, "A microfluidic system for automatic cell culture," *Journal of Micromechanics and Microengineering*, vol. 17, no. 7, pp. 1266–1274, 2007.
- [24] M. Anvari and G. Khayati, "In situ recovery of 2,3-butanediol from fermentation by liquid-liquid extraction," *Journal of Industrial Microbiology & Biotechnology*, vol. 36, no. 2, pp. 313–317, 2009.
- [25] R. Zautsen, F. Maugeri, C. Vaz-Rossell, A. Straathof, L. van der Wielen, and J. de Bont, "Liquid-Liquid extraction of fermentation inhibiting compounds in lignocellulose hydrolysate," *Biotechnology and Bioengineering*, vol. 102, no. 5, pp. 1354–1360, 2009.
- [26] E. Purcell, "Life at low Reynolds-Number," *Americal Journal of Physics*, vol. 45, no. 1, pp. 3–11, 1977.
- [27] V. Hessel and H. Löwe, "Micromixers - a review on passive and active mixing principles," *Chemical Engineering Science*, vol. 60, pp. 2479–2501, 2005.
- [28] S. Hardt and F. Schönfeld, *Microfluidic Technologies for Miniaturized Analysis Systems*. MEMS Reference Shelf, New York: Springer, 2007.
- [29] Z. Zhang, G. Perozziello, P. Boccazzi, A. J. Sinskey, O. Geschke, and K. F. Jensen, "Microbioreactors for bioprocess development," *Journal of the association for laboratory automation*, vol. 12, pp. 143–151, 2007.
- [30] Z. Zhang, N. Szita, P. Boccazzi, A. J. Sinskey, and K. F. Jensen, "A well-mixed, polymer-based microbioreactor with integrated optical measurements," *Biotechnology and Bioengineering*, vol. 93, no. 2, pp. 286–296, 2005.
- [31] A. D. Stroock, S. K. W. Dertinger, A. Ajdari, I. Mezic, H. A. Stone, and G. M. Whitesides, "Chaotic mixer for microchannels," *Science*, vol. 295, no. 5555, pp. 647–651, 2002.
- [32] X. Li, G. van der Steen, G. van Dedem, L. van der Wielen, M. van Leeuwen, W. van Gulik, J. Heijnen, E. Krommenhoek, J. Gardeniers, A. van den Berg, and M. Ottens, "Improving mixing in microbioreactors," *Chemical Engineering Science*, vol. 63, no. 11, pp. 3036–3046, 2008.
- [33] E. Berthier, J. Warrick, H. Yu, and D. J. Beebe, "Managing evaporation for more robust microscale assays. part 2. characterization of convection and diffusion for cell biology," *Lab on a Chip*, vol. 8, pp. 860–864, 2008.
- [34] A. Olsson, G. Stemme, and E. Stemme, "Diffuser-element design investigation for valve-less pumps," *Sensors and Actuators A: Physical*, vol. 57, no. 2, pp. 137–143, 1996.
- [35] O. C. Jeong, S. W. Park, S. S. Yang, and J. J. Pak, "Fabrication of a peristaltic PDMS micropump," *Sensors and Actuators A*, vol. 123–124, pp. 453–458, 2005.
- [36] C. Fredrickson and Z. Fan, "Macro-to-micro interfaces for microfluidic devices," *Lab on a Chip*, vol. 4, no. 6, pp. 526–533, 2004.

- [37] G. Perozziello, *Packaging of Microfluidic Systems: A microfluidic Motherboard Integrating Fluidic and Optical Interconnections*. PhD thesis, Technical University of Denmark, 2006.
- [38] H. Kortmann, L. M. Blank, and A. Schmid, "A rapid, reliable, and automatable lab-on-a-chip interface," *Lab Chip*, vol. 9, pp. 1455–1460, 2009.
- [39] V. Vojinovic, J. Cabral, and L. Fonseca, "Real-time bioprocess monitoring part i: In situ sensors," *Sensors and Actuators B: Chemical*, vol. 114, no. 2, pp. 1083–1091, 2005.
- [40] S. Petronis and M. Stangegaard, "Transparent polymeric cell culture chip with integrated temperature control and uniform media perfusion," *Biotechniques*, vol. 40, no. 3, pp. 368–376, 2006.
- [41] T. Maiti, "A novel lead-wire-resistance compensation technique using two-wire resistance temperature detector," *IEEE Sensors Journal*, vol. 6, no. 6, pp. 1454–1458, 2006.
- [42] E. Krommenhoek, M. van Leeuwen, H. Gardeniers, W. van Gulik, A. van den Berg, X. Li, M. Ottens, L. van der Wielen, and J. Heijnen, "Lab-scale fermentation tests of microchip with integrated electrochemical sensors for pH, temperature, dissolved oxygen and viable biomass concentration," *Biotechnology and Bioengineering*, vol. 99, no. 4, pp. 884–892, 2008.
- [43] M. Vervliet-Scheebaum, R. Ritzenthaler, J. Normann, and E. Wagner, "Short-term effects of benzalkonium chloride and atrazine on elodea canadensis using a miniaturised microbioreactor system for an online monitoring of physiologic parameters," *Ecotoxicology and Environmental Safety*, vol. 69, no. 2, pp. 254–262, 2008.
- [44] J. Gimbun, A. Radiah, and T. Chuah, "Bioreactor design via spreadsheet - a study on the monosodium glutamate (MSG) process," *Journal of Food Engineering*, vol. 64, no. 3, pp. 277–283, 2004.
- [45] M. Assael, K. Antoniadis, and J. Wu, "New measurements of the thermal conductivity of PMMA, BK7, and pyrex 7740 up to 450K," *International Journal of Thermophysics*, vol. 29, no. 4, pp. 1257–1266, 2008.
- [46] Y. Shin, K. Cho, S. Lim, S. Chung, S. Park, C. Chung, D. Han, and J. Chang, "PDMS-based micro PCR chip with parylene coating," *Journal of Micromechanics and Microengineering*, vol. 13, no. 5, pp. 768–774, 2003.
- [47] L. Liu, S. Peng, X. Niu, and W. Wen, "Microheaters fabricated from a conducting composite," *Applied Physics Letters*, vol. 89, no. 22, pp. 223521–1:223521–3, 2006.
- [48] T. Yamamoto, T. Nojima, and T. Fujii, "PDMS-glass hybrid microreactor array with embedded temperature control device. application to cell-free protein synthesis," *Lab on a Chip*, vol. 2, no. 4, pp. 197–202, 2002.

- [49] M. van Leeuwen, J. Heijnen, H. Gardeniers, A. Oudshoorn, H. Noorman, J. Visser, L. van der Wielen, and W. van Gulik, "A system for accurate on-line measurement of total gas consumption or production rates in microbioreactors," *Chemical Engineering Science*, vol. 64, no. 3, pp. 455–458, 2009.
- [50] K. Isett, H. George, W. Herber, and A. Amanullah, "Twenty-four-well plate miniature bioreactor high-throughput system: Assessment for microbial cultivations," *Biotechnology and Bioengineering*, vol. 98, no. 5, pp. 1017–1028, 2007.
- [51] Presens, "Non-Invasive pH sensors." <http://www.presens.de/>, 2009.
- [52] Microsens, "ISFET (Ion sensitive Field-Effect transistor)." <http://www.microsens.ch/products/chemical.htm>, 2009.
- [53] G. T. John, D. Goelling, I. Klimant, H. Schneider, and E. Heinzle, "pH-Sensing 96-Well microtitre plates for the characterization of acid production by dairy starter cultures," *Journal of Dairy Research*, vol. 70, no. 03, pp. 327–333, 2003.
- [54] E. E. Krommenhoek, J. G. E. Gardeniers, J. Bomer, X. Li, M. Ottens, G. van Dedem, M. van Leeuwen, W. van Gulik, L. van der Wielen, J. Heijnen, and A. van den Berg, "Integrated electrochemical sensor array for on-line monitoring of yeast fermentations," *Analytical Chemistry*, vol. 79, no. 15, pp. 5567–5573, 2007.
- [55] M. Wu, S. Huang, Z. Cui, Z. Cui, and G. Lee, "A high throughput perfusion-based microbioreactor platform integrated with pneumatic micropumps for three-dimensional cell culture," *Biomedical Microdevices*, 2007.
- [56] Applikon, "Micro 24 bioreactor." <http://www.applikon-bio.com/>, 2009.
- [57] K. Jensen, M. Alam, B. Scherer, A. Lambrecht, and N. Mortensen, "Slow-light enhanced light-matter interactions with applications to gas sensing," *Optics Communications*, vol. 281, no. 21, pp. 5335–5339, 2008.
- [58] A. Cervera, N. Petersen, A. Lantz, A. Larsen, and K. V. Gernaey, "Application of Near-Infrared spectroscopy for monitoring and control of cell culture and fermentation," *Biotechnology Progress*, vol. 25, no. 6, pp. 1561–1581, 2009.
- [59] Sartorius, "FUNDALUX II." <http://www.sartorius-stedim.com>, 2009.
- [60] L. Villain, L. Meyer, S. Kroll, S. Beutel, and T. Scheper, "Development of a novel membrane aerated hollow-fiber microbioreactor," *Biotechnology Progress*, vol. 24, no. 2, pp. 367–371, 2008.
- [61] D. Papkovsky, "New oxygen sensors and their application to biosensing," *Sensors and Actuators B: Chemical*, vol. 29, no. 1-3, pp. 213–218, 1995.

- [62] R. Islam, D. Tisi, M. Levy, and G. Lye, "Scale-up of escherichia coli growth and recombinant protein expression conditions from microwell to laboratory and pilot scale based on matched  $k(L)a$ ," *Biotechnology and Bioengineering*, vol. 99, no. 5, pp. 1128–1139, 2008.
- [63] X. Ge, Y. Kostov, and G. Rao, "Low-cost noninvasive optical CO<sub>2</sub> sensing system for fermentation and cell culture," *Biotechnology and Bioengineering*, vol. 89, no. 3, pp. 329–334, 2004.
- [64] G. Liebsch, I. Klimant, B. Frank, G. Holst, and O. Wolfbeis, "Luminescence lifetime imaging of oxygen, pH, and carbon dioxide distribution using optical sensors," *Applied Spectroscopy*, vol. 54, no. 4, pp. 548–559, 2000.
- [65] M. Scarff, S. A. Arnold, L. Harvey, and B. McNeil, "Near infrared spectroscopy for bioprocess monitoring and control: Current status and future trends," *Critical Reviews in Biotechnology*, vol. 26, pp. 17–39, 2006.
- [66] H. Lee, P. Boccazzi, N. Gorret, R. Ram, and A. Sinskey, "In situ bioprocess monitoring of escherichia coli bioreactions using raman spectroscopy," *Vibrational Spectroscopy*, vol. 35, no. 1-2, pp. 131–137, 2004.
- [67] E. Cao, S. Firth, P. McMillan, and A. Gavriilidis, "Application of micro-fabricated reactors for operando raman studies of catalytic oxidation of methanol to formaldehyde on silver," *Catalysis Today*, vol. 126, no. 1-2, pp. 119–126, 2007.
- [68] W. Ferstl, T. Klahn, W. Schweikert, G. Billeb, M. Schwarzer, and S. Loebbecke, "Inline analysis in microreaction technology: A suitable tool for process screening and optimization," *Chemical Engineering & Technology*, vol. 30, no. 3, pp. 370–378, 2007.
- [69] "Biomass Research and Development, Technical Advisory Committee (2006) Vision for bioenergy and biobased products in the United States." <http://www.brdisolutions.com/default.aspx>.
- [70] SusChem, "European Technology Platform, Industrial Biotechnology Section (2005)." <http://www.suschem.org/>, 2009.
- [71] D. Riesenberger and R. Guthke, "High-cell-density cultivation of microorganisms," *Applied Microbiology and Biotechnology*, vol. 51, no. 4, pp. 422–430, 1999.
- [72] M. Åkesson, P. Hagander, and J. Axelsson, "A probing feeding strategy for escherichia coli cultures," *Biotechnology Techniques*, vol. 13, no. 8, pp. 523–528, 1999.
- [73] L. de Maré, C. Cimander, A. Elfving, and P. Hagander, "Feeding strategies for e-coli fermentations demanding an enriched environment," *Bioprocess and Biosystems Engineering*, vol. 30, no. 1, pp. 13–25, 2007.
- [74] Sartorius, "BIOSTAT CultiBag RM." <http://www.sartorius-stedim.com/>, 2009.

- [75] R. Sathuluri, S. Yamamura, and E. Tamiya, "Microsystems technology and biosensing," in *Biosensing for the 21st Century*, pp. 285–350, Springer, 2008.
- [76] B. Lennox, G. Montague, H. Hiden, G. Kornfeld, and P. Goulding, "Process monitoring of an industrial fed-batch fermentation," *Biotechnology and Bioengineering*, vol. 74, no. 2, pp. 125–135, 2001.
- [77] H. Sundström and S. Enfors, "Software sensors for fermentation processes," *Bioprocess and Biosystems Engineering*, vol. 31, no. 2, pp. 145–152, 2008.
- [78] W. A. Duetz, "Microtiter plates as mini-bioreactors: miniaturization of fermentation methods," *Trends in Microbiology*, vol. 15, pp. 469–475, Oct. 2007.
- [79] M. Micheletti, T. Barrett, S. Doig, F. Baganz, M. Levy, J. Woodley, and G. Lye, "Fluid mixing in shaken bioreactors: Implications for scale-up predictions from microlitre-scale microbial and mammalian cell cultures," *Chemical Engineering Science*, vol. 61, pp. 2939–2949, May 2006.
- [80] A. Akgün, B. Maier, D. Preis, B. Roth, R. Klingelhöfer, and J. Büchs, "A novel parallel shaken bioreactor system for continuous operation," *Biotechnology Progress*, vol. 20, pp. 1718–1724, 2004.
- [81] A. Chen, R. Chitta, D. Chang, and A. Amanullah, "Twenty-four well plate miniature bioreactor system as a scale-down model for cell culture process development," *Biotechnology and Bioengineering*, vol. 102, no. 1, pp. 148–160, 2009.
- [82] G. Rao, A. Moreira, and K. Brorson, "Disposable bioprocessing: The future has arrived," *Biotechnology and Bioengineering*, vol. 102, no. 2, pp. 348–356, 2009.
- [83] J. de Jong, R. G. Lammertink, and M. Wessling, "Membranes and microfluidics: a review," *Lab on a Chip*, vol. 6, pp. 1125–139, 2006.
- [84] J. J. Horvath, S. A. Glazier, and C. J. Spangler, "In situ fluorescence cell mass measurements of *saccharomyces cerevisiae* using cellular tryptophan," *Biotechnolgy Progresses*, vol. 9, pp. 666–670, 1993.
- [85] J. Li, E. Asali, and A. Humphrey, "Monitoring cell concentration and activity by multiple excitation fluorometry," *Biotechnology Progress*, vol. 7, no. 1, pp. 21–27, 1991.
- [86] R. Matanguihan, K. Konstantinov, and T. Yoshida, "Dielectric measurement to monitor the growth and the physiological states of biological cells," *Bioprocess Engineering*, vol. 11, no. 6, pp. 213–222, 1994.
- [87] A. Ferreira, L. Vieira, J. Cardoso, and J. Menezes, "Evaluation of a new annular capacitance probe for biomass monitoring in industrial pilot-scale fermentations," *Journal of Biotechnology*, vol. 116, no. 4, pp. 403–409, 2005.

- [88] J. M. Ottino and S. Wiggins, "Introduction: mixing in microfluidics," *Philosophical Transactions of the Royal Society of London Series A - Mathematical, Physical and Engineering Sciences*, vol. 362, no. 1818, pp. 923–935, 2004.
- [89] H. Zhu, Z. Zhou, R. Yang, and A. Yu, "Discrete particle simulation of particulate systems: A review of major applications and findings," *Chemical Engineering Science*, vol. 63, no. 23, pp. 5728–5770, 2008.
- [90] H. Zhu, Z. Zhou, R. Yang, and A. Yu, "Discrete particle simulation of particulate systems: Theoretical developments," *Chemical Engineering Science*, vol. 62, no. 13, pp. 3378–3396, 2007.
- [91] E. Berthier, J. Warrick, H. Yu, and D. J. Beebe, "Managing evaporation for more robust microscale assays. part 1: Volume loss in high throughput assays," *Lab on a Chip*, vol. 8, pp. 852–859, 2008.
- [92] F. Arroyo-Lopez, S. Orlic, A. Querol, and E. Barrio, "Effects of temperature, pH and sugar concentration on the growth parameters of *saccharomyces cerevisiae*, *s. kudriavzevii* and their interspecific hybrid," *International Journal of Food Microbiology*, vol. 131, no. 2-3, pp. 120–127, 2009.
- [93] S. Chuppa, Y. Tsai, S. Yoon, S. Shackleford, C. Rozales, R. Bhat, G. Tsay, C. Matanguihan, K. Konstantinov, and D. Naveh, "Fermentor temperature as a tool for control of high-density perfusion cultures of mammalian cells," *Biotechnology and Bioengineering*, vol. 55, no. 2, pp. 328–338, 1996.
- [94] P. Kromer, R. Robinett, R. Bengtson, and C. Hays, "PC-Based digital Lock-In detection of small signals in the presence of noise," tech. rep., Department of Physics, University of Texas at Austin.
- [95] J. H. Scofield, "A frequency-domain description of a lock-in amplifier," *American Journal of Physics*, vol. 62, no. 2, pp. 129–133, 1994.
- [96] M. A. Eddings and B. K. Gale, "A PDMS-based gas permeation pump for on-chip fluid handling in microfluidic devices," *Journal of Micromechanics and Microengineering*, vol. 16, no. 11, pp. 2396–2402, 2006.
- [97] M. Johnson, G. Liddiard, M. Eddings, and B. Gale, "Bubble inclusion and removal using PDMS membrane-based gas permeation for applications in pumping, valving and mixing in microfluidic devices," *Journal of Micromechanics and Microengineering*, vol. 19, p. 095011, 2009.
- [98] C. Roosen, M. Ansorge-Schumacher, T. Mang, W. Leitner, and L. Greiner, "Gaining pH-control in water/carbon dioxide biphasic systems," *Green Chemistry*, vol. 9, pp. 455–458, May 2007.
- [99] S. Clegg and P. Brimblecombe, "Solubility of ammonia in pure aqueous and multicomponent solutions," *Journal of Physical Chemistry*, vol. 93, no. 20, pp. 7237–7248, 1989.
- [100] D. Green and R. Perry, *Perry's Chemical Engineers' Handbook*. McGraw-Hill, 8th edition ed., 2008.

- [101] N. L. Morgan, G. Higton, and J. S. Rockey, *Industrial Microbiology: An Introduction*. Wiley-Blackwell, 2001.
- [102] A. H. Rose and J. S. Harrison, *The yeasts*. London: Academic Press, 2nd ed., 1991.
- [103] DTU Department of Systems Biology, “Exercise manual: Yeast cultivations.”
- [104] P. Wildberger, *Comparison of the cultivation of *S. cerevisiae* in micro-bioreactors and bench-scale fermentors*. Masters thesis, Technical University of Denmark, Kgs. Lyngby, Denmark, 2009.
- [105] H. G. Choi, Z. Zhang, P. Boccazzi, P. E. Laibinis, A. J. Sinskey, and K. F. Jensen, “Poly(ethylene glycol) (PEG)- modified poly(dimethylsiloxane) (PDMS) for protein- and cell-resistant surfaces in microbioreactor,” in *7th International Conference on Miniaturized Chemical and Biochemical Analysis Systems*, pp. 1105–1108, 2003.
- [106] F. Okkels and H. Bruus, “Design of micro-fluidic bio-reactors using topology optimization,” *Journal of Computational and Theoretical Nanoscience*, vol. 4, no. 4, pp. 814–816, 2007.
- [107] M. P. Bendsoe and O. Sigmund, *Topology Optimization -Theory, Methods and Applications*. Springer, 2nd ed., 2002.
- [108] M. P. Bendsoe and N. Kikuchi, “Generating optimal topologies in structural design using a homogenization method,” *Computer Methods in applied Mechanics and Engineering*, vol. 71, no. 2, pp. 197–224, 1988.
- [109] T. Borrvall and J. Petersson, “Topology optimization of fluids in stokes flow,” *International Journal for Numerical Methods in Fluids*, vol. 41, no. 1, pp. 77–107, 2003.
- [110] L. Olesen, F. Okkels, and H. Bruus, “A high-level programming-language implementation of topology optimization applied to steady-state Navier-Stokes flow,” *International Journal for Numerical Methods in Engineering*, vol. 65, no. 7, pp. 975–1001, 2006.
- [111] F. Okkels and H. Bruus, “Scaling behavior of optimally structured catalytic microfluidic reactors,” *Physical Review E*, vol. 75, no. 1, 2007.
- [112] H. A. Eschenauer and N. Olhoff, “Topology optimization of continuum structures: A review,” *Applied Mechanics Reviews*, vol. 54, no. 4, p. 331, 2001.
- [113] M. Bendsoe, E. Lund, N. Olhoff, and O. Sigmund, “Topology optimization - broadening the areas of application,” *Control and Cybernetics*, vol. 34, no. 1, pp. 7–35, 2005.
- [114] K. V. Gernaey, A. E. Lantz, P. Tufvesson, J. Woodley, and G. Sin, “Application of mechanistic models to fermentation and biocatalysis for next generation processes,” *Trends in Biotechnology*, vol. accepted for publication, 2010.

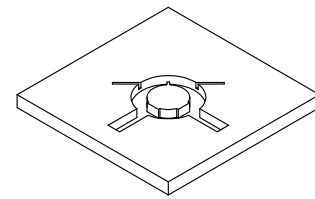
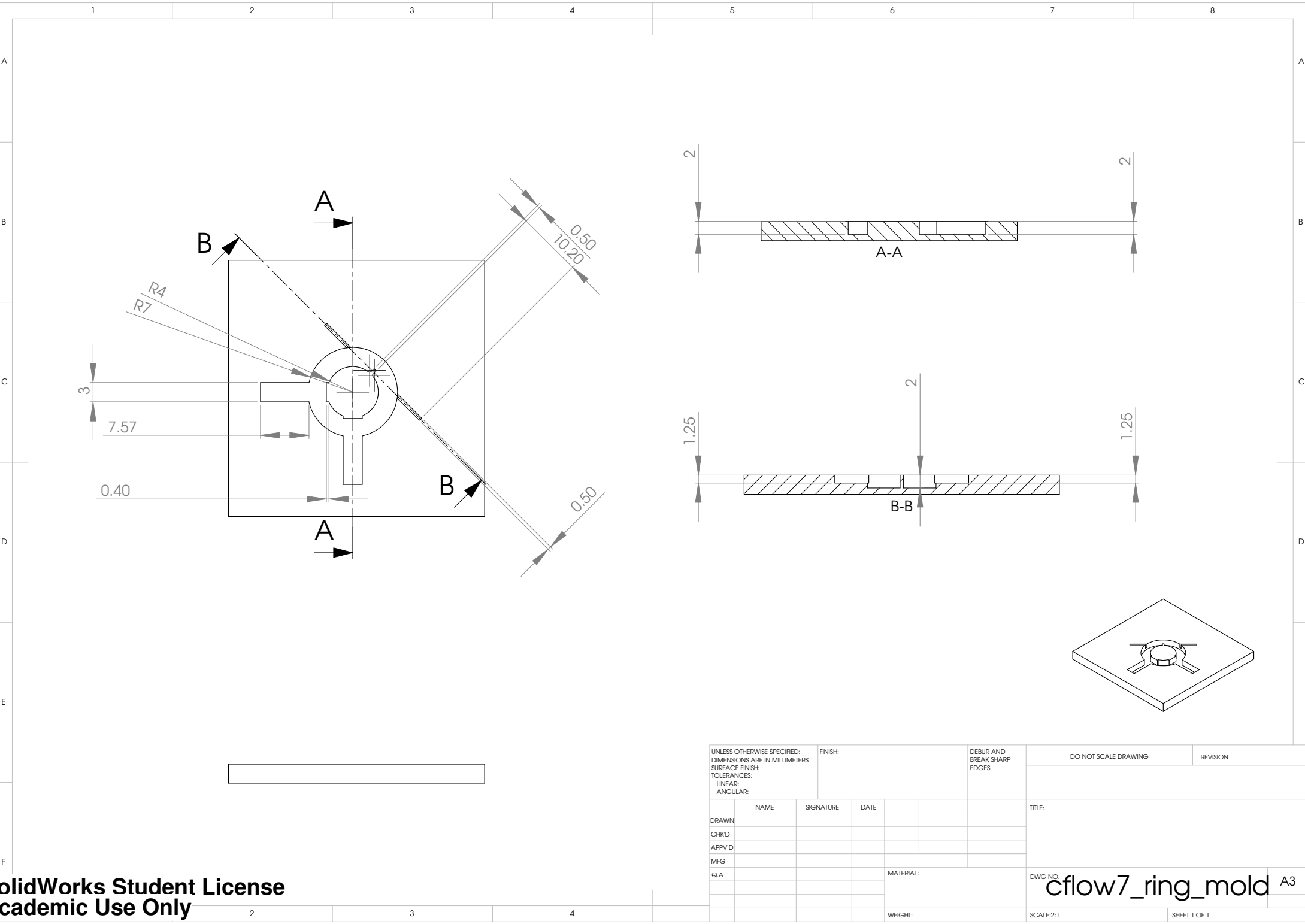


- [115] S. Enfors, M. Jahic, A. Rozkov, B. Xu, M. Hecker, B. Jurgen, E. Kruger, T. Schweder, G. Hamer, D. O'Beirne, N. Noisommit-Rizzi, M. Reuss, L. Boone, C. Hewitt, C. McFarlane, A. Nienow, T. Kovacs, C. Tragardh, L. Fuchs, J. Revstedt, P. Friberg, B. Hjertager, G. Blomsten, H. Skogman, S. Hjort, F. Hoeks, H. Lin, P. Neubauer, R. van der Lans, K. Luyben, P. Vrabel, and A. Manelius, "Physiological responses to mixing in large scale bioreactors," *Journal of Biotechnology*, vol. 85, no. 2, pp. 175–185, 2001.
- [116] A. Lapin, D. Muller, and M. Reuss, "Dynamic behavior of microbial populations in stirred bioreactors simulated with Euler-Lagrange methods: Traveling along the lifelines of single cells," *Industrial & Engineering Chemistry Research*, vol. 43, no. 16, pp. 4647–4656, 2004.
- [117] T. Branyik, A. Vicente, G. Kuncova, O. Podrazky, P. Dostalek, and J. Teixeira, "Growth model and metabolic activity of brewing yeast biofilm on the surface of spent grains: A biocatalyst for continuous beer fermentation," *Biotechnology Progress*, vol. 20, no. 6, pp. 1733–1740, 2004.
- [118] G. Desmet, J. D. Greef, H. Verelst, and G. Baron, "Performance limits of isothermal packed bed and perforated monolithic bed reactors operated under laminar flow conditions. i. general optimization analysis," *Chemical Engineering Science*, vol. 58, no. 14, pp. 3187–3202, 2003.
- [119] Z. Zhang, J. M. Scharer, and M. Moo-Young, "Mathematical model for aerobic culture of a recombinant yeast," *Bioprocess and Biosystems Engineering*, vol. 17, no. 4, pp. 235–240, 1997.
- [120] M. Reichen, *Development of a Microbioreactor with Integrated Mixing and Oxygen Monitoring*. Masters thesis, Technical University of Denmark, Kgs. Lyngby, Denmark, Feb. 2006.

APPENDIX A

# Microbioreactor: Mechanical drawings

---



UNLESS OTHERWISE SPECIFIED: DIMENSIONS ARE IN MILLIMETERS SURFACE FINISH: TOLERANCES: LINEAR: ANGULAR:						FINISH:	DEBUR AND BREAK SHARP EDGES	DO NOT SCALE DRAWING	REVISION
DRAWN						NAME		TITLE:	
CHK'D						SIGNATURE	DATE	cflow7_ring_mold A3	
APPV'D									
MFG									
Q.A									
						MATERIAL:		DWG NO.	
						WEIGHT:		SCALE:2:1	SHEET 1 OF 1

1

2

3

4

A

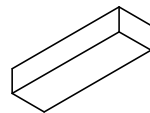
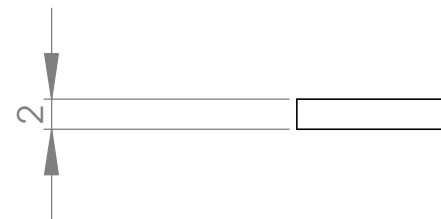
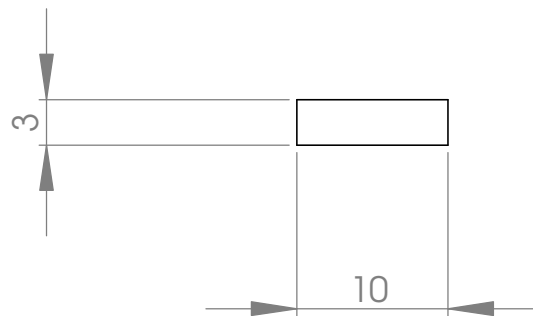
B

C

D

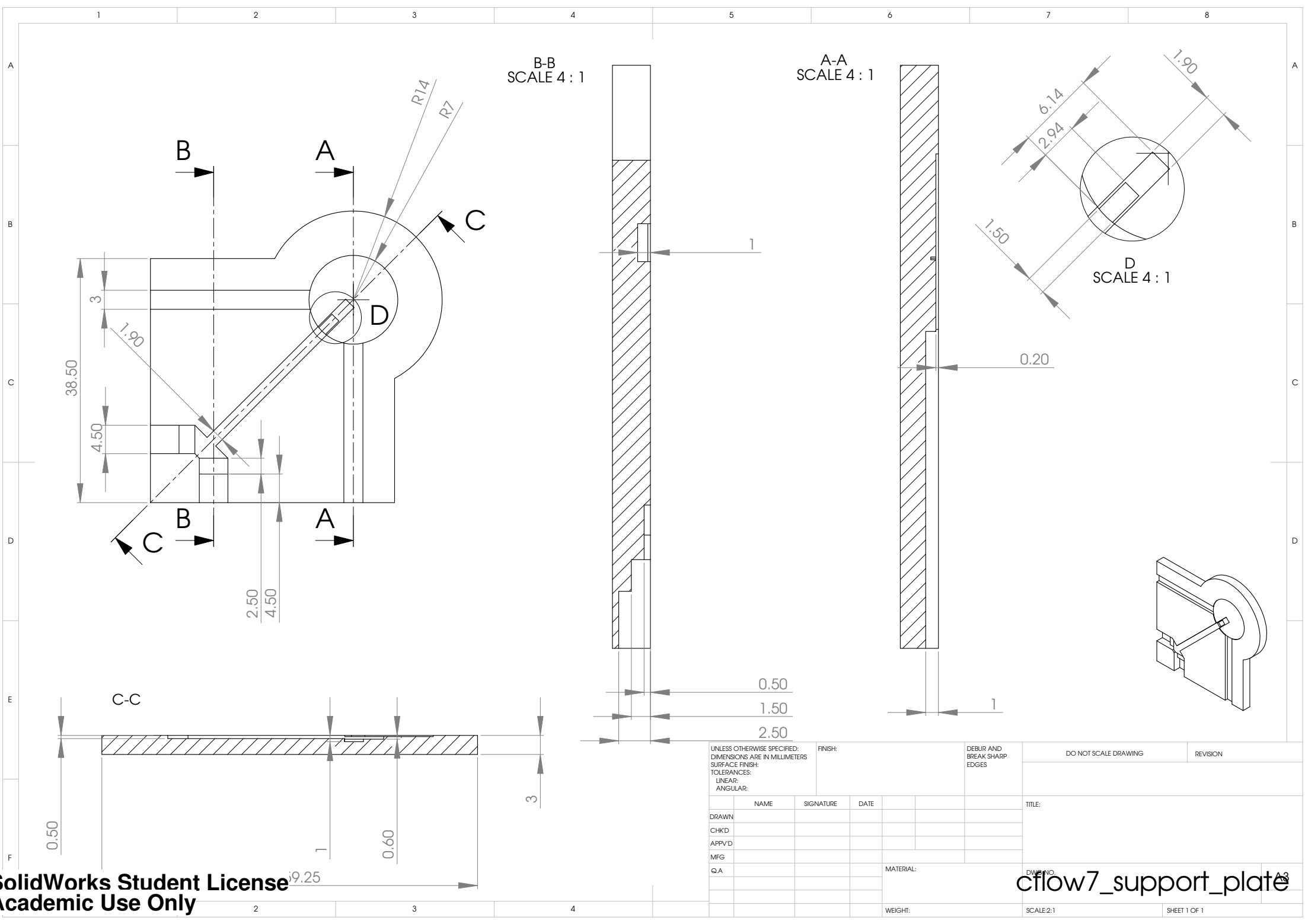
E

F



UNLESS OTHERWISE SPECIFIED: DIMENSIONS ARE IN MILLIMETERS SURFACE FINISH: TOLERANCES: LINEAR: ANGULAR:				FINISH:		DEBUR AND BREAK SHARP EDGES		DO NOT SCALE DRAWING		REVISION	
	NAME	SIGNATURE	DATE			TITLE:					
DRAWN											
CHK'D											
APPV'D											
MFG											
Q.A				MATERIAL:			DWG NO.		cflow7_plug		A4
WORKS Student License Non-Commercial Use Only				WEIGHT:			SCALE: 1:1		SHEET 1 OF 1		

UNLESS OTHERWISE SPECIFIED: DIMENSIONS ARE IN MILLIMETERS SURFACE FINISH: TOLERANCES: LINEAR: ANGULAR:				FINISH:		DEBUR AND BREAK SHARP EDGES		DO NOT SCALE DRAWING		REVISION		
	NAME		SIGNATURE		DATE				TITLE:			
DRAWN												
CHK'D												
APPV'D												
MFG												
Q.A							MATERIAL:		DWG NO.		A4	
works Student License mic Use Only						WEIGHT:		SCALE:2:1			SHEET 1 OF 1	



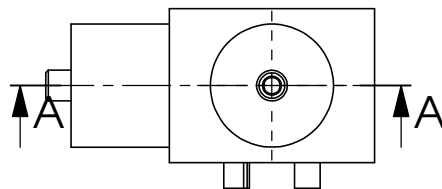
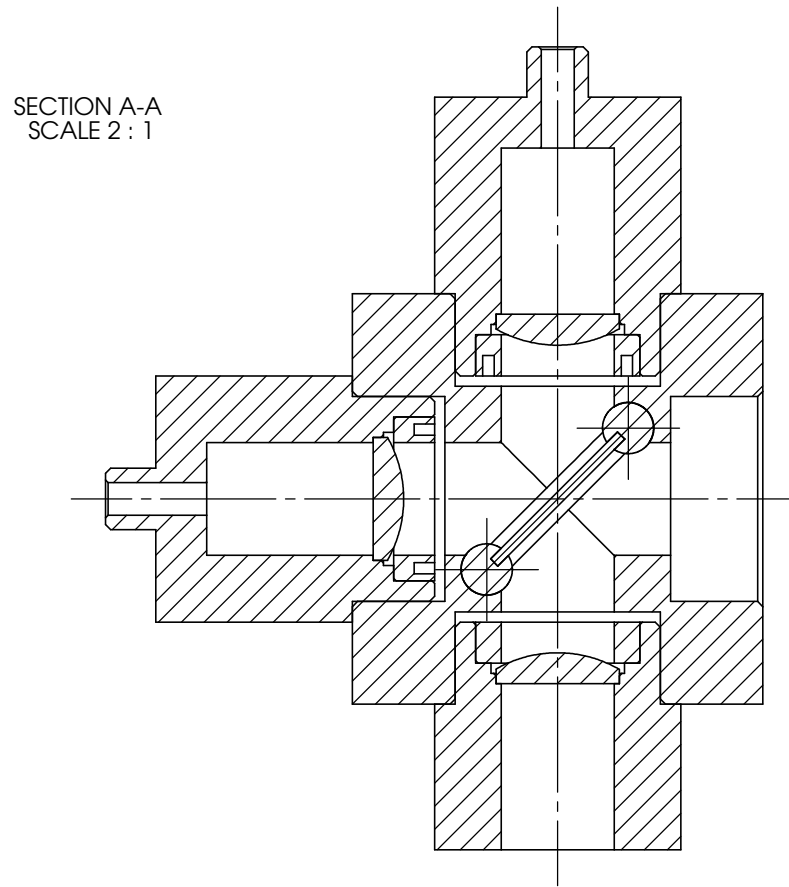


APPENDIX B

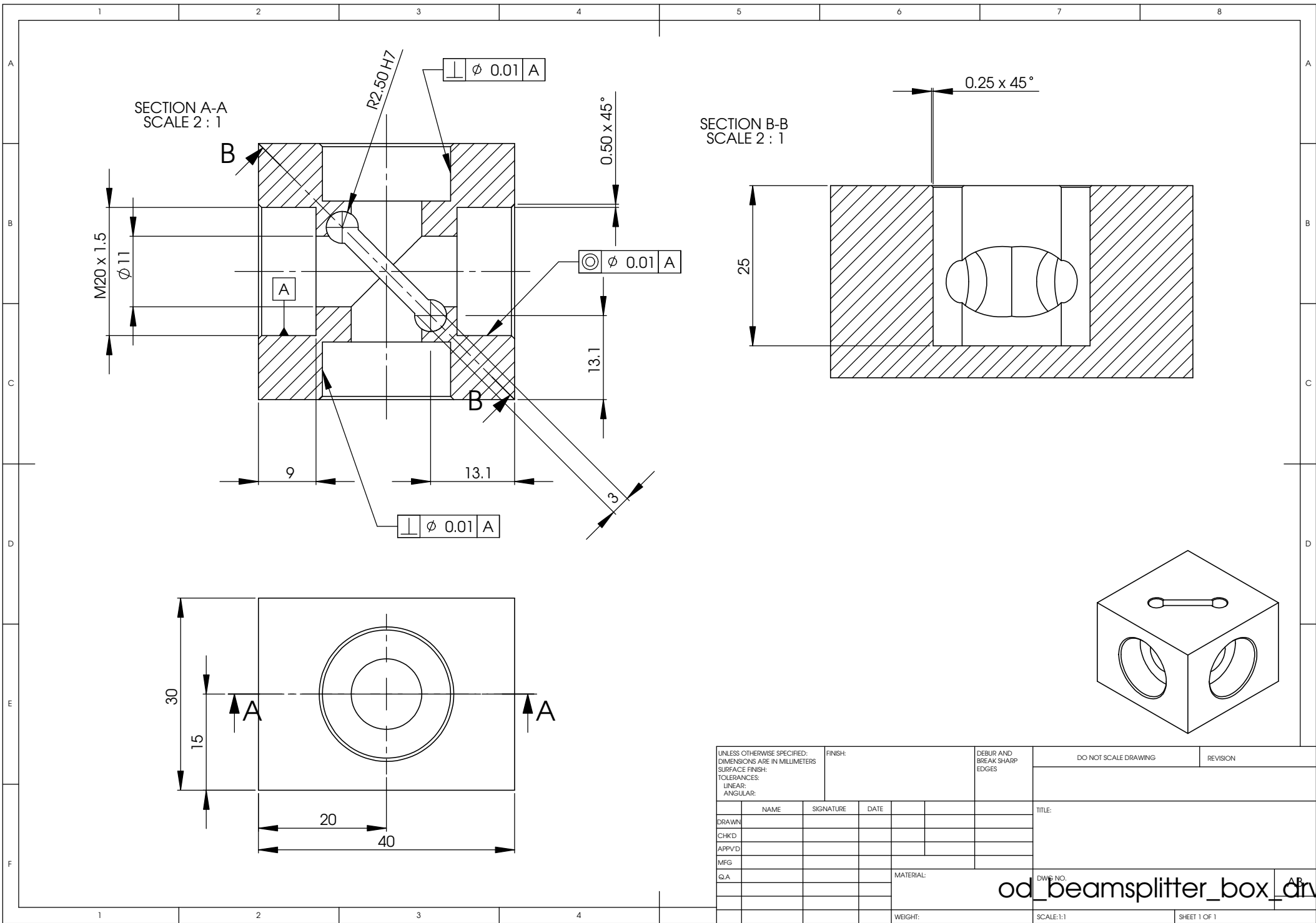
# Optical density: Mechanical drawings

---



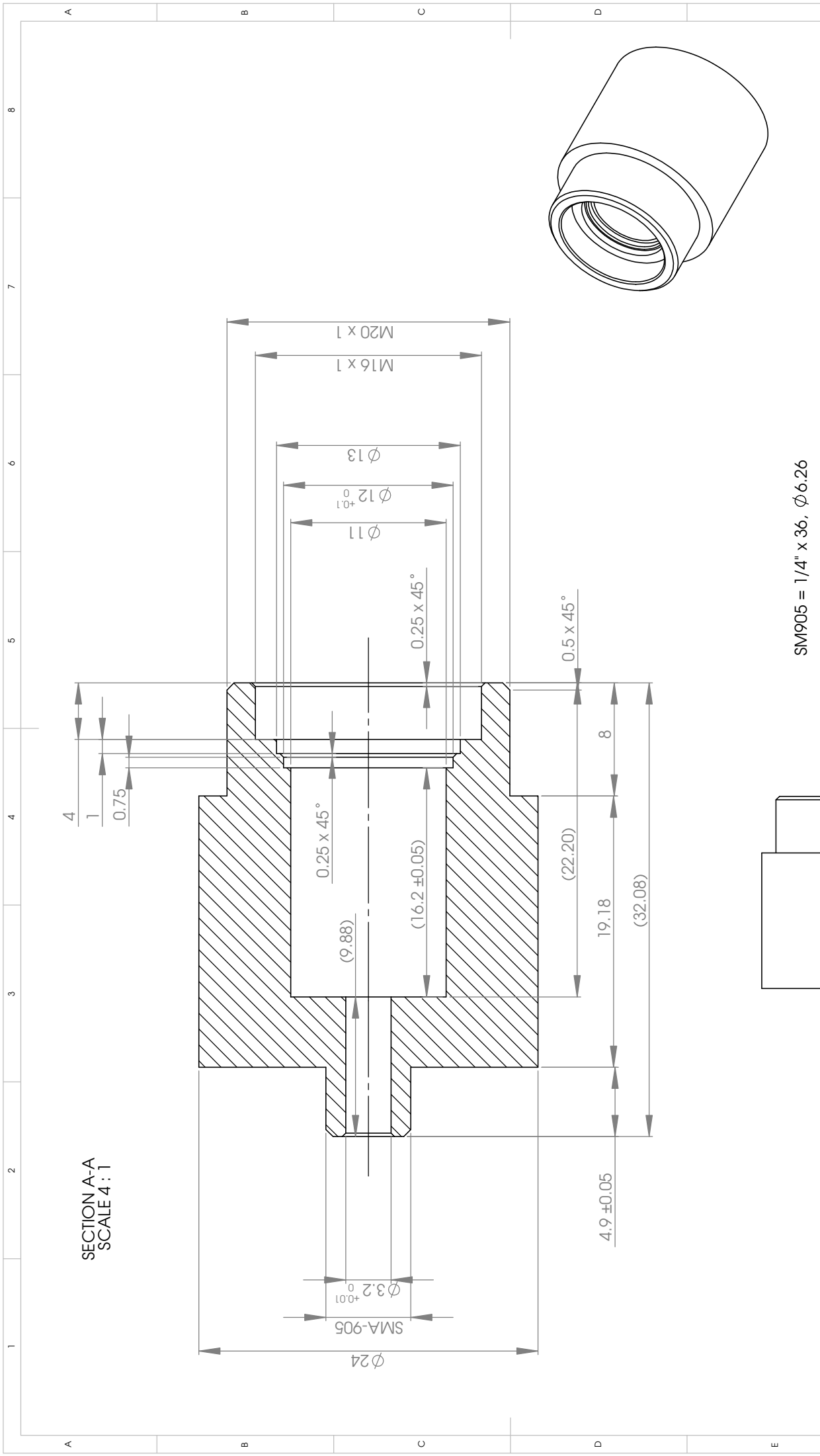


UNLESS OTHERWISE SPECIFIED: DIMENSIONS ARE IN MILLIMETERS SURFACE FINISH: TOLERANCES: LINEAR: ANGULAR:						FINISH:		DEBUR AND BREAK SHARP EDGES		DO NOT SCALE DRAWING		REVISION	
NAME		SIGNATURE		DATE						TITLE:			
DRAWN													
CHKD													
APPVD													
MFG													
Q.A.						MATERIAL:				DWG NO.		A3	
						WEIGHT:				SCALE: 1:1		SHEET 1 OF 1	



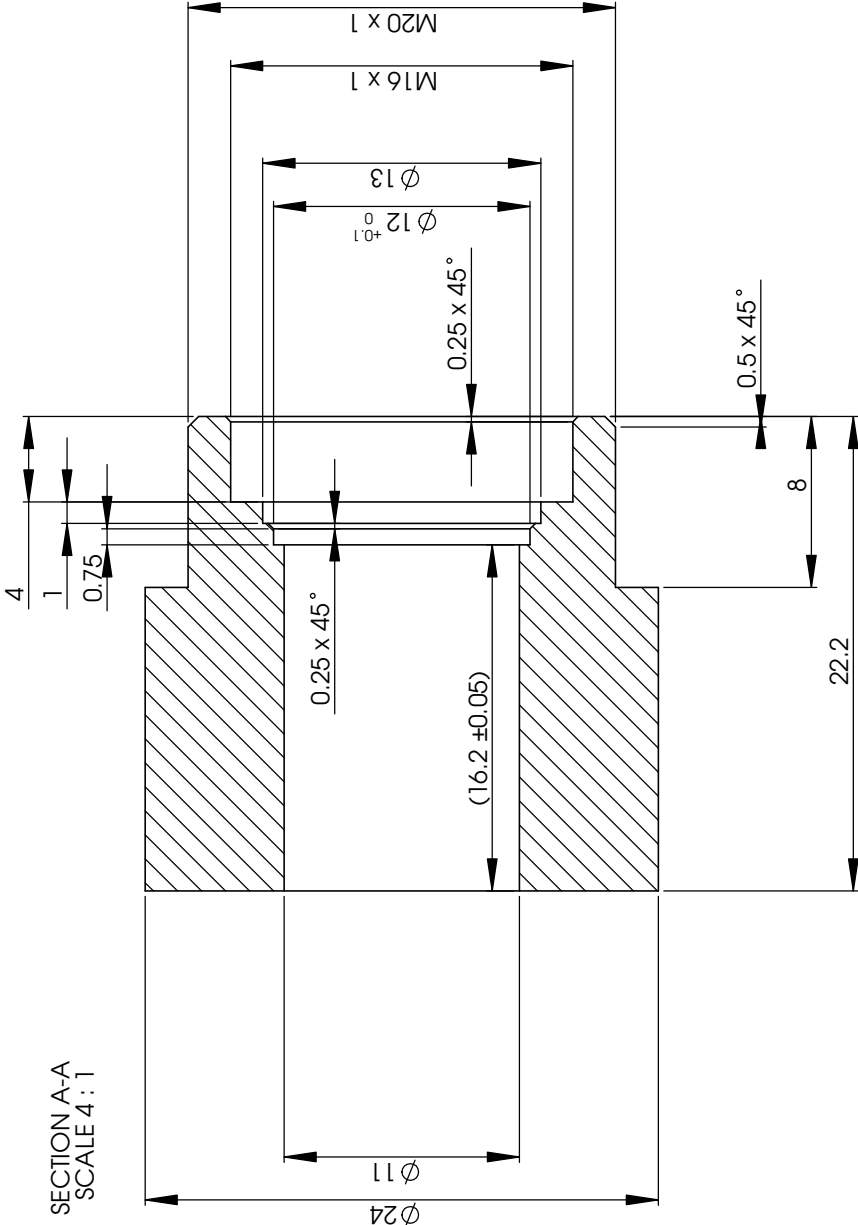
UNLESS OTHERWISE SPECIFIED: DIMENSIONS ARE IN MILLIMETERS SURFACE FINISH: TOLERANCES: LINEAR: ANGULAR:				FINISH:		DEBUR AND BREAK SHARP EDGES		DO NOT SCALE DRAWING	REVISION
	NAME	SIGNATURE	DATE					TITLE:	
DRAWN									
CHK'D									
APP'VD									
MFG									
Q.A								DWG NO.	
								SCALE:1:1	
								SHEET 1 OF 1	

od\_beamsplitter\_box\_drw

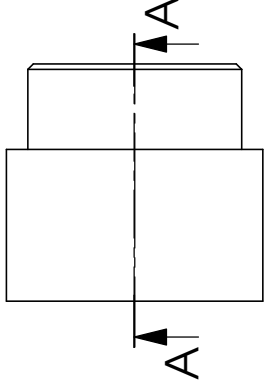
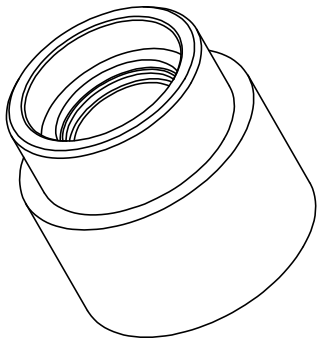


SM905 = 1/4" x 36,  $\phi 6.26$

										2		3		4	
SolidWorks Student License Academic Use Only															
UNLESS OTHERWISE SPECIFIED: DIMENSIONS ARE IN MILLIMETERS				FINISH:		DEBUR AND BREAK SHARP EDGES		DO NOT SCALE DRAWING		REVISION					
TOLERANCES: LINEAR: ANGULAR:															
NAME		SIGNATURE		DATE		TITLE:									
DRAWN															
CHKD															
APPVD															
MFG															
Q.A						MATERIAL:		DWG NO.		od_beamsplitter_fiber_holder					
										SCALE: 1:1					
						WEIGHT:				SHEET 1 OF 1					



SECTION A-A  
SCALE 4 : 1



UNLESS OTHERWISE SPECIFIED: DIMENSIONS ARE IN MILLIMETERS SURFACE FINISH: TOLERANCES: LINEAR: ANGULAR:				FINISH:	DEBUR AND BREAK SHARP EDGES		DO NOT SCALE DRAWING	REVISION
NAME	SIGNATURE	DATE						
DRAWN								
CHKD								
APPVD								
MFG								
Q.A								
							TITLE:	

1

2

3

4

A

B

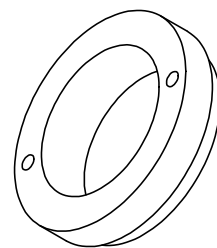
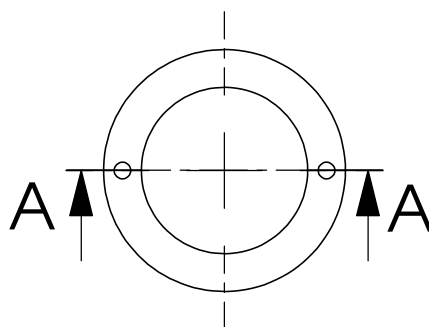
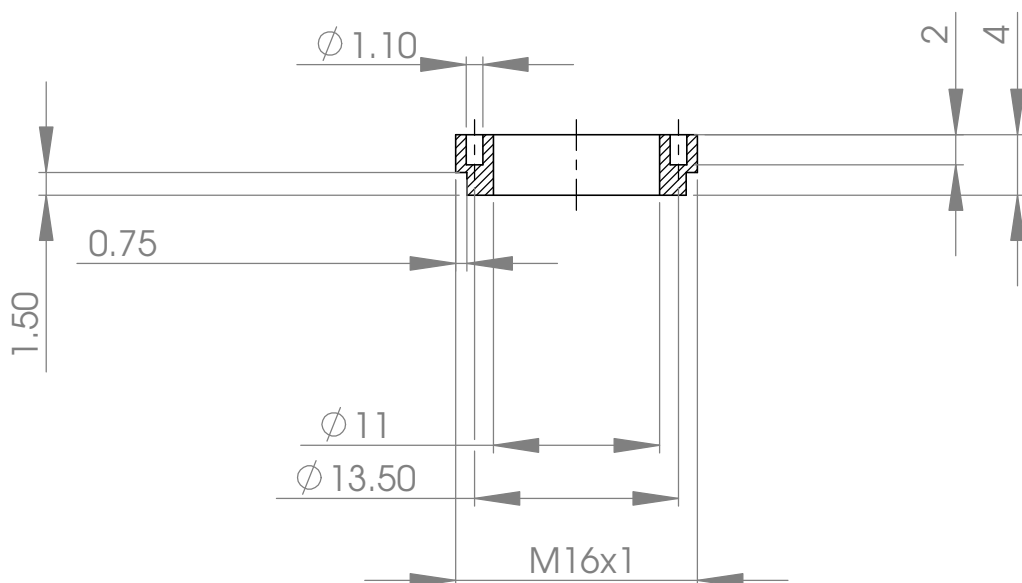
C

D

E

F

SECTION A-A



UNLESS OTHERWISE SPECIFIED:  
DIMENSIONS ARE IN MILLIMETERS  
SURFACE FINISH:  
TOLERANCES:  
LINEAR:  
ANGULAR:

FINISH:

DEBUR AND  
BREAK SHARP  
EDGES

DO NOT SCALE DRAWING

REVISION

	NAME	SIGNATURE	DATE			
DRAWN						
CHK'D						
APPV'D						
MFG						
Q.A						

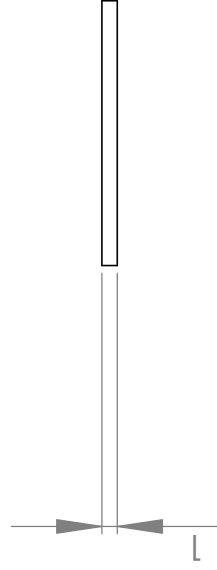
MATERIAL:

DWG NO.

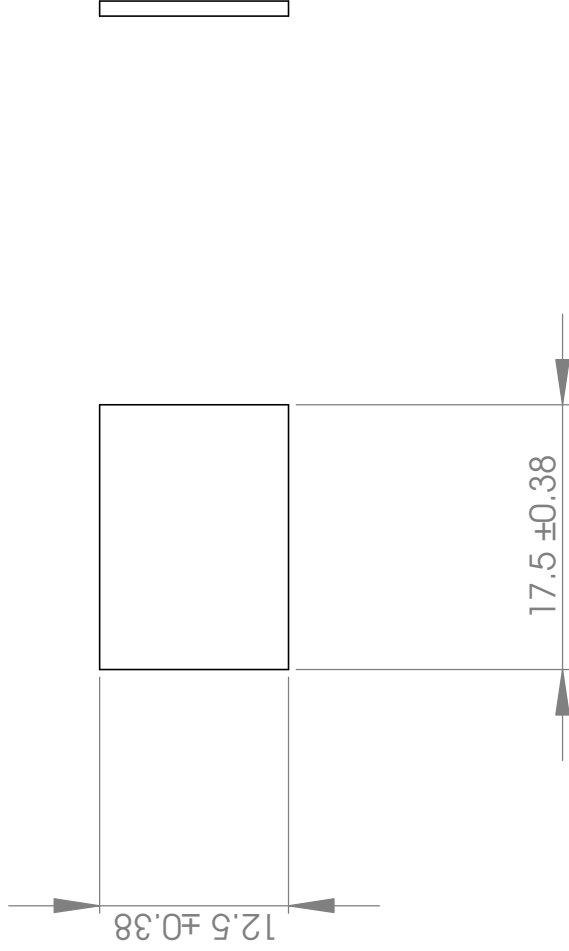
WEIGHT:

SCALE:2:1

SHEET 1 OF 1

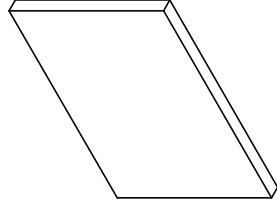


B



C

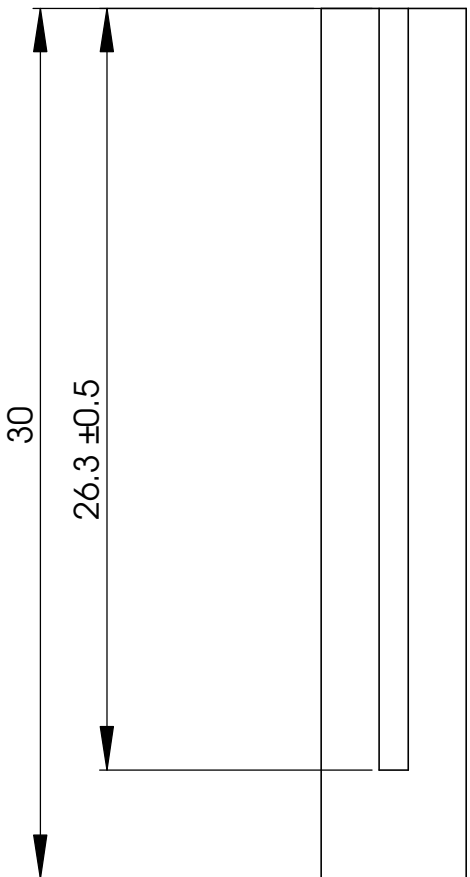
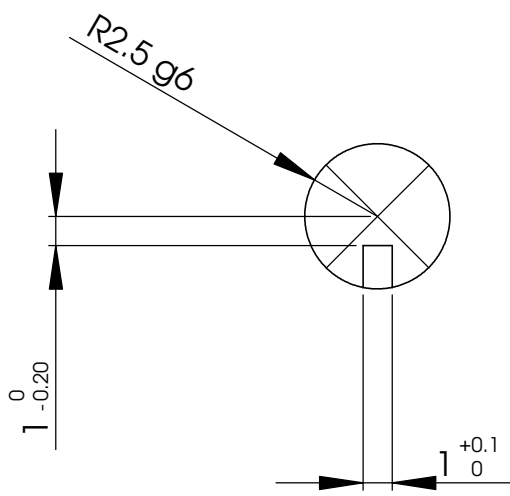
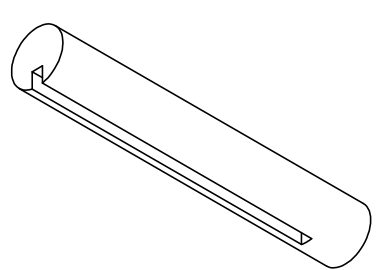
D



Does not have to be fabricated - only for information purposes!  
Edmund Optics R45-317 (70%R - 30%T)

E

<b>SolidWorks Student License</b> <b>Academic Use Only</b>		FINISH:  OTHERWISE SPECIFIED: DIMENSIONS ARE IN MILLIMETERS FINISH: TOLERANCES: LINEAR: ANGULAR:	DEBUR AND BREAK SHARP EDGES	DO NOT SCALE DRAWING	REVISION

	1	2	3	4																																																																																										
A																																																																																														
B																																																																																														
C																																																																																														
D																																																																																														
E																																																																																														
F	<table><tr><td colspan="2">UNLESS OTHERWISE SPECIFIED: DIMENSIONS ARE IN MILLIMETERS SURFACE FINISH: TOLERANCES:   LINEAR:   ANGULAR:</td><td colspan="2">FINISH:</td><td colspan="2">DEBUR AND BREAK SHARP EDGES</td><td colspan="2">DO NOT SCALE DRAWING</td><td colspan="2">REVISION</td></tr><tr><td colspan="2">DRAWN</td><td colspan="2">NAME</td><td colspan="2">SIGNATURE</td><td colspan="2">DATE</td><td colspan="2">TITLE:</td></tr><tr><td colspan="2">CHK'D</td><td colspan="2"></td><td colspan="2"></td><td colspan="2"></td><td colspan="2"></td></tr><tr><td colspan="2">APP'V'D</td><td colspan="2"></td><td colspan="2"></td><td colspan="2"></td><td colspan="2"></td></tr><tr><td colspan="2">MFG</td><td colspan="2"></td><td colspan="2"></td><td colspan="2"></td><td colspan="2"></td></tr><tr><td colspan="2">Q.A</td><td colspan="2"></td><td colspan="2"></td><td colspan="2">MATERIAL:</td><td colspan="2">DWG NO.</td></tr><tr><td colspan="2"></td><td colspan="2"></td><td colspan="2"></td><td colspan="2"></td><td colspan="2">od_beamsplitter_holder_dr</td></tr><tr><td colspan="2"></td><td colspan="2"></td><td colspan="2"></td><td colspan="2">WEIGHT:</td><td colspan="2">SCALE: 1:1</td></tr><tr><td colspan="2"></td><td colspan="2"></td><td colspan="2"></td><td colspan="2"></td><td colspan="2">SHEET 1 OF 1</td></tr></table>				UNLESS OTHERWISE SPECIFIED: DIMENSIONS ARE IN MILLIMETERS SURFACE FINISH: TOLERANCES: LINEAR: ANGULAR:		FINISH:		DEBUR AND BREAK SHARP EDGES		DO NOT SCALE DRAWING		REVISION		DRAWN		NAME		SIGNATURE		DATE		TITLE:		CHK'D										APP'V'D										MFG										Q.A						MATERIAL:		DWG NO.										od_beamsplitter_holder_dr								WEIGHT:		SCALE: 1:1										SHEET 1 OF 1	
UNLESS OTHERWISE SPECIFIED: DIMENSIONS ARE IN MILLIMETERS SURFACE FINISH: TOLERANCES: LINEAR: ANGULAR:		FINISH:		DEBUR AND BREAK SHARP EDGES		DO NOT SCALE DRAWING		REVISION																																																																																						
DRAWN		NAME		SIGNATURE		DATE		TITLE:																																																																																						
CHK'D																																																																																														
APP'V'D																																																																																														
MFG																																																																																														
Q.A						MATERIAL:		DWG NO.																																																																																						
								od_beamsplitter_holder_dr																																																																																						
						WEIGHT:		SCALE: 1:1																																																																																						
								SHEET 1 OF 1																																																																																						

1

2

3

4

A

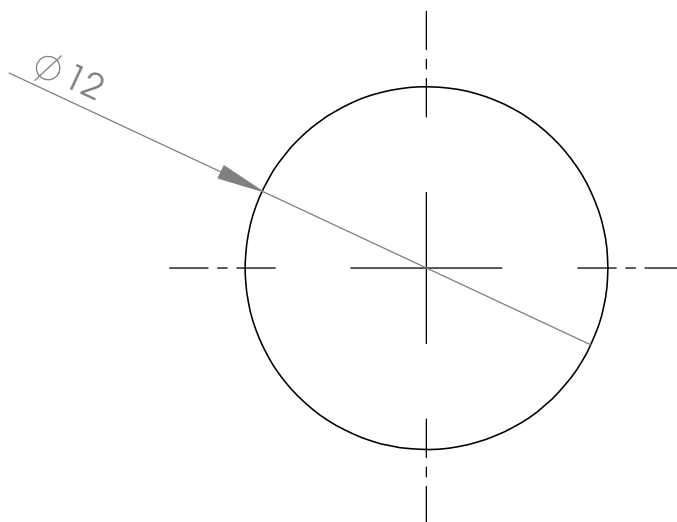
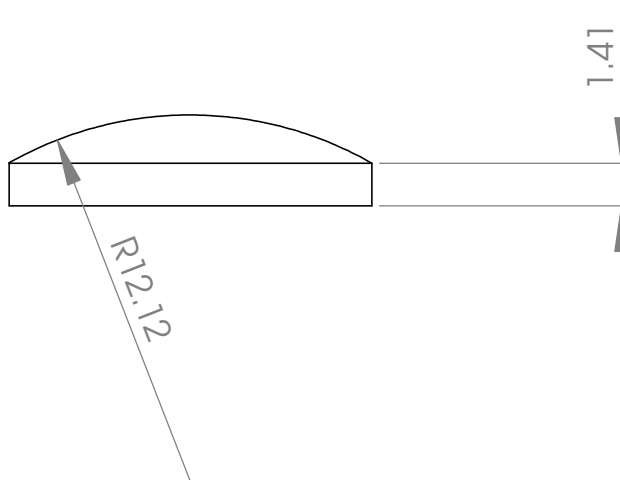
B

C

D

E

F



Does not have to be fabricated - only for information purposes!  
Edmund Optics, PCX 12/18 VIS-NIR Coated

UNLESS OTHERWISE SPECIFIED: DIMENSIONS ARE IN MILLIMETERS SURFACE FINISH: TOLERANCES: LINEAR: ANGULAR:				FINISH:		DEBUR AND BREAK SHARP EDGES		DO NOT SCALE DRAWING		REVISION	
NAME		SIGNATURE		DATE				TITLE:			
DRAWN											
CHK'D											
APPV'D											
MFG											
Q.A								MATERIAL:		DWG. NO.	
								od_beamsplitter_lens_pcx12_18		A4	
WEIGHT:				SCALE: 1:1				SHEET 1 OF 1			



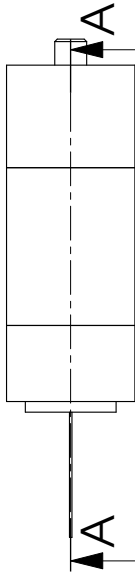
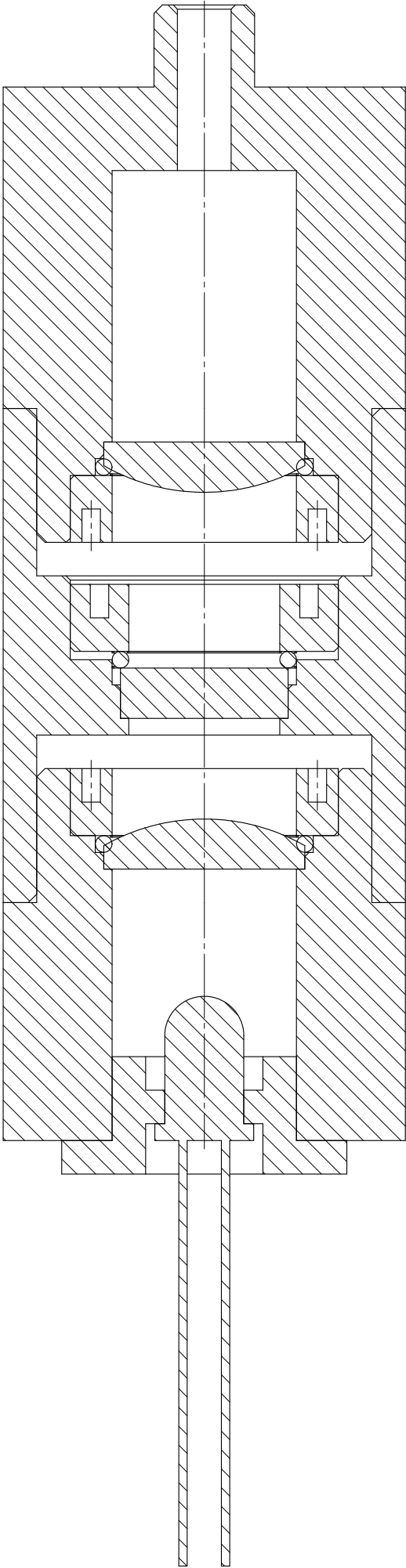


APPENDIX C

## **Dissolved oxygen & pH: Mechanical drawings**

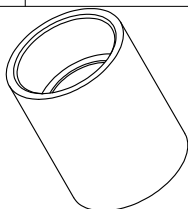
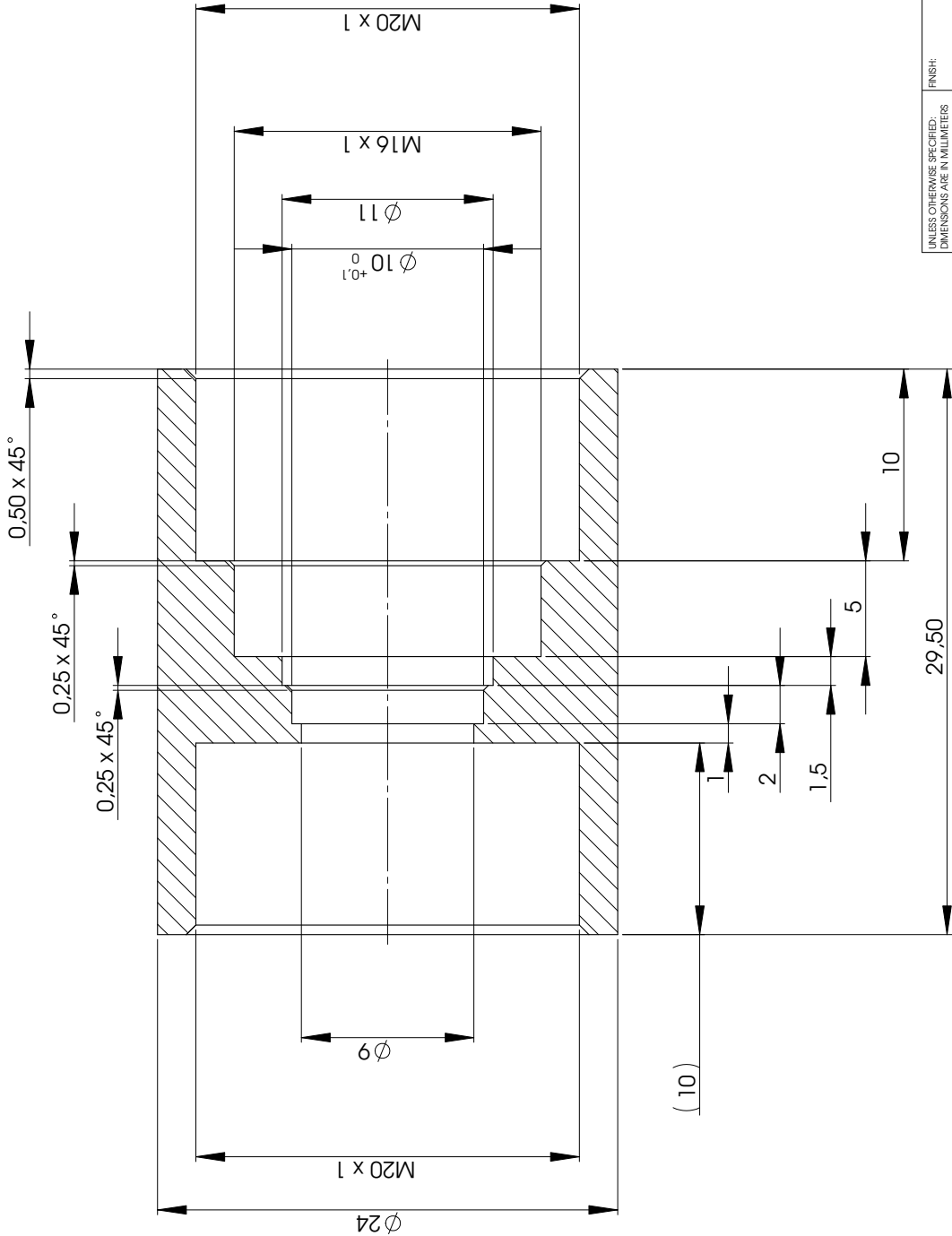
---

SECTION A-A  
SCALE 4:1



UNLESS OTHERWISE SPECIFIED: DIMENSIONS ARE IN MILLIMETERS SURFACE FINISH: TOLERANCES: LINEAR: ANGULAR:				FINISH:		DEBUR AND BREAK SHARP EDGES	DO NOT SCALE DRAWING		REVISION		
NAME		SIGNATURE		DATE			TITLE:				
DRAWN											
CHK'D											
APP'D											
MFG											
QA							DWG NO.				
							pH_assembly				
						SCALE: 1:1					
						SHEET 1 OF 1					

SECTION A-A  
SCALE 4 : 1



UNLESS OTHERWISE SPECIFIED: DIMENSIONS ARE IN MILLIMETERS				FINISH:		DEBUR AND BREAK SHARP EDGES	DO NOT SCALE DRAWING	REVISION
SURFACE FINISH:				TOLERANCES:				
LINEAR:				ANGULAR:				
	NAME	SIGNATURE	DATE				TITLE:	
DRAWN								
CHKD								
APP'D								
MFG								
Q.A								
MATERIAL:							DWG NO.	A3
							pH_coupling_drw	
							SCALE:1:1	SHEET 1 OF 1

1

2

3

4

A

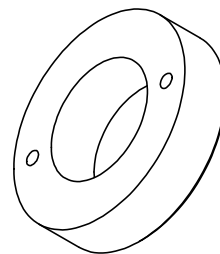
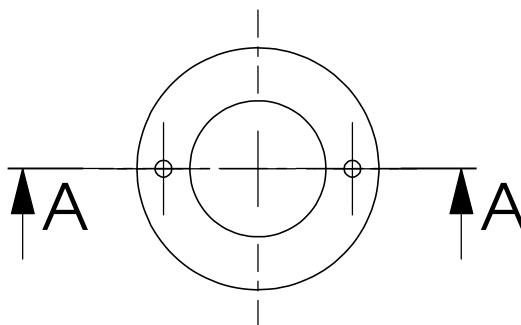
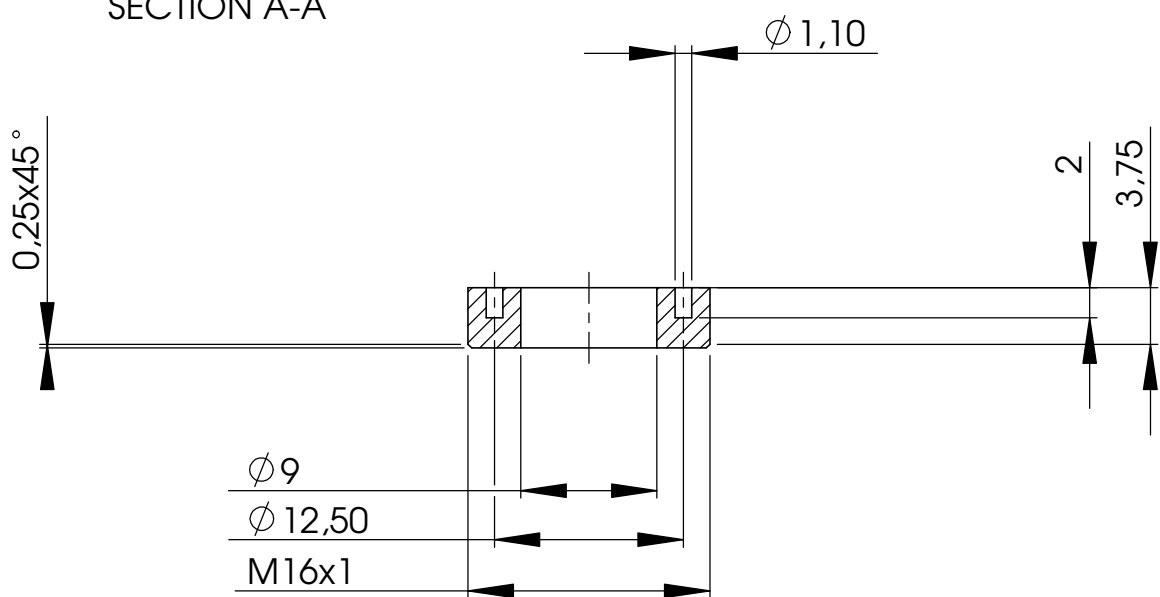
B

C

D

E

SECTION A-A



UNLESS OTHERWISE SPECIFIED:  
DIMENSIONS ARE IN MILLIMETERS  
SURFACE FINISH:  
TOLERANCES:  
LINEAR:  
ANGULAR:

FINISH:

DEBUR AND  
BREAK SHARP  
EDGES

DO NOT SCALE DRAWING

REVISION

	NAME	SIGNATURE	DATE		
DRAWN					
CHKD					
APPV'D					
MFG					
Q.A					

MATERIAL:

WEIGHT:

TITLE:

DWG NO.

SCALE:2:1

pH\_klemmring

A4

SHEET 1 OF 1

APPENDIX D

# Photodiodes: Mechanical drawings

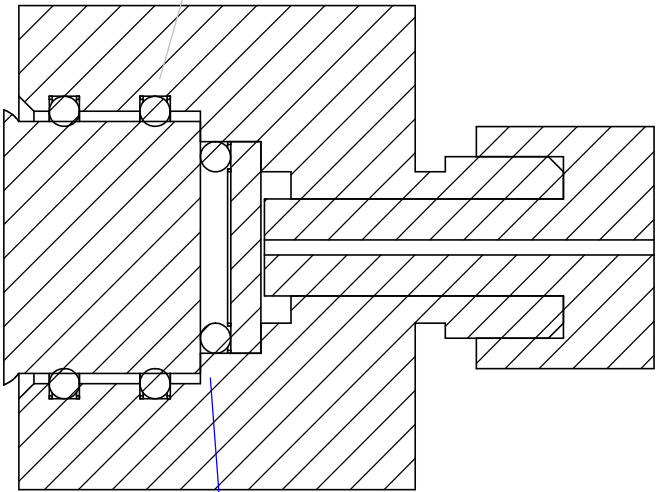
---

A

SECTION A-A  
SCALE 4 : 1

O-Ring 10-8-1 (2 pcs per assembly)

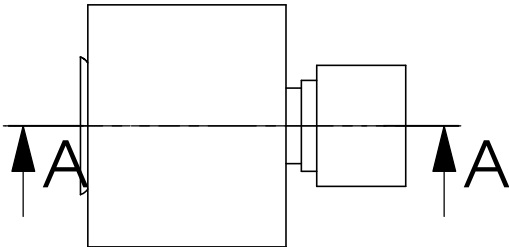
B



C

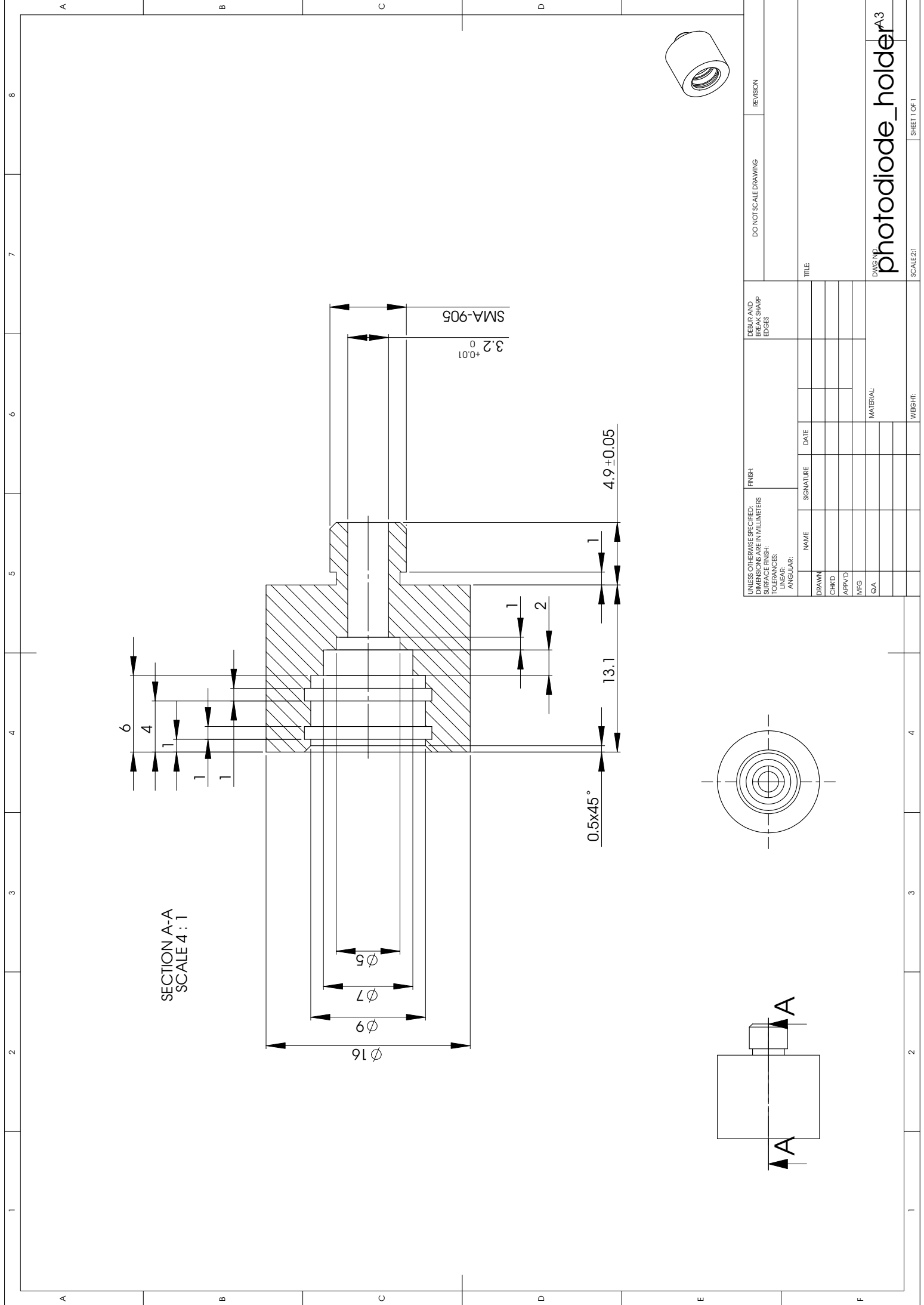
O-Ring 7-5-1 (1 pcs per assembly)

D



E

UNLESS OTHERWISE SPECIFIED: DIMENSIONS ARE IN MILLIMETERS SURFACE FINISH: TOLERANCES: LINEAR: ANGULAR:				FINISH:		DEBUR AND BREAK SHARP EDGES		DO NOT SCALE DRAWING		REVISION	
NAME		SIGNATURE		DATE				TITLE:			
DRAWN											
CHK'D											
APPV'D											
MFG								DWG NO. <b>photodiode_assembly</b>			
Q.A											
						MATERIAL:		A4			
						WEIGHT:		SCALE: 1:1		SHEET 1 OF 1	







# Procedure for the production of PDMS membranes

---

## Introduction

PDMS membranes are used in MicroBioReactors for the aeration of the cultures and also the removal of  $\text{CO}_2$  which is produced during fermentation. Until recently, these membranes were produced by spinning PDMS onto a silicon wafer with an antistiction coating. However, as the preparation of these wafers requires lengthy clean room processes another, simpler, solution was sought after. As PMMA is used when casting PDMS parts this was an obvious alternative. In these tests the PDMS membranes were spun onto PMMA discs of 5cm diameter (Fig. E.5). The basic feasibility has already been proven. These tests now investigate the influence of different spinning parameters on the resulting membrane thickness.

## Tests & Results

For the spinning process the parameters as given by (120) were used. These parameters have proven to be well suited to the silicon-wafer spinning process. Also, the same two-step approach was chosen. In the first step, a slow spinning was chosen to get the PDMS well distributed across the wafer and in the second step the final spinning was applied. The parameters and the resulting thicknesses can be summarized as follows:

There is a large difference between the two sets of measurements, the membranes spun on PMMA consequently being much thicker than those on the antistiction coated silicon wafers. Reasons for this difference might lie in the different surface properties or in viscosity differences of the PDMS when spinning. However, as the new results for each parameter variation closely resemble each other, there is no reason not to believe the results. An investigation into the causes for the differences is out of the scope of this experiment.

	Acceleration rpm/sec	Speed rpm	Time sec	Av. Thickness $\mu\text{m}$	Thickness acc. (120) $\mu\text{m}$
Step 1	5000	500	20	-	-
Step 2	5000	2000	30	$80.69 \pm 1.02$	33
	5000	3000	30	$41.81 \pm 0.39$	27
	5000	4000	30	$27.92 \pm 0.32$	19
	5000	5000	30	$21.11 \pm 0.14$	15

**Table E.1:** Summary of Results

The bottom line of these tests is that it should at least for the thicker membranes be well possible to use PMMA as wafer material. Should much thinner membranes be required then either antistiction coated silicon wafers should be used or alternatively the PDMS should be allowed to cure to higher viscosities before spinning.

## Production of the Membranes

PDMS was fabricated according to the standard recipe (10:1), thoroughly mixed and then dessicated until the mass was bubble-free (approximately 30 minutes). Thereafter, in short procession, the fluid was transferred to the PMMA wafers with a syringe and immediately spun according to the parameters in Table E.1. After spinning, the membranes were hardened out at 70 °C for one hour. The resulting membranes were then cut in half with a scalpel and one half was pulled off the PMMA wafer (Fig. E.5).

## Measurement Process

The measurements of the different membranes were done with the Dektak-8 at DanChip. Basically every membrane was measured once, only if the results did not prove satisfactory were additional measurements done on other parts of the membrane. Especially in the thinner membranes the effect of cutting the membrane apart can clearly be seen as an overshoot in material where probably some material was ‘shoved’ to the side. Also, from a purely qualitative point of view, the thinnest membranes (series D) seemed to have the most inconsistent membrane quality with lots of pits. The resulting measurement curves can be seen in Figures E.1 - E.4.

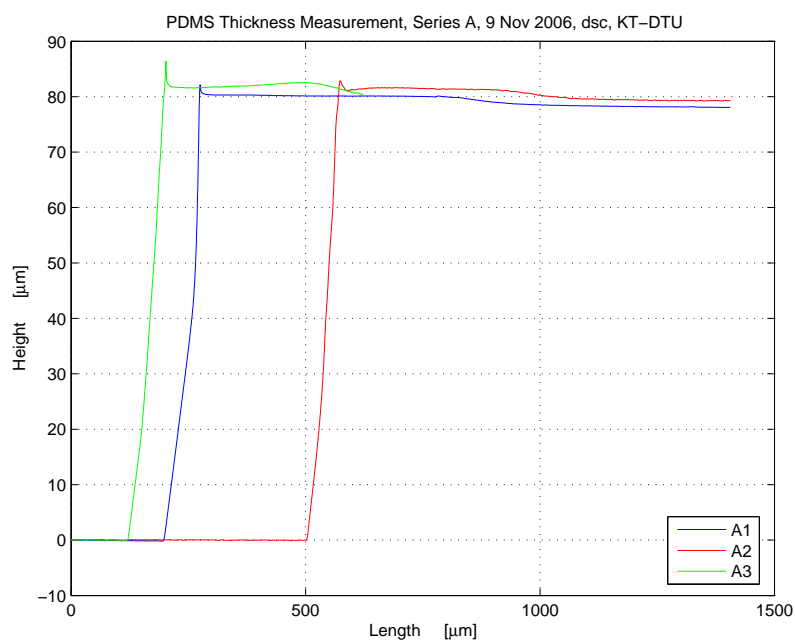


**Figure E.1:** Membranes of Series A

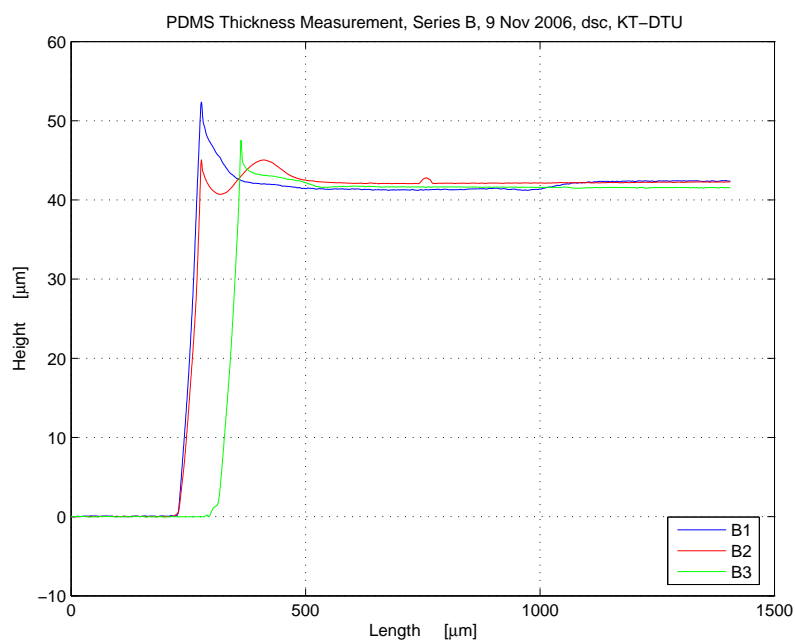


**Figure E.2:** Membranes of Series B

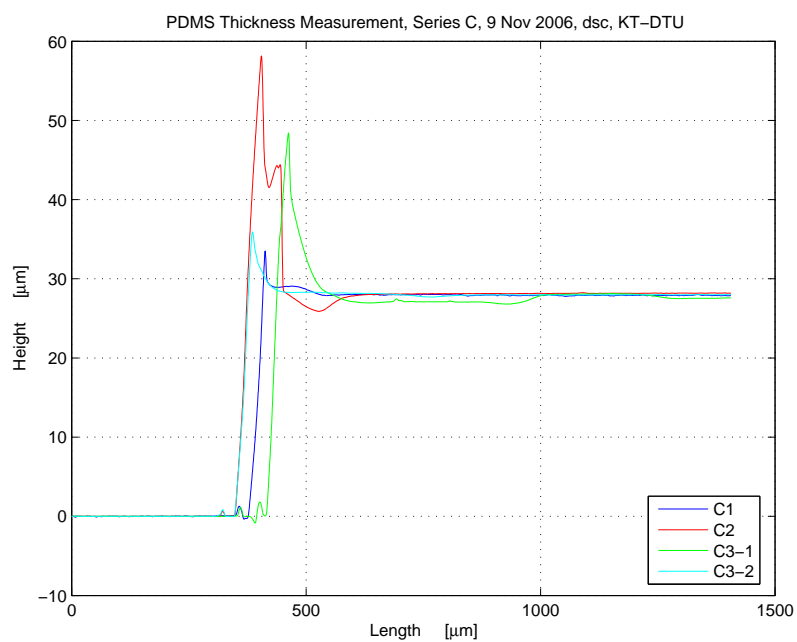


Figure E.3: Membranes of Series C

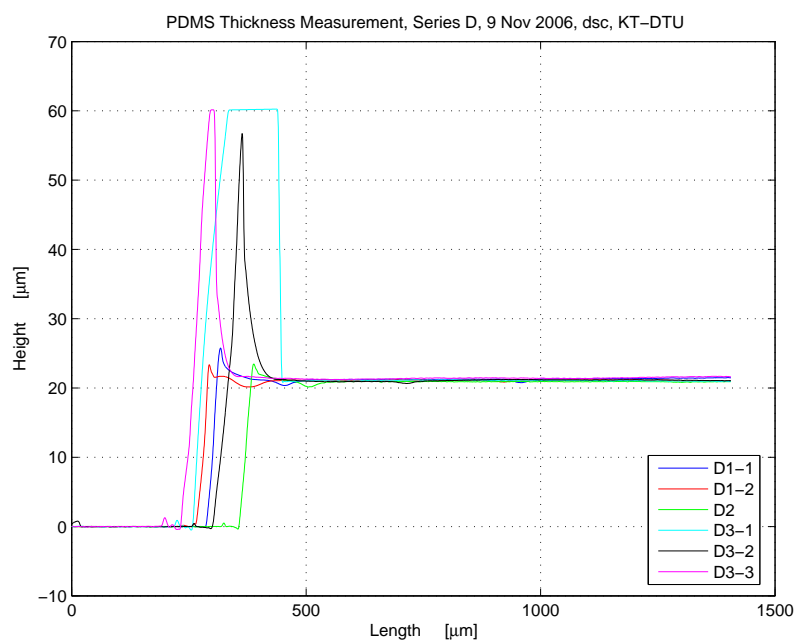
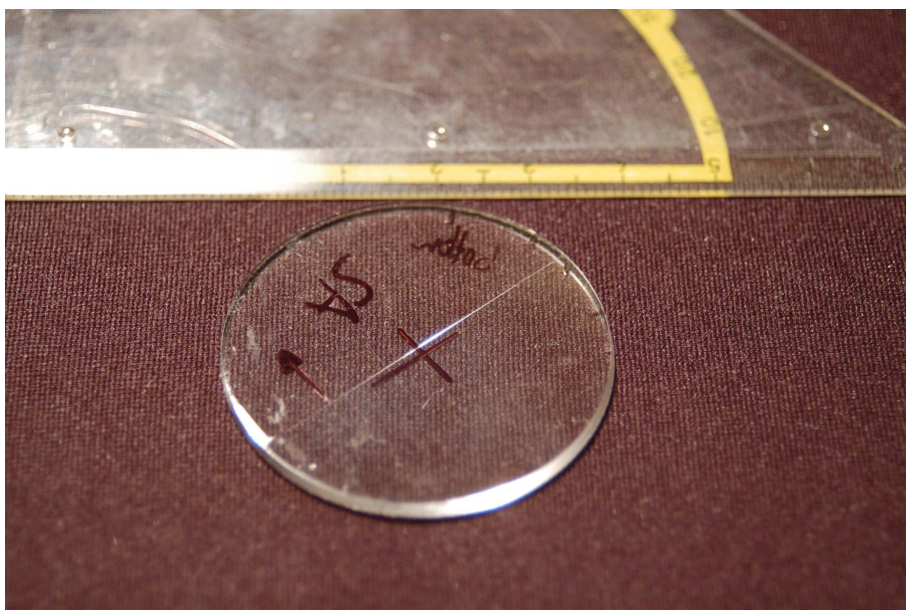


Figure E.4: Membranes of Series D



**Figure E.5:** Membrane of Series A



APPENDIX F

**Transmittance/absorbance  
measurements of different  
materials**

---



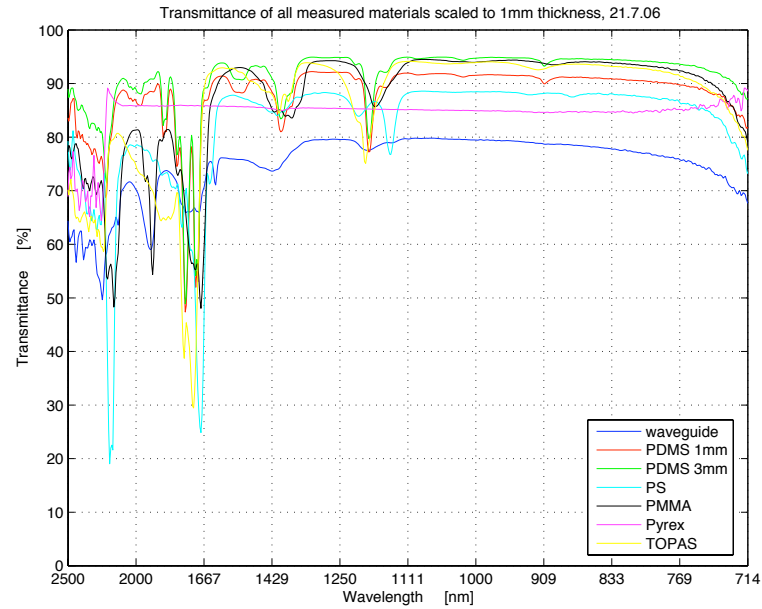


Figure F.1: Transmittance for various transparent materials

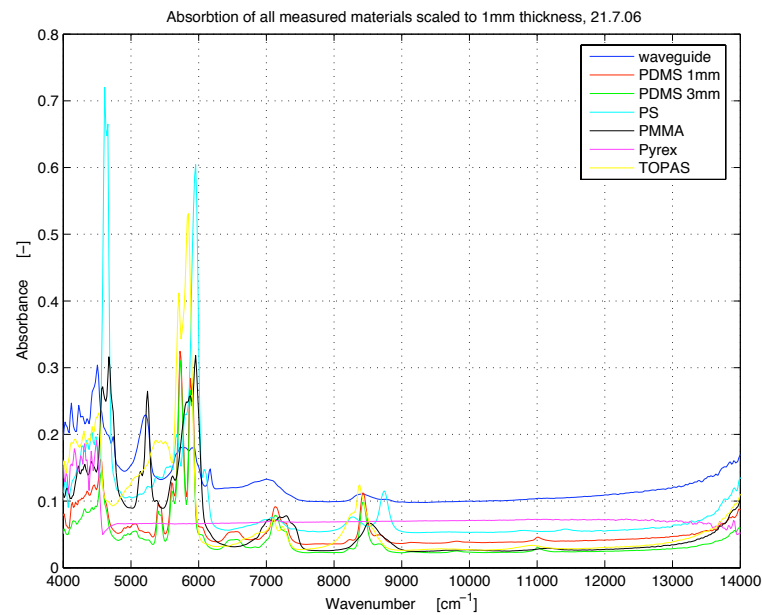


Figure F.2: Scaled absorbtion for various transparent materials

## APPENDIX G

# Culture media

---

All cultivations were done either in *CBS / Delft medium* or *YPD* rich medium. Both recipes are according to the DTU-Department of Systems Biology 'Course notes for the yeast fermentation exercise, June 2006. Course 27031. Experimental fermentation technology'.

### G.1 YPD

YPD is a complex medium for routine growth of yeast. Preparation as follows:

*Composition:*

Yeast extract	10	g
Peptone	20	g
Carbon source	20	g
H <sub>2</sub> O		up to 900 mL

(in addition 20 g/L of agar was added when medium was used for plates).

Weigh and mix together the yeast extract and the peptone in 800 mL of H<sub>2</sub>O. Add 20 g of Bacto Agar (2%) before autoclaving. Adjust the volume of the solution to 900 mL. Autoclave.

Prepare separately the carbon source (glucose for YPD medium; galactose for YPGal medium) in H<sub>2</sub>O to have a concentration of 20 g · L<sup>-1</sup>. Autoclave.

When autoclaved and cooled down to about 50 °C, add 100 mL of the carbon source to the solution containing agar, yeast extract and peptone. Shake vigorously.

## G.2 CBS / Delft medium

The CBS / Delft medium is a standard minimal medium for yeast cultivations. It is composed of salt solutions, a trace metal solution, a vitamin solution and a carbon source. Preparation as follows:

All solutions are made from distilled water.

### *Salt solutions:*

$(\text{NH}_4)_2\text{SO}_4$	500	g	in 5000	mL
$\text{KH}_2\text{PO}_4$	240	g	in 2000	mL
$\text{MgSO}_4, 7\text{H}_2\text{O}$	50	g	in 1000	mL

### *Solution of trace metals:*

The following amounts of salts (-EDTA) are dissolved/suspended in 1000 mL distilled water. Keep the pH at 6 and add the components one by one. The solution is gently heated (lukewarm/hand warm) and the EDTA is added. In the end, the pH is adjusted to 4, and the solution is autoclaved or sterilized by filtration.

$\text{FeSO}_4, 7\text{H}_2\text{O}$	3.0	g
$\text{ZnSO}_4, 7\text{H}_2\text{O}$	4.5	g
$\text{CaCl}_2, 6\text{H}_2\text{O}$	4.5	g
$\text{MnCl}_2, 2\text{H}_2\text{O}$	0.84	g
$\text{CoCl}_2, 6\text{H}_2\text{O}$	0.3	g
$\text{CuSO}_4, 5\text{H}_2\text{O}$	0.3	g
$\text{Na}_2\text{MoO}_4, 2\text{H}_2\text{O}$	0.4	g
$\text{H}_3\text{BO}_3$	1.0	g
KI	0.1	g
$\text{Na}_2\text{EDTA}$	15	g

### *Vitamins:*

For 500 mL 25 mg d-biotin is dissolved in 10 mL 0.1 M NaOH and approximately 400 mL  $\text{H}_2\text{O}$ . Adjust the pH to 6.5 with HCl, and add the following vitamins one by one:

Ca-Pantothenat	500	mg
Thiamin-HCl	500	mg
Pyridoxin-HCl	500	mg
Nicotinic acid	500	mg
p-aminobenzoic acid	100	mg

Again adjust pH to 6.5. Add 12.5 g m-Inositol and adjust pH to 6.5 filling up to 500 mL. Sterilize by filtration and store in the cold.

### *Preparation of CBS-medium from stock solutions:*

The stock solutions for

---

TOTAL	1	L
$(\text{NH}_4)_2\text{SO}_4$	200	mL
$\text{KH}_2\text{PO}_4$	100	mL
$\text{MgSO}_4, 7\text{H}_2\text{O}$	40	mL
Trace metals	4	mL
Sigma 204 antifoam	200	$\mu\text{L}$

are poured together and water is added to give 3.5 L. Adjust pH to 5.0. Pour the medium into the bioreactor and sterilize it by autoclaving it in the bioreactor. The carbon source is dissolved in water to reach volume of 500 mL and autoclaved separately in a flask outfitted with inoculation bulb. Different carbon sources or amounts can be used depending on the experiment. A total of 4 mL of vitamins is added to the bioreactor after autoclavation by sterile filtration.

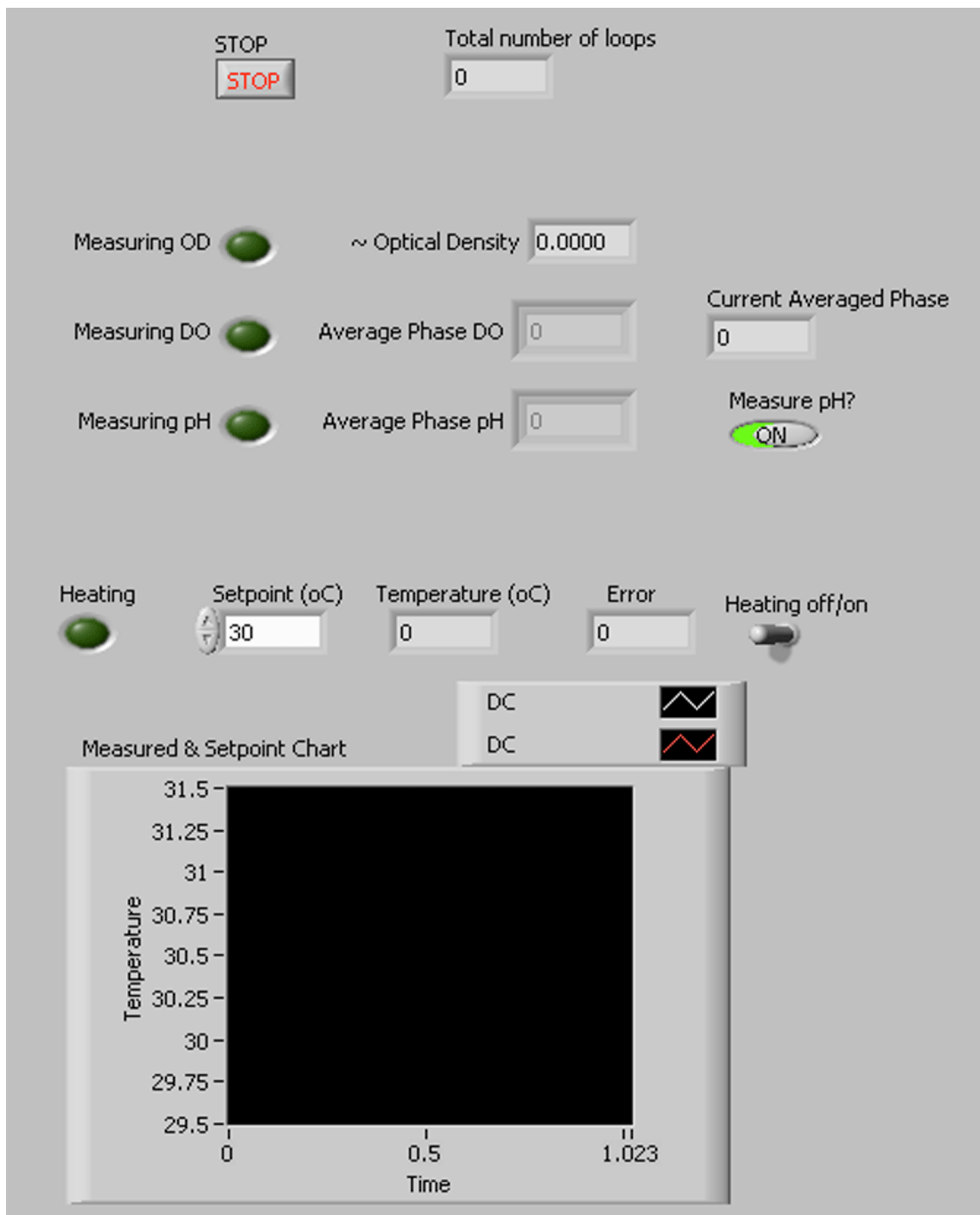


APPENDIX H

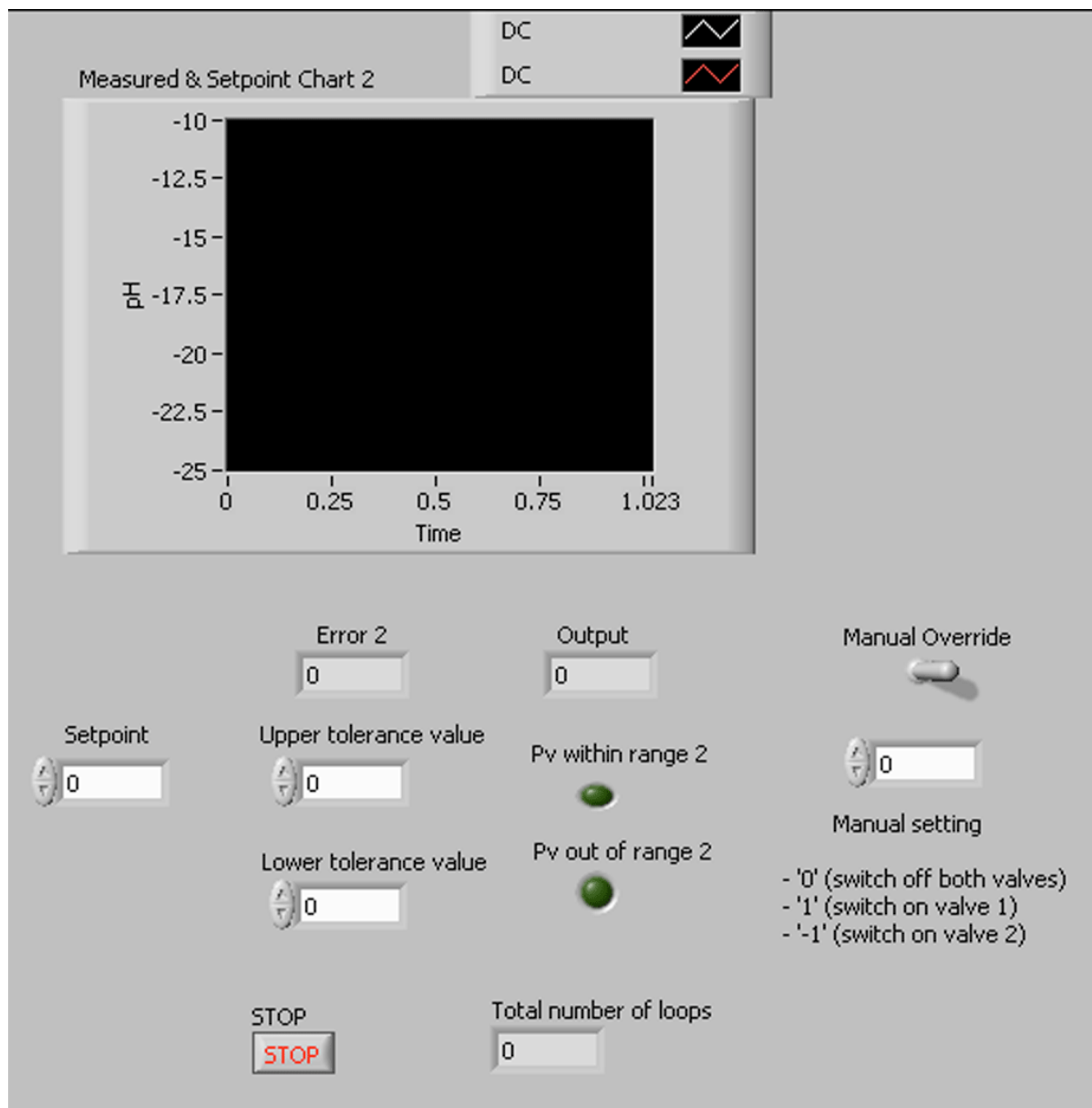
## LabView program

---

LabView front panel for process overview/control



## LabView front panel for pH measurement

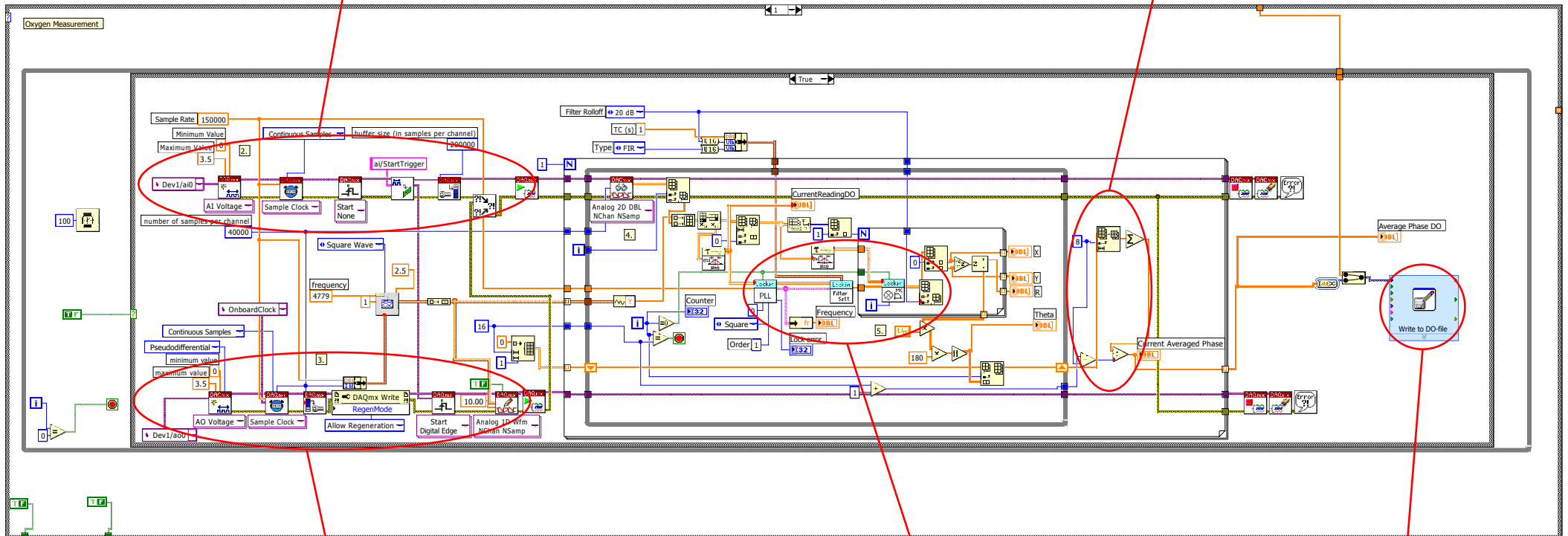




## Measurement of dissolved oxygen

Set up AI channel (read in photodiode voltages)

average over 8 loops

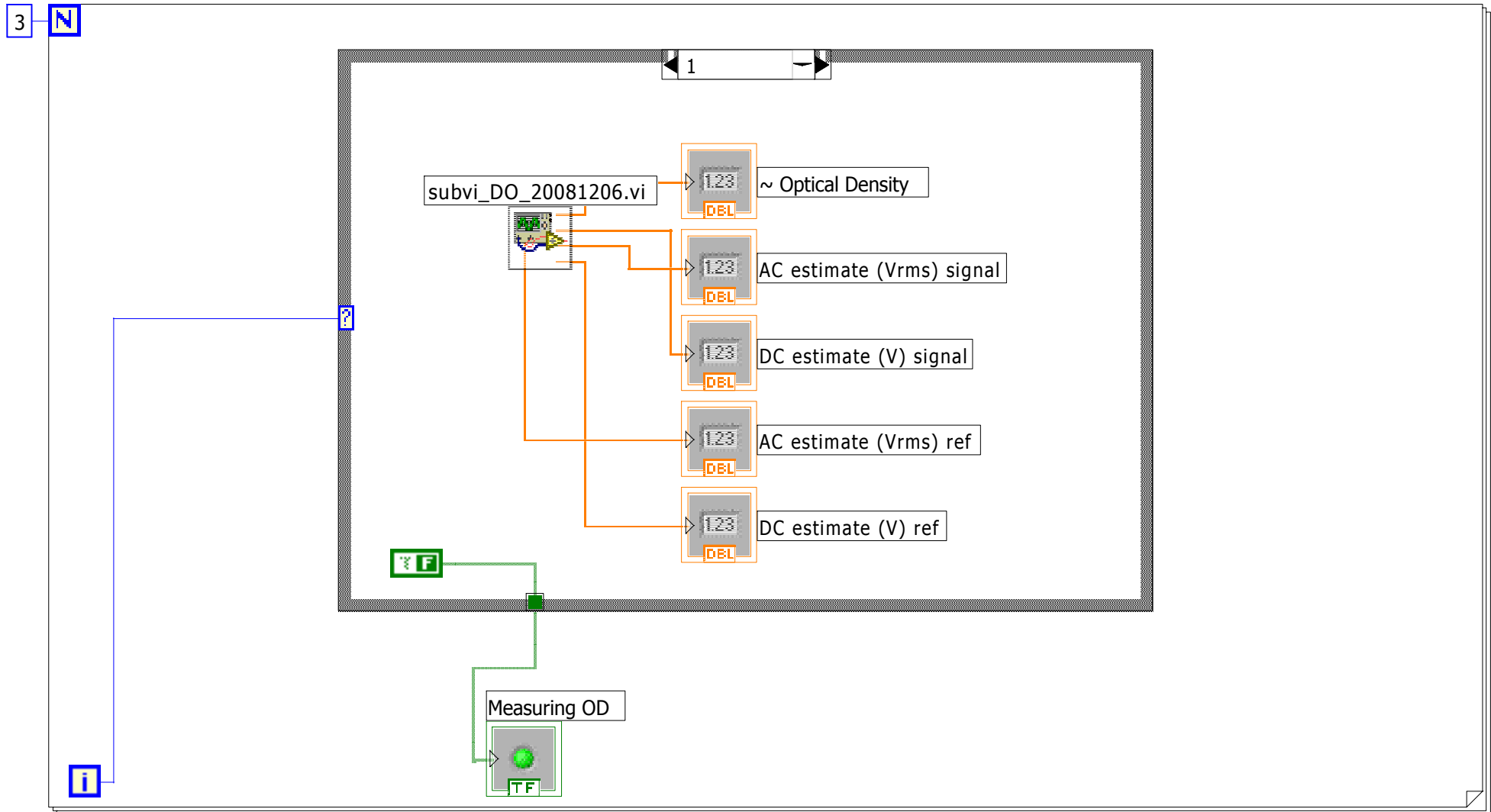


Set up AO channel (send sine wave to LED)

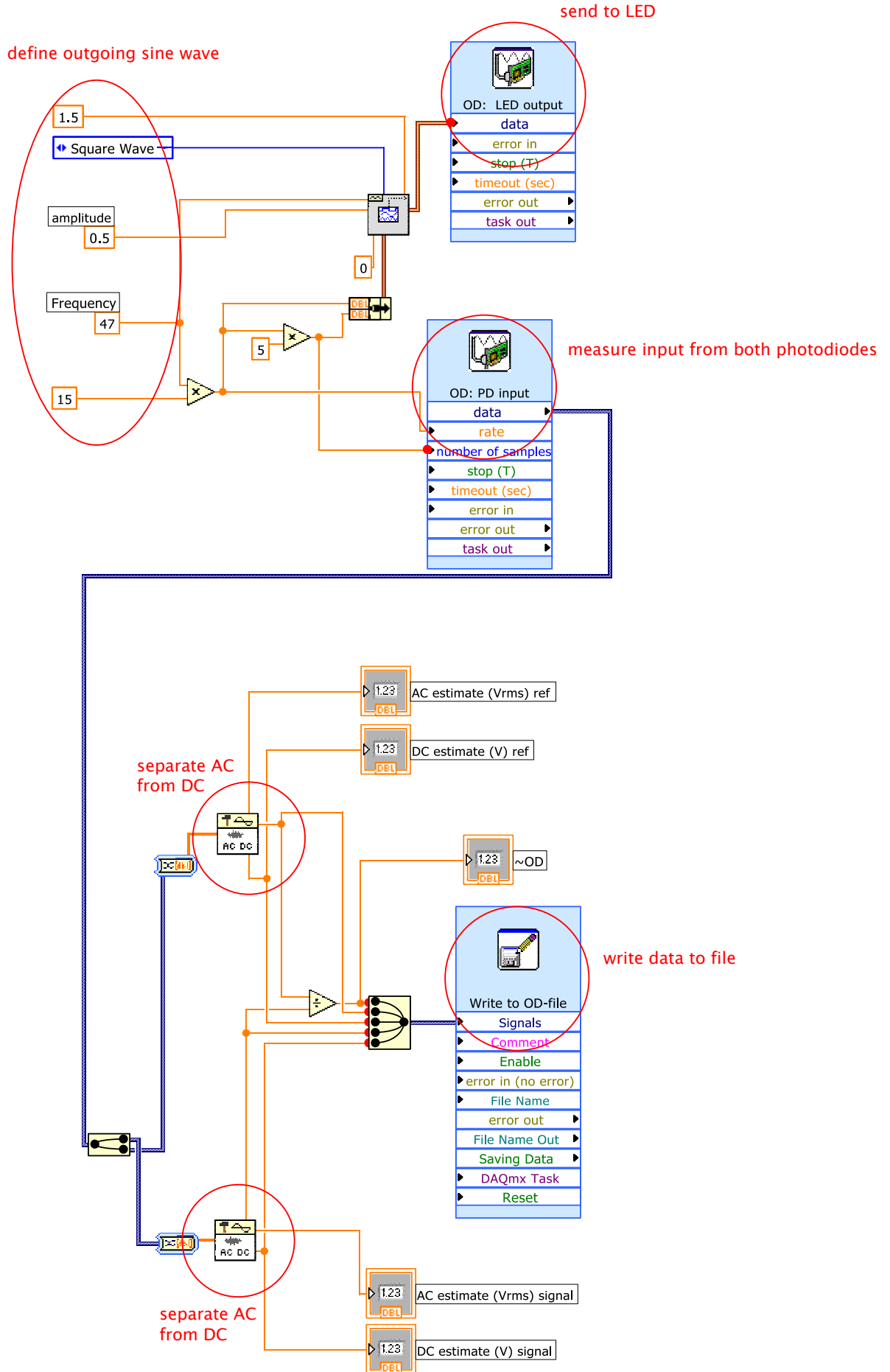
determine phase difference

write to file

## USB-6229: Measurement of Optical Density



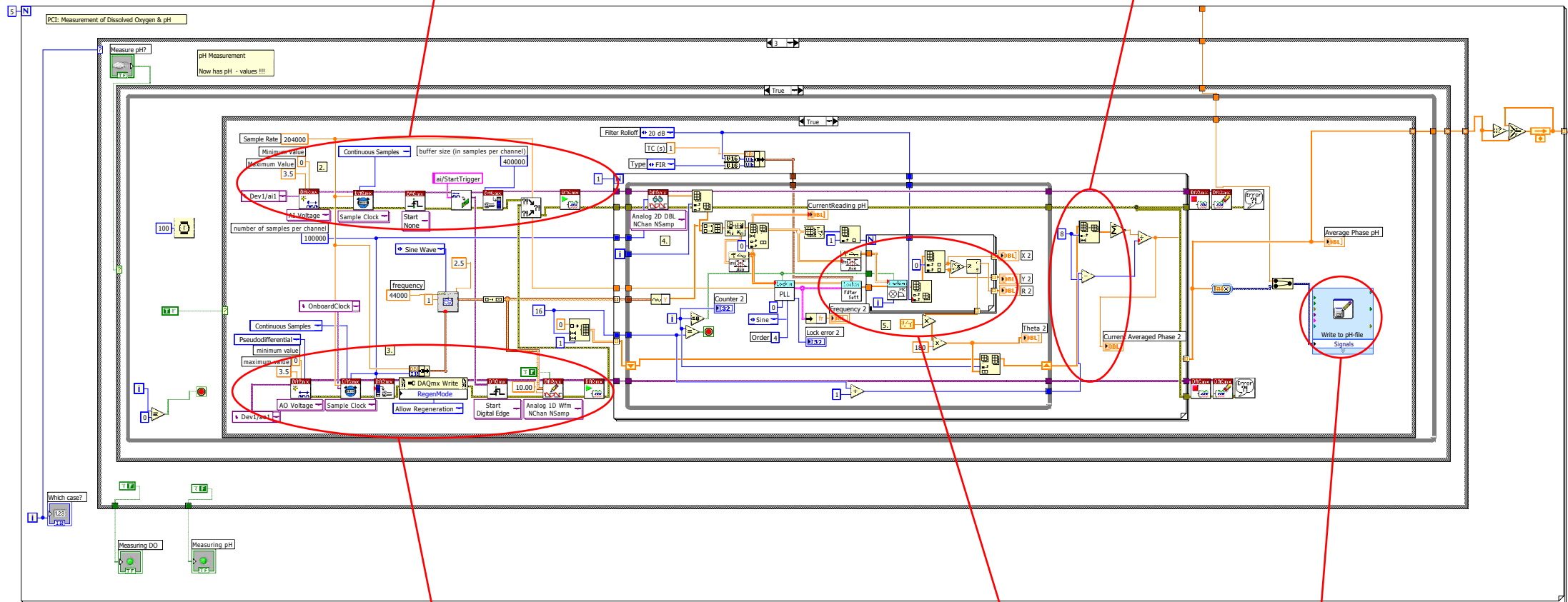
# Measurement of optical density



## Measurement of pH

Set up AI channel (read in photodiode voltages)

average over 8 loops

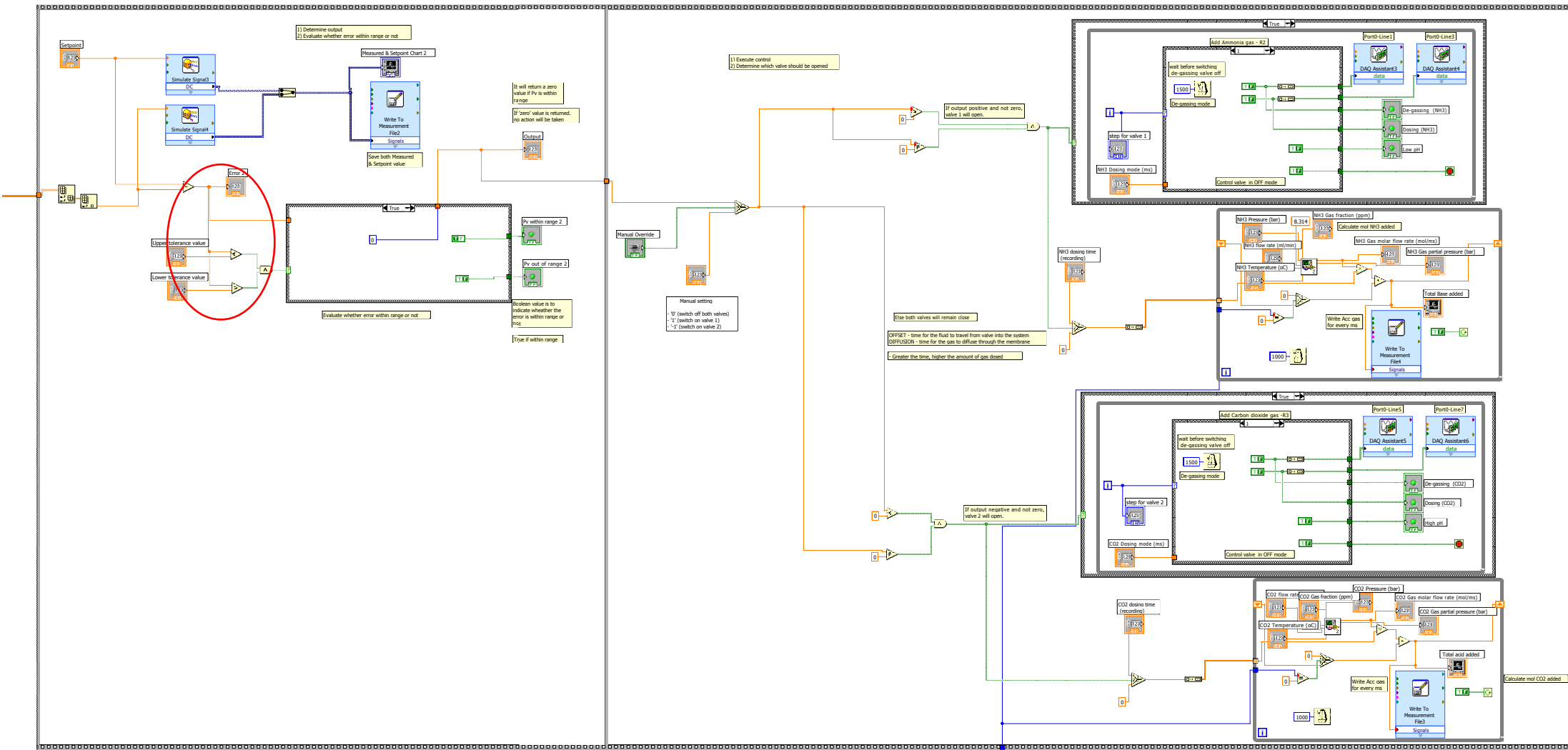


Set up AO channel (send sine wave to LED)

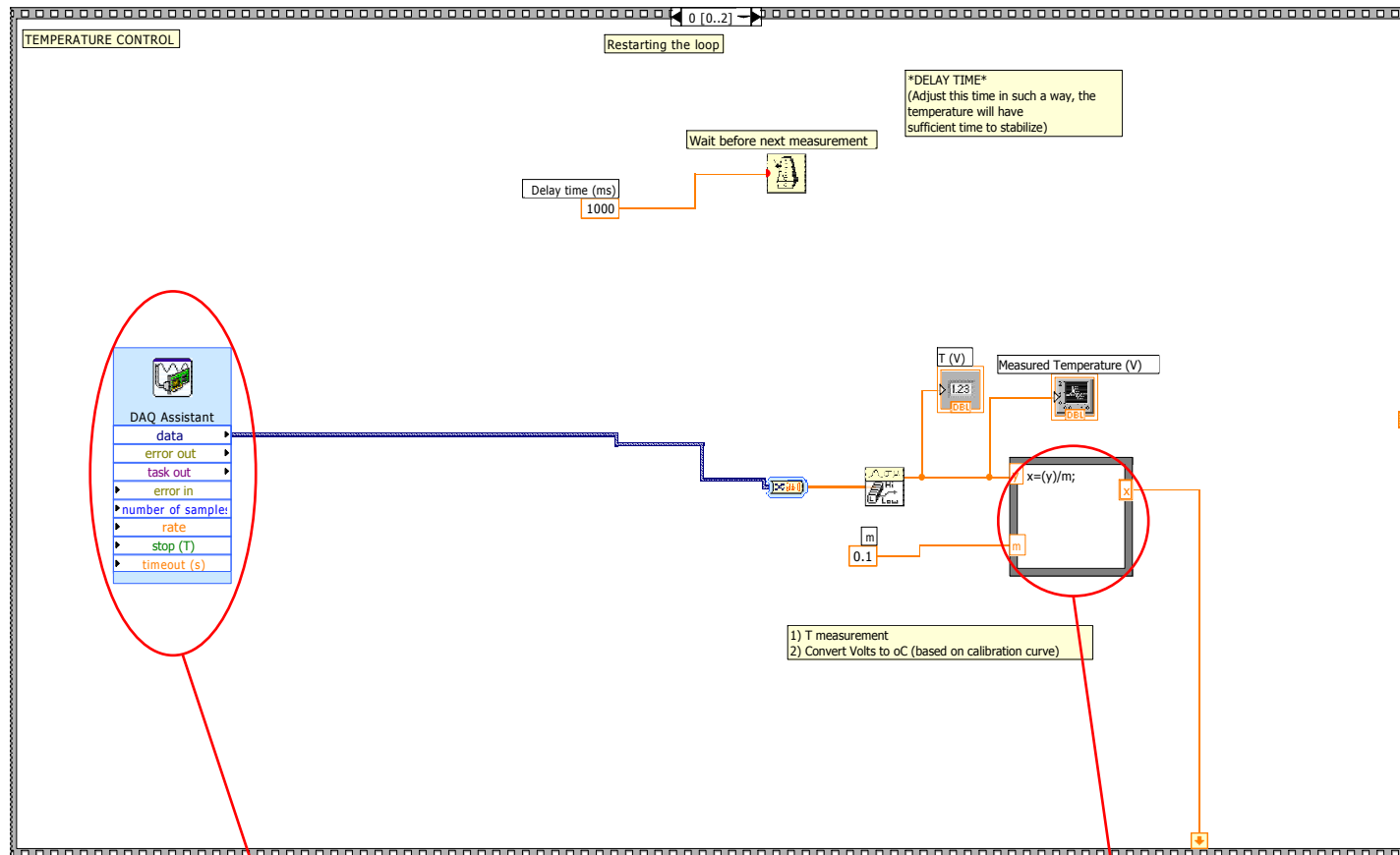
determine phase difference

write to file

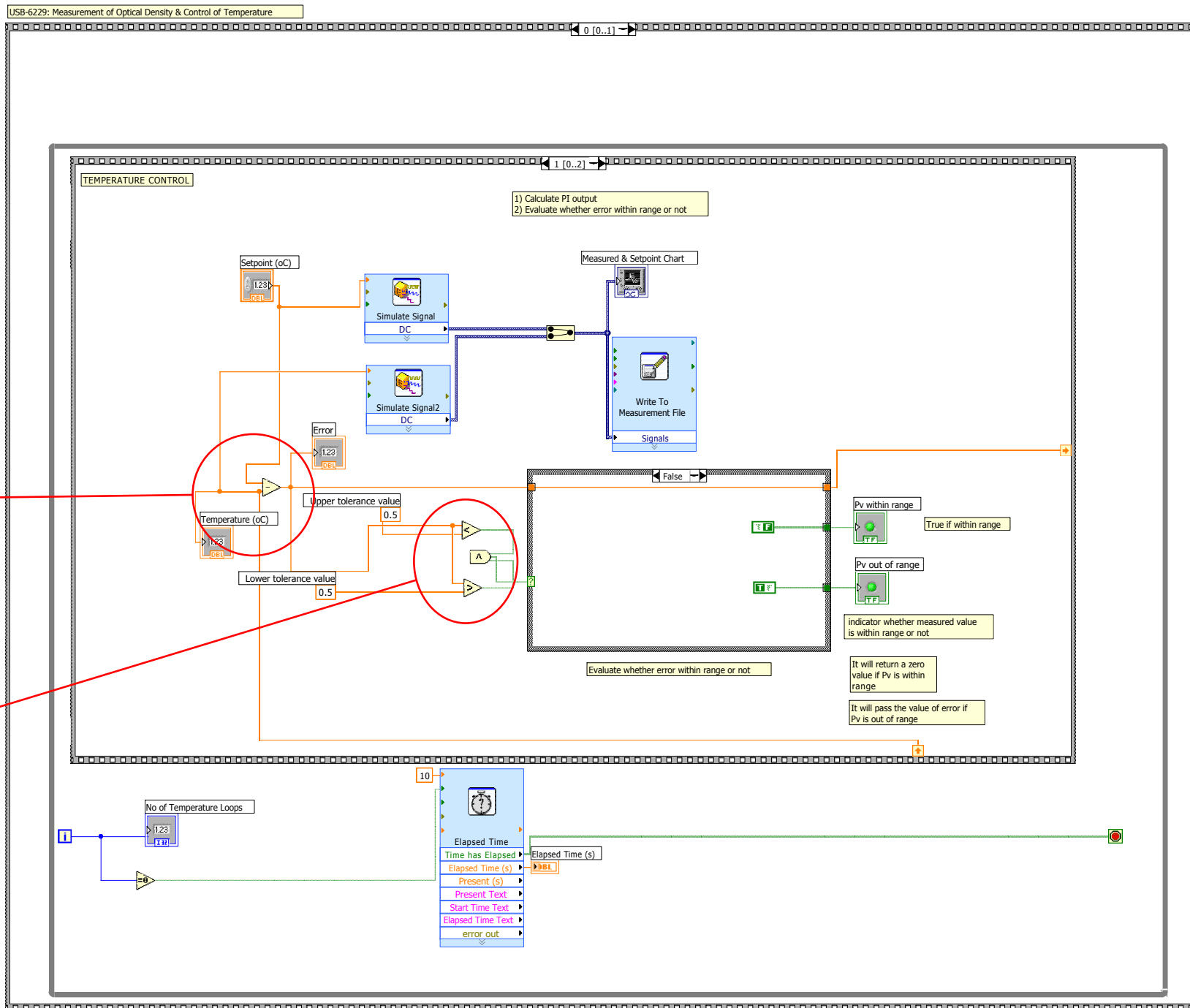
pH control



## Temperature measurement



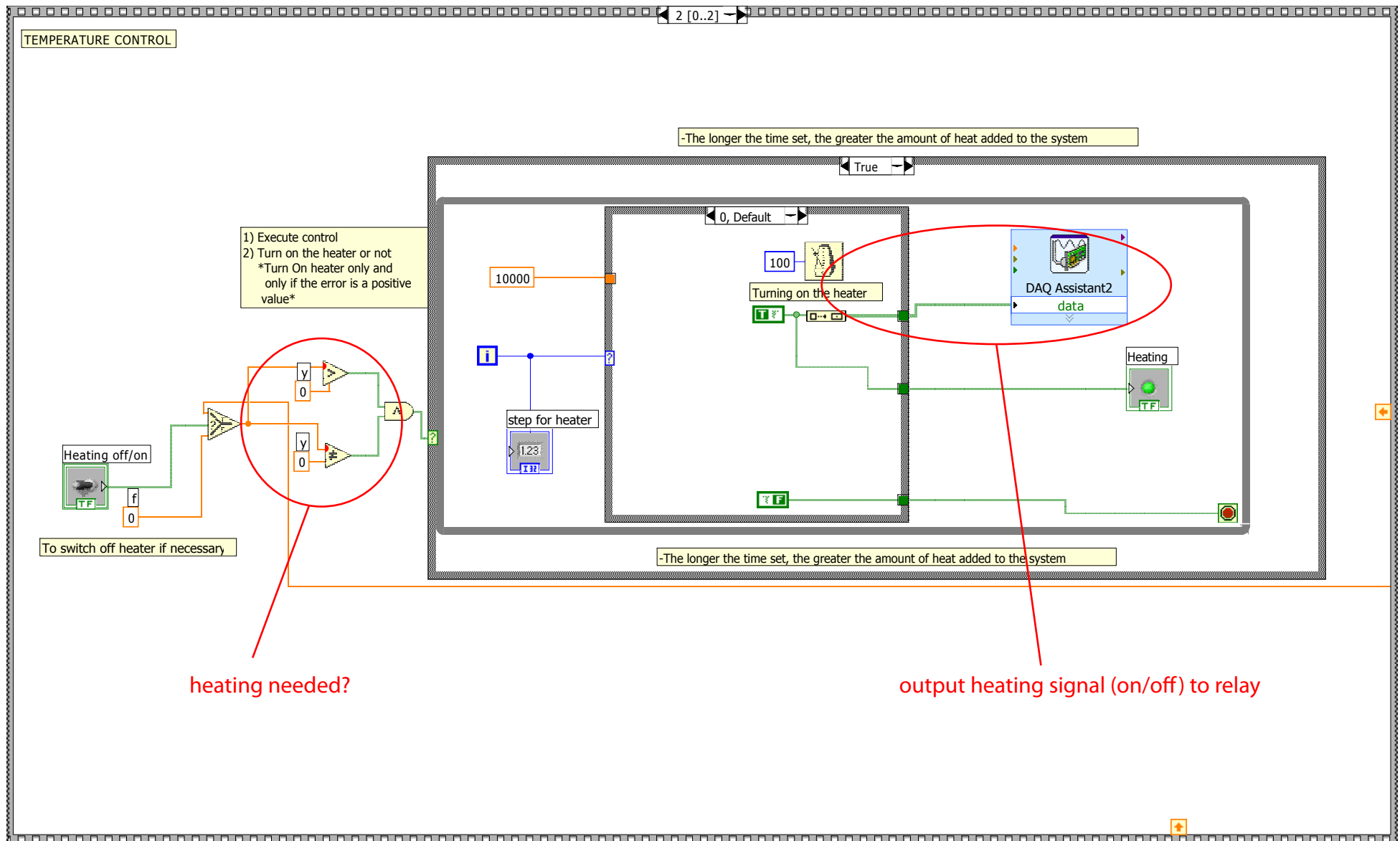
## Temperature control - evaluation of error



Calculate error

Error within  
setpoint?

## Temperature control - heating







## Details of the topology optimization routine

---

The model used within the topology optimization routine is presented below. It was implemented and solved using the commercial software COMSOL®. A list of parameters and corresponding values is given in Table I.1.

The total immobilized biomass is the actuator variable. It is defined based on a design parameter,  $\gamma$ , that will be varied in the routine iterations.  $(1 - \gamma)$  represents the fraction of carrier used by the immobilized biomass (Eq. I.1).

$$X_{im} = (1 - \gamma) \cdot X_{im}^{max} \quad (I.1)$$

The plasmid bearing immobilized biomass, i.e., the fraction of immobilized that possess the genetic information necessary to the production of the desired protein, can be determined by multiplying the total immobilized biomass by  $p$ , constant factor of plasmid loss (Eq. I.2).

$$X_{im}^+ = (1 - p) \cdot X_{im} \quad (I.2)$$

The transport of the suspended (free) biomass, glucose and ethanol is carried out by fluid convection and diffusion, and are mathematically described by the Equations I.3 to I.6, where

$$\frac{X_{im}^{act}}{X_{im}^{act} + X_{im}}$$

accounts for the fact that not all immobilized cells are actively growing.

$$\begin{aligned} \vec{u} \cdot \nabla X_f = (\mu_1 + \mu_2 + \mu_3) \cdot \left( \frac{X_{im}^{act}}{X_{im}^{act} + X_{im}} \frac{X_{im} P_C}{V_r} + X_f \right) \\ + D_X f \nabla^2 X_f \end{aligned} \quad (I.3)$$

$$\vec{u} \cdot \nabla X_f^+ = (\mu_1 + \mu_2 + \mu_3) \cdot \left( \frac{X_{im}^{act}}{X_{im}^{act} + X_{im}^+} \frac{X_{im}^+ P_C}{V_r} + X_f^+ \right) + D_{Xf} \nabla^2 X_f^+ \quad (I.4)$$

$$\vec{u} \cdot \nabla G = - \left( \frac{mu_1}{Y_{X/G}^F} + \frac{\mu_2}{Y_{X/G}^O} \right) \left( \frac{X_{im}^{act}}{X_{im}^{act} + X_{im}^+} \frac{X_{im}^+ P_C}{V_r} + X_f^+ \right) + D_G \cdot \nabla^2 G \quad (I.5)$$

$$\vec{u} \cdot \nabla E = - \left( Y_{E/X, \mu_1} - \frac{\mu_2}{Y_{X/E}} \right) \left( \frac{X_{im}^{act}}{X_{im}^{act} + X_{im}^+} \frac{X_{im}^+ P_C}{V_r} + X_f^+ \right) + D_E \cdot \nabla^2 E \quad (I.6)$$

The growth rates for each of the pathways (Eq. I.7 - I.9) consist of modified Monod equations where  $K_{i'}$  and  $k_{i'}$  are saturation and regulation constants which have been recalculated in order to obtain explicitly defined functions which where mathematically equivalent to the implicitly defined expressions proposed in the work of Zhang et al. The term  $(1 - \tanh G)$  in Eq. I.9 operates as switch function that tends to 0 when G concentration is high and to 1 when G approaches zero.

$$\mu_1 = \mu_{1,max} \frac{G}{K_{1'} + G} \frac{1 + k_{a'} G}{k_{b'} + k_{a'} G} \quad (I.7)$$

$$\mu_2 = \mu_{2,max} \frac{G}{K_{2'} + G} \frac{1 + k_{c'} G}{1 + k_{c'} k_{d'} G} \quad (I.8)$$

$$\mu_3 = \mu_{3,max} \frac{E}{K_3 + E} \cdot (1 - \tanh G) \quad (I.9)$$

In a topology optimization routine, the optimization function is, by default, minimized. As in the case of the presented work, it is desired that the protein product rate is maximized rather than minimized, a negative signal is added when writing the optimization function  $\Phi$  (Eq. I.10)

$$-\Phi = (\alpha_2 \mu_2 - \alpha_3 \mu_3) \left( \frac{X_{im}^+ P_c}{V_r} + X_f^+ \right) \quad (I.10)$$

**Table I.1:** List of model parameters

$X_{im}^{act}$	fraction of active immobilized cells (117)	0.62	$gX_{im}/gC$
$P_c/V_r$	carrier mass/reactor volume (117)	13.6	g/L
$p$	plasmid loss factor (119)	0.05	-
$Y_{X/G}^F$	Yield coefficient of biomass on glucose for glucose fermentation (119)	0.12	$gX/gG$
$Y_{X/G}^O$	Yield coefficient of biomass on glucose for glucose oxidation (119)	0.48	$gX/gG$
$Y_{E/X}$	Yield coefficient of ethanol on biomass for glucose fermentation (119)	3.35	$gE/gX$
$Y_{X/E}$	Yield coefficient of biomass on ethanol for ethanol oxidation (119)	0.65	$gX/gE$
$\alpha_2$	Protein yield coefficient for glucose oxidation (119)	32.97	units/gX
$\alpha_3$	Protein yield coefficient for ethanol oxidation (119)	33.80	units/gX
$\mu_{max,1}$	Maximum specific growth rate for glucose fermentation (119)	0.38	$0.38 \text{ h}^{-1}$
$\mu_{max,2}$	Maximum specific growth rate for glucose oxidation (119)	0.25	$\text{h}^{-1}$
$\mu_{max,3}$	Maximum specific growth rate for ethanol oxidation (119)	0.10	$\text{h}^{-1}$
$K_{1'}$	Saturation constant	0.18	-
$K_{2'}$	Saturation constant	$0.01\text{exp} -2$	-
$k_{a'}$	Enzyme pool regulation constant	-0.0044	-
$k_{b'}$	Enzyme pool regulation constant	2.3	-
$dp$	Pressure drop	0.1	Pa
$DX_f^+$	Diffusion coefficient	$1\text{e}-10$	$\text{m}^2/\text{s}$
$DG$	Diffusion coefficient	number	unit
$DE$	Diffusion coefficient	number	unit
$l$	Reactor length	0.0012	m
$w$	Reactor width	0.0012	m
$h$	Reactor height	0.001	m
$\eta$	Fluid viscosity	0.001	$\text{Pa} \cdot \text{s}$
$G_{inlet}$	Glucose feed concentration	0.001–1	g/L





**[www.kt.dtu.dk](http://www.kt.dtu.dk)**

Department of Chemical and Biochemical Engineering  
Center for Process Engineering and Technology (PROCESS)  
Technical University of Denmark  
Søltofts Plads  
Building 229  
DK-2800 Kgs. Lyngby  
Denmark  
Tel: (+45) 45 25 28 00  
Fax: (+45) 45 93 29 06  
Email: [kt@kt.dtu.dk](mailto:kt@kt.dtu.dk)